Intensificación de Procesos de Oxidación Avanzada mediante radiación microondas para el tratamiento de aguas residuales

Alicia Loreto García Costa

Madrid - 2019

UNIVERSIDAD AUTÓNOMA DE MADRID
FACULTAD DE CIENCIAS
Departamento de Ingeniería Química

INTENSIFICACIÓN DE PROCESOS DE OXIDACIÓN AVANZADA MEDIANTE RADIACIÓN MICROONDAS PARA EL TRATAMIENTO DE AGUAS RESIDUALES

ADVANCED OXIDATION PROCESSES INTENSIFICATION BY MEANS OF MICROWAVE RADIATION FOR WASTEWATER TREATMENT

Tesis Doctoral

ALICIA LORETO GARCÍA COSTA

Madrid, 2019

UNIVERSIDAD AUTÓNOMA DE MADRID
FACULTAD DE CIENCIAS
Departamento de Ingeniería Química

INTENSIFICACIÓN DE PROCESOS DE OXIDACIÓN AVANZADA MEDIANTE RADIACIÓN MICROONDAS PARA EL TRATAMIENTO DE AGUAS RESIDUALES

ADVANCED OXIDATION PROCESSES INTENSIFICATION BY MEANS OF MICROWAVE RADIATION FOR WASTEWATER TREATMENT

MEMORIA

para optar al grado de

Doctor con Mención Internacional

y al sello

International PhD on AOPs

que presenta

Alicia Loreto García Costa

bajo la dirección de:

Dr. José Antonio Casas de Pedro

Dr. Juan Antonio Zazo Martínez

Madrid, 2019

D. José Antonio Casas de Pedro y D. Juan Antonio Zazo Martínez, Profesores Titulares del Departamento de Ingeniería Química de la Universidad Autónoma de Madrid

HACEN CONSTAR: que el presente trabajo, titulado "*Intensificación de procesos de oxidación avanzada mediante microondas para el tratamiento de aguas residuales*", presentado por Dña. Alicia L. García Costa, ha sido realizado bajo su dirección, en los laboratorios del Departamento de Ingeniería Química, en la Universidad Autónoma de Madrid y que, a su juicio, reúne los requisitos de originalizad y rigor científico necesarios para ser presentados como Tesis Doctoral mediante compendio de artículos conforme al artículo 8 del Procedimiento relativo al tribunal, defensa y evaluación de la tesis doctoral en la Universidad Autónoma de Madrid

Y, para que conste a efectos oportunos, firmamos el presente informe en Madrid a 25 de febrero de 2019.

José Antonio Casas de Pedro Juan Antonio Zazo Martínez

La realización de este trabajo ha sido posible gracias al apoyo económico del Ministerio de Economía y Competitividad con los proyectos CTQ2013-41963-R y CTM2016-76454-R, además del contrato predoctoral BES-2014-067598 cofinanciado por el Fondo Social Europeo y las ayudas económicas de movilidad predoctoral EEBB-I-17-12532 y EST2019-013106-I

Asimismo, han contribuido en la financiación de este trabajo la Comunidad Autónoma de Madrid a través del proyecto REMTAVARES S2013/MAE-2716 y Campus France con una beca de movilidad predoctoral dentro del programa *Make Our Planet Great Again*.

La vida de un gran científico en el laboratorio no es idílica, como se suele creer, sino que acostumbra a ser una lucha obstinada contra las cosas, contra el entorno y, ante todo, contra sí mismo. *Marie Curie*

¡GRACIAS!

En primer lugar, me gustaría agradecer a mis directores de tesis su enorme contribución a esta tesis y a mi formación como investigadora.

Gracias al Dr. José Antonio Casas, *Houses*, por cargar conmigo en un inesperado cambio de planes, por confiar en mí y por mantener mi cordura a salvo estos últimos cuatro años. Gracias por todas y cada una de las horas dedicadas, presenciales y en remoto, para solventar crisis hasta de nivel internacional. Gracias por todas las lecciones, incluidas las de mus y tu tremenda paciencia en esos momentos en los que no entra más en esta alborotada cabeza que llevo sobre los hombros. Gracias por hacer de profesor, director y hasta psicólogo. Gracias por ser un modelo a seguir.

Gracias al Dr. Juan Antonio Zazo, el eterno tutor, que lleva aconsejándome desde que pusiera mi primer pie en la UAM allá por 2009. Gracias, porque sin esos consejos y ánimos no hubiera acabado a tiempo para iniciar esta aventura con vosotros. Gracias por estar a mi lado desde el principio, desde las tutorías del PAT a mis inicios en investigación del TFG y, sobre todo, por aguantar alguna que otra crisis existencial y nuestros cafés.

¡A los dos en conjunto, por vuestro genial matrimonio! Ambos habéis sido un apoyo y una referencia, con nuestras comidas, partidas de mus con el alcalde o cualquier paisano que se uniera y los pokepaseos. No puedo imaginar jefes mejores.

No puedo olvidarme en estas palabras de agradecimiento del, por fin, Departamento de Ingeniería Química en su totalidad. Todos y cada uno de vosotros habéis contribuido a mi formación como Ingeniera Química e indirectamente como persona, a través del Grado, Máster y más recientemente en el Doctorado. Dentro de este apartado, mi sincero agradecimiento al Dr. Juan José Rodríguez tanto por sus conocimientos y ayuda en la redacción de artículos, como por confiar en mí e impulsarme a través del grupo especializado de la RSEQ y del WCCE10. Gracias por valorar mi esfuerzo y confiar en mí.

Sin duda otro apartado especial dentro del Departamento va dedicado a mis compañeros de laboratorio. Compañeros de fatigas que han conseguido amenizar, muy mucho, las horas de laboratorio. Gracias a Anita y Lucía por las largas horas de laboratorio y de peleas con los equipos que hemos sufrido juntas. Gracias a Sandra, Pepelu y Cris por vuestra acogida y cariño. Gracias a Cristian, Rubén, Lemus, los Danis y Gon, chicos LIs, por los momentos chop, por aguantarme en el mismo despacho con una hartura de paciencia y por estar siempre dispuestos a ayudar con lo que sea. Gracias a los plantíferos, Isma, Esther, Inés S., Javi y Andrés, especialmente a los dos primeros, que han compartido viajes, comidas y muchas tonterías. Gracias Jeff por tu calma y disposición y, obviamente, ¡por las barbacoas y esa yuca frita! Gracias a Inés A., ese mini-me que ha revolucionado el IQ3. Gracias a las chicas escapistas: Adri, Julia, Blanca y Estefanía, por vuestro entusiasmo y nuestros momentos juntas. Gracias a todos y cada uno de los cohabitantes del lab: Álvaro, Silvia, Maca, Xu, Esbi, Almu, Virginia, Jaime, Javi, Dani R., Sichen, etc. También imprescindibles en la sección laboratorio todos los que habéis confiado en mí con los TFG/TFM: Laura R., Raúl, Luis, Alberto (por partida doble, ¡qué osadía repetir la experiencia con nosotros!), Esbi, Carmen, Laura C., Lucía, Claudia, Ángela y Ramón. No sabéis la alegría que ha sido poder trabajar con todos vosotros y poner un granito de arena en vuestra formación.

Thanks to Dr. Dionysios Dionysiou and his group for hosting me in Cincinnati for 3 months. My very special thanks to Ming Hao and Nathalie, who introduced me to the amazing people in the GSGA and changed completely my stay in the States. To my Cincy family: Mary Rita, Buddy, Rie and Akira, thanks for our little special moments.

Un gros merci va aussi en France, vers le groupe de Dr. Karine Groenen-Serrano, de l'université Toulouse III-Paul Sabatier. Je te remercie énormément pour m'accueillir en deux occasions suivantes pour mieux apprendre sur les procèdes d'oxydation électrochimique. J'ai bien profité le double stage, non seulement dès le point de vue scientifique, mais aussi pour l'opportunité d'être part d'un group grand et motivateur avec des gens merveilleuses comme André, Theo, Laure, Brigitte, Sandrine et les autres doctorants.

A partir de aquí he de agradecer a los más cercanos de la parte no estrictamente científica. A mis compañeros de carrera, que habéis seguido apoyándome en cada uno de mis pasos: Irene, Carmen, Laura, Nai, Dani, Emilio, Juan, Vassi, Julián y Javi. A mis niñas del cole, creáis o no en los electrones, siempre habéis creído en mí: Moni, Sonia, Palo, Cris, Lourdes, Pili, Marta, Sandra e Iara. A mis lastreños, los Arakiri, las escapadas rurales, las fiestas de nuestra comarca y por acogerme siempre con una sonrisa.

Dentro de mi familia tengo que agradecer a mi mayor fan, la que siempre tiene tiempo para sacarme una sonrisa. Nuria, Nurieta o *mi prima la de Valencia*. Mi prima-hermana, esa prima que es como si fuera una hermana y aguanta todas y cada una de mis chorradas (y son muchas). A mi grupo de primos + tíos esquiadores: Elena, Vicen, Pati, Pepón e Ina. Gracias por esa semana anual que tenemos para nosotros, para desconectar y ponernos al día. Al Rober, mi padrino y joya recuperada dentro de la familia. A todos mis tíos y primos.

Gracias a mi hermano, Álvaro, Alvi, Güess, gords, por enseñarme a perseguir mis sueños y que el cielo es el límite. Por acogerme siempre con los brazos abiertos, por seguirme ahí a donde voy con viajes increíbles. Este señor ha cruzado la frontera de las cataratas del Niágara a pie y cogido un Uber a un sitio cercado por contaminación solo porque a la niña le hacía ilusión… ¡Gracias por todas y cada una de nuestras lemongadas, que seguirán sorprendiendo al mundo entero!

Gracias a mi padre, Andrés, papá, Sr. Alcalde, por enseñarme lo que es la perseverancia, el hacer las cosas bien o no hacerlas y por haber compartido cargo público conmigo los últimos cuatro años.

Por último y, sí por ello más importante, gracias a mi madre, la Geno, mamá, mamichula, por tu apoyo incondicional, tu fuerza y tus ganas de salir adelante de todo lo que se cruce, siempre que estemos juntas. Gracias por creer en mí y en mis sueños. ¡No hay otra mami más chula que tú y lo sabes!

¡A todos… GRACIAS!

INDEX

1. INTRODUCTION

Water is a scarce resource, essential for life, but it can be endangered by the anthropogenic activity. According to the United Nations (UN), approximately 70% of water usage goes for agricultural purposes, 20% for domestic use and 10% for industrial applications [1]. Nonetheless, this distribution varies depending on the economic development of the countries. Figure 1.1 shows the latest available water distribution data for Spain, provided by the National Institute of Statistics [2]. As may be seen, the industrial sector gets around 20% of the total water consumption.

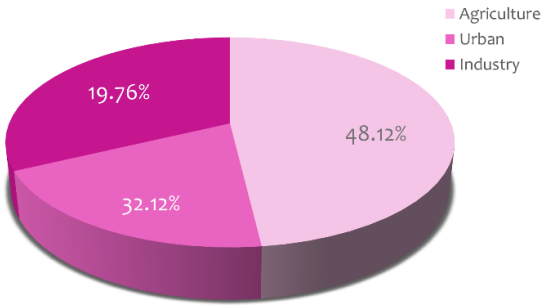

Figure 1.1. Water usage in Spain, 2016 [2]

Whilst each of these activities results in a deterioration of water quality, industrial effluents carry the most concentrated and toxic pollution. Hence, in order to fulfill target 6.3 of the UN Water Agenda for Sustainable Development, which aims to improve water quality by reducing pollution, eliminating waste discharges and minimizing the release of hazardous chemicals and materials, efficient water treatments must be implemented [3].

Industrial water treatments can be classified in two main groups: non-transformative and transformative methods, as listed in Table 1.1. The first one implies the concentration or transference of the pollutant into another phase, without changes in its chemical structure. Thus, they are usually employed as a pretreatment prior to chemical depollution. On the other hand, the transformative methods aim for the partial or total degradation of the contaminants towards CO_2 and water or non-toxic compounds. The selection of an adequate technology relies on economic and environmental factors, as well as the pollutant nature.

Table 1.1. Industrial wastewater treatments classification.

Non-Transformative	Transformative	
Adsorption Filtration Stripping	Reduction	
	Biological oxidation	
	Chemical oxidation	Supercritical wet oxidation Wet air oxidation Advanced oxidation processes

NON-TRANSFORMATIVE METHODS

Amongst the non-transformative processes, **adsorption** is one of the most commonly employed. It consists on the retention of soluble or suspended species on the surface of solid adsorbents. The most common adsorbents are activated carbon [4, 5], zeolites [6, 7], clays [8, 9], etc. These are typically employed as tertiary treatment in wastewater treatment plants to retain organic compounds in relatively diluted streams. However, the spent adsorbents must be efficiently regenerated in order to avoid hazardous waste generation.

Filtration processes are based on the use of membranes as semipermeable physical barriers, which allow pollutant separation from a water stream. As a result, two effluents are generated, a clean permeate and a concentrated polluted stream. Depending on the membrane pore diameter the filtration processes are classified as: microfiltration (MF, 10 μm-100 nm) [10], ultrafiltration (UF, 100-10 nm) [11, 12], nanofiltration (NF, 10-1 nm) [13, 14] and reverse osmosis (RO, <1 nm) [15, 16]. The main drawback of these technologies relies on the energy requirements, as pressure may rise to 70 bar. Also, membrane deterioration and fouling may pose a threat in the application of membrane filtration systems.

Stripping or desorption processes use an air flow to sweep volatile compounds from an aqueous influent. This technology has been widely applied at industrial scale for the removal of diverse contaminants such as ammonia, benzene, toluene, mercaptans, etc. [17, 18], but is also used in potable and groundwater

treatment [19, 20]. As for the previous processes, the stripping results in a contaminated gaseous stream, which must be treated.

TRANSFORMATIVE METHODS

The application of transformative processes depends on the nature of the contaminants and the amount of wastewater to treat. Figure 1.2 outlines the usual criteria as a function of the effluent flow and the organic content expressed as total organic carbon.

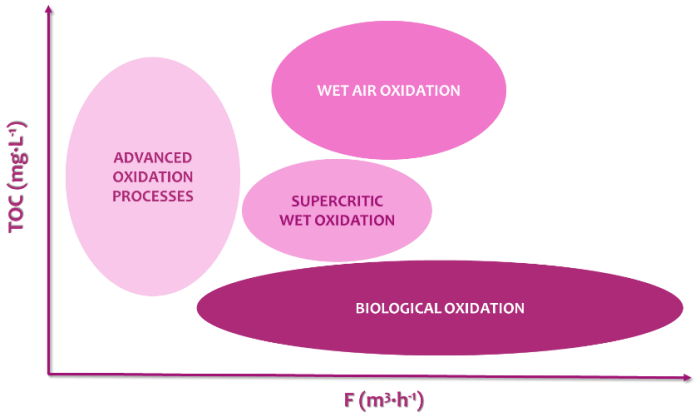

Figure 1.2. Traditional application criteria for transformative methods in wastewater treatment [21] .

Reduction treatments have been widely employed for water decontamination. Catalytic hydrotreatments have been successfully applied for dehalogenation, reducing the toxicity of the effluent [22, 23]. Nevertheless, this technology does not eliminate organic matter and is usually applied as a pre-treatment, to reduce the toxicity of the pollutants or to transform the molecule into a more reactive one in an oxidation process. The direct oxidation of halogenated compounds can give rise to the formation of non-biodegradable and highly toxic pollutants such as biphenyls, chlorofuranes or chlorodioxines.

Biological aerobic oxidation is vastly extended due to its reduced operating costs. These processes employ microorganisms that can transform or even eliminate the biodegradable organic matter in presence of oxygen. Their versatility relies on the wide range of flow and organic matter that may be

treated with these methods. They include activated sludge, sequential batch reactors (SBR), membrane biological reactors (MBR) and rotating biological contactors (RBC), amongst others [24-26]. Despite their several applications, these systems are not always effective, especially when facing non-biodegradable toxic or recalcitrant pollutants.

Supercritical Wet Oxidation (SWO) is based in the oxidation at water supercritical conditions (T: 374ºC, P: 221 bar), or above them, commonly 650ºC and 250 bar [27-29]. This technique is only economically competitive for wastewater with an elevated organic load, when it is possible the autothermic sustainability of the process. This technology achieves high conversion rates with >99.9% of organic carbon transformed to CO_2, nitrogen to N_2 and halogens to their corresponding acids in a very short time reaction (30-60 s). On the other hand, inorganic salts deposition poses a major threat towards its application as it causes reactor corrosion. Altogether, this is a rather expensive treatment considering both the equipment and the operative costs, which are very elevated due to the pressure and temperature requirements.

Wet Air Oxidation (WAO) aims to oxidize organic matter in presence of O_2 as oxidant. In order to maximize the dissolved O_2 concentration and generate free radicals for pollutant depletion, high temperature and pression are required (T: 200-350ºC, P: 5-200 bar) [30, 31]. This process is applied to high organic load wastewaters (TOC: 5-500 $g \cdot L^{-1}$) in order to generate autothermic conditions and it is currently used by the petrochemical, chemical and pharmaceutical industries [32]. WAO has been intensified using solid catalysts, typically with noble or transition metals as active phase, such as Pd, Pt, Ru, Fe, Co or Ni, in the so called **Catalytic Wet Air Oxidation (CWAO)** [33-35]. These allow working at lower pressure and temperature, reducing significantly the costs for its application. The main drawback for WAO is, as for SWO, the high economic expense due to the operating conditions, whereas for CWAO the low catalyst stability, along with their cost compromises the feasibility of the process.

Due to the limited applications of the aforementioned, **advanced oxidation processes** arise as a reasonable alternative for industrial wastewater treatment.

1.1. Advanced Oxidation Processes

Advanced oxidation processes (AOPs) are based on the generation of strong oxidizing radicals able to oxidize a wide variety of pollutants [36]. At the beginning, this definition for AOPs only considered hydroxyl ($HO^{\bullet}$) radicals and mild operating conditions (T: 25ºC). Nowadays, this classification has been expanded and it includes a wide variety of oxidants, such as hydroperoxyl ($HOO^{\bullet}$), sulfate ($SO_4^{2-\bullet}$) and chlorine-based radicals ($Cl_2^{-\bullet}$, $Cl^{\bullet}$). These are very reactive and non-selective species, able to deplete organic matter at higher reaction rates than classical oxidants, such as Cl_2, H_2O_2, O_2, or even O_3. Table 1.2 collects the standard oxidation potential for all these oxidants.

Table 1.2. Standard electrode oxidation potentials [37-39]

Oxidant	E^0 (V)
F_2	+ 3.03
$HO^{\bullet}$	**+ 2.74**
$SO_4^{2-\bullet}$	+ 2.44
$Cl^{\bullet}$	+ 2.43
O	+ 2.42
$Cl_2^{-\bullet}$	+ 2.13
O_3	+ 2.08
H_2O_2	**+ 1.76**
$HOO^{\bullet}$	**+ 1.70**
HClO	+ 1.49
Cl_2	+ 1.36
O_2	+ 1.23

Despite the increasing interest in the action of sulfate and chlorine radicals [40-42], the salinity introduced to the bulk reaction by these AOPs may suppose an additional water pollution. Contrarily, the use of H_2O_2 as a $HO_X^{\bullet}$ promoter is more environmentally sustainable, as it decomposes towards H_2O and O_2. Hence, for the sake of concision, we will focus our attention in H_2O_2-based AOPs.

FENTON PROCESS

One of the most employed AOPs, due to the ease of operation and high catalyst availability is the Fenton process [43]. This redox reaction consists on the H_2O_2 decomposition towards hydroxyl and hydroperoxyl radicals ($HO_X^{\bullet}$) using iron salts in acidic media, as depicted in Figure 1.3 [44]. The key of this mechanism is the dual character of H_2O_2 as oxidant and reducer, which allows to regenerate the catalyst giving rise to hydroperoxyl radicals.

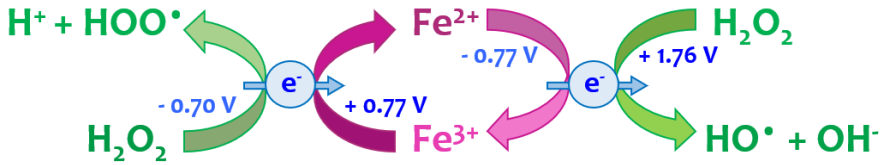

Figure 1.3. Fenton redox mechanism.

Besides iron, other metals, such as Ni, Cu, Au, Cr, etc., can also act as Fenton-like catalysts, carrying out the H_2O_2 reduction, as shown in Table 1.3, and have been successfully applied for water treatment [45]. However, these catalysts present either a higher price or toxicity than Fe. Therefore, their use is very limited.

Table 1.3. Standard reduction potentials for Fenton-like catalysts.

Redox pair	Semi-reaction	E^0 (V)
Cr^{3+}/Cr	$Cr^{3+} + 3e^- \rightleftarrows Cr$	- 0.74
Ni^{2+}/Ni	$Ni^{2+} + 2e^- \rightleftarrows Ni$	- 0.25
Cu^{2+}/Cu	$Cu^{2+} + 2e^- \rightleftarrows Cu$	+ 0.34
Hg^{2+}/Hg	$Hg^{2+} + 2e^- \rightleftarrows Hg$	+ 0.79
Ag^{+}/Ag	$Ag^{+} + e^- \rightleftarrows Ag$	+ 0.80
Au^{3+}/Au^{+}	$Au^{3+} + 3e^- \rightleftarrows Au$	+ 1.50

Fenton oxidation is usually carried out at ambient conditions (T: 25-40ºC and atmospheric pressure) and pH around 3, being especially sensitive to this parameter. At pH below 2.5, the efficiency of the treatment decreases due to a significant increase of the scavenging effect of $HO^{\bullet}$ radicals by H^+ [46]. This effect has been also observed at basic pH, in which the $HO^{\bullet}$ interact with hydroxyl ions giving rise to oxygen and water [47].

The main drawback presented by this homogeneous process is the catalyst loss as $Fe(OH)_3$ sludge, generated in the neutralization stage prior to the effluent discharge. This implies that the catalyst cannot be reused, with a continuous need of raw material, but also an extra charge associated to the sludge management and disposal. In order to overcome this issue, heterogeneous catalysts have been developed for heterogeneous Fenton or Catalytic Wet Peroxide Oxidation.

CATALYTIC WET PEROXIDE OXIDATION (CWPO)

The main challenge of heterogeneous catalysis is to obtain highly active and stable materials. Traditionally, CWPO catalysts have been synthesized placing a metallic active phase (Fe, Cu, Ni, Au, etc.) on the surface of a porous support, being the most employed carbon materials, clays, zeolites, alumina and silica [48-52]. These tailor-made catalysts have shown a great activity towards H_2O_2 decomposition and organic matter depletion. Still, most of them have very sophisticated synthesis procedures which increase their cost and limit their industrial application. On the search of inexpensive catalysts, there is an uprising trend on the use of iron bearing minerals as magnetite or hematite [53-55], or even iron mining residues [56, 57]. The main advantage of these materials is that, given their wide availability and low cost, their stability is not as decisive as for the traditional catalysts.

However, in the usual operating conditions at acidic pH, metal leaching can occur. Thus, the effluents are contaminated, and the catalyst activity is compromised. This drawback can be prevented employing metal-free catalysts. Carbon materials like activated carbon, graphite, carbon black and graphene, amongst others, have been widely studied for CWPO [58-61]. Despite presenting a lower activity in relation to traditional catalysts, their great stability makes them an interesting alternative. In order to boost the activity of these catalysts, AOP intensification has gained a great attention over the past decades.

1.1.1. Advanced Oxidation Processes intensification

Process intensification is defined as any chemical engineering development that leads to a substantially smaller, cleaner, safer, and more energy efficient technology [62]. Referred to AOP, intensification strategies are applied to either enhance the activity and overall performance of the process, or to enlarge the catalyst lifetime. Furthermore, it allows to expand the operating range, working at higher organic loads than those outlined in Figure 1.2. These technologies, depicted in Figure 1.4, can be classified in three main groups: electro-assisted, high-temperature and radiation-mediated processes.

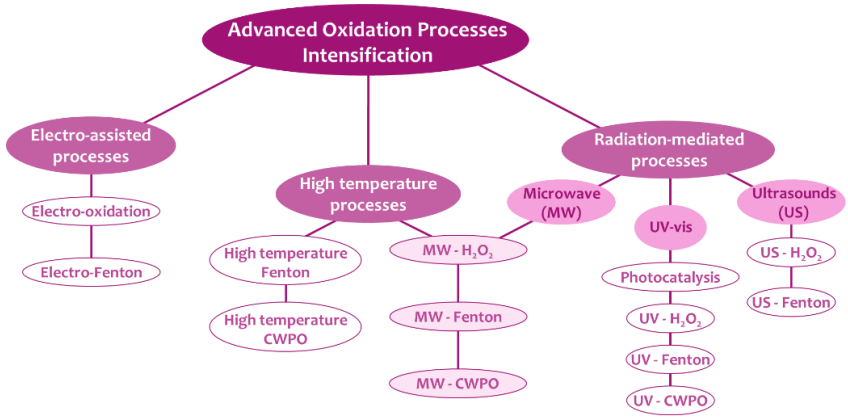

Figure 1.4. H_2O_2 AOP intensification strategies.

ELECTRO-ASSISTED PROCESSES

Electro-assisted processes can achieve pollutant oxidation by means of:

- Direct anodic oxidation, which implies pollutant degradation on the anode surface either by direct electron transfer or by chemical reaction with electrogenerated reactive oxygen species (ROS) produced as intermediates of oxidation of water to oxygen (physisorbed $HO^{\bullet}$) [63].
- Indirect oxidation, when strong oxidants are generated during the electro-treatment. For instance, chloride anodic oxidation gives rise to free chlorine and chlorine/oxygen species that can interact with the pollutants in the bulk reaction, giving rise to their partial or total oxidation [63, 64].

The efficiency of anodic electro-oxidation is highly dependent on the mass transfer of pollutants from the bulk to the anode surface or its vicinity. For these processes, the most common anodes are boron doped diamond (BDD), SnO_2 or PbO_2 [65-67].

The main disadvantage of these materials is their high cost in the case of BDD and the polluting potential for Pb and Sn anodes.

Electro-Fenton (EF) is an example of indirect oxidation in which $HO^{\bullet}$ radicals are formed by electro-generated H_2O_2 decomposition in presence of Fe^{2+} salts [68]. In this case, iron can be regenerated by cathodic reduction of Fe^{3+}. H_2O_2 is produced by the two-electron reduction of injected $O_{2(g)}$ (pure or from air) using a carbonaceous cathode with high surface area like carbon felt, reticulated vitreous carbon (RVC), carbon-polytetrafluoroethylene (PTFE) or even BDD, according to the following reaction (E° = 0.68 V):

$$O_{2\,(g)} + 2H^+ + 2e^- \rightarrow H_2O_2 \qquad \text{Eq. 1}$$

This technology, compared to the traditional Fenton, presents several advantages such as easy regulation of the on-site H_2O_2 production, higher degradation rate of pollutants due to the quicker regeneration of Fe^{2+} at the cathode and lower operating cost if experimental variables are optimized [63]. Nonetheless, iron sludge production is still present in EF.

HIGH TEMPERATURE PROCESSES

Against the general believe that high temperature processes would promote an inefficient H_2O_2 decomposition towards H_2O and O_2, several studies have successfully applied high temperature Fenton and CWPO processes for organic pollution removal. By increasing the temperature, H_2O_2 decomposition rate towards $HO_X^{\bullet}$ is greatly enhanced. Furthermore, these radicals react with the pollutants, rather than between themselves, avoiding the auto-scavenging reactions. Besides, some species, like oxalic acid, which can form iron complexes reducing the catalyst availability, are further oxidized when increasing the temperature over 90°C.

High temperature Fenton (HTF) has been applied in the range of 50-130ºC to different industrial effluents, including cosmetic, inks, sulfonation plant and power plant wastewaters [69-71]. In all cases, a high mineralization degree was reached (X_{TOC}>70%) with a high H_2O_2 consumption efficiency.

Ever since the development of HTF, process temperature in both Fenton and CWPO has been studied to enhance the mineralization rate and degree, especially when using non-traditional catalysts (minerals, iron tailings or metal-free catalysts) in order to boost their activity.

In this sense, Dominguez et al. have studied the application of activated carbon, graphite and carbon black in CWPO working at 80ºC for phenol degradation [60, 61]. Furthermore, they treated a high organic load wastewater from the winery industry using graphite as catalyst at 125ºC, achieving outstanding results with 80% TOC removal after 4h [72].

RADIATION-MEDIATED PROCESSES

Microwave-assisted processes fall between the high temperature and the radiation-mediated intensification strategies, as the bulk reaction is heated by means of microwave (MW) radiation. These technologies will be further discussed in Section 1.2.

UV-visible radiation has been widely applied for water treatment. Coupled to the Fenton process, UV radiation can enhance Fe^{2+} regeneration and carry on the photodecomposition of iron complexes formed on the oxidation processes, increasing the mineralization rate and degree [73].

Photocatalytic processes have also been widely developed during the past two decades. They are based on the use of a solid semiconductor or photocatalyst that, when irradiated with enough energy to overcome the bandgap, experiments an electron excitation from the valence band to the conduction band, generating an electron-hole pair. These species can migrate to the catalyst surface and take an active part in the redox cycle for radical generation and pollutant degradation, as depicted in Figure 1.5. The most popular photocatalyst

is TiO_2, which can be employed in a wide range of pH [74]. However, photocatalysis is a rather slow process and high intensity radiation is needed (UV-C) to activate TiO_2. To overcome this issue, UV-CWPO arises as a feasible technique, with higher mineralization rate and degree and lower electron-hole pair recombination. For this purpose, Fe-activated carbon and natural ilmenite have been successfully applied for water treatment under UV-A radiation [75, 76].

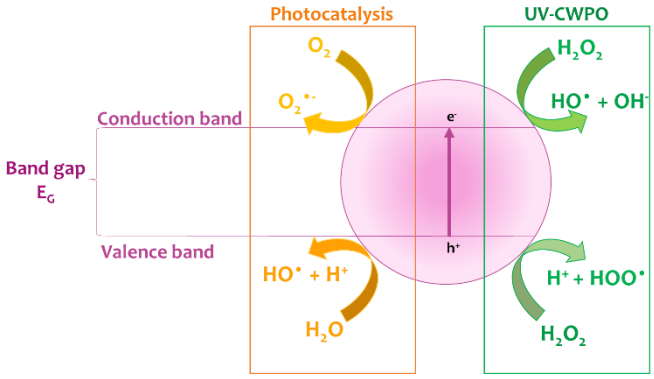

Figure 1.5. Photocatalysis and UV-CWPO mechanisms.

Ultrasound-assisted processes are based on the bulk sonication, which produces cavitation bubbles that generate local heating when collapsing. During acoustic cavitation, highly reactive hydrogen atoms (H•) and HO• radicals are generated [77]. When coupling US to the Fenton process, the overall pollutant degradation is increased due to the combined effects of contaminant sonolysis, Fenton reaction and HO• sono-generation [78].

1.2. Microwave-assisted processes

1.2.1. Microwave fundamentals

MW radiation lies between radio frequencies (RF) and infrared radiation (IR), at frequencies between 0.3-300 GHz. Nonetheless, commercial MW ovens usually operate at 2.45 GHz in order to avoid interferences with radar and telecommunication frequencies. The corresponding wavelength for these conventional devices, 12 cm, is not energetic enough to cause an interaction between MW and matter at either the atomic or molecular levels. [79, 80]. MW

heating has been widely extended since the invention of the domestic MW oven in 1950 [81]. Ever since, thanks to its quick heating, improved reaction rates, enhanced energy efficiency and reduced equipment size, this technology has been employed for a wide variety of applications in chemistry. These include sample pretreatments by means of MW digestion or ashing [82-84], polymerization [85, 86] and for both organic and inorganic synthesis [87-89], amongst others.

The main difference between conventional and MW heating is that the latter relies on the ability of the different substances to absorb MW energy, resulting in two basic mechanisms, dipole polarization and ionic conduction. In contrast, traditional heating depends on the thermal conductivity of a vessel with a higher temperature than its content. In consequence, the temperature profile is inverted with MW, as the increase of temperature builds up in the bulk, as shown in Figure 1.6.

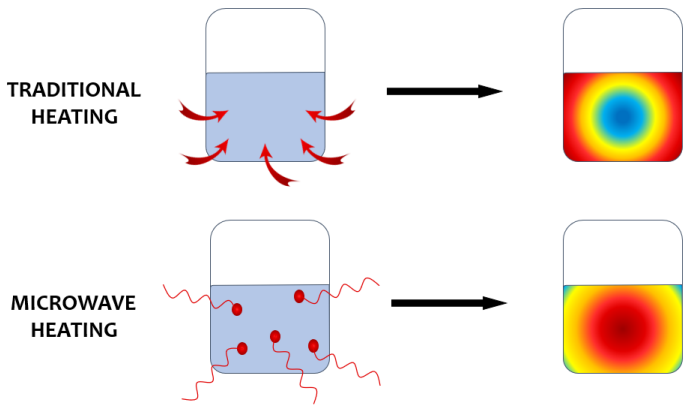

Figure 1.6. Heating mechanisms and temperature profiles in conventional and MW devices [79].

MW heating works at a molecular level, where the interaction of a certain material with an alternating electromagnetic field leads to its polarization. These interactions, which include electronic, dipolar, ionic and interfacial polarizations are dissipative, resulting in heat generation [90-92]. Figure 1.7 illustrates these polarization mechanisms.

- Electronic polarization takes place when the electrons are shifted under an electric field with respect to the positive nuclei, generating a nonzero dipole moment. In covalent solids, the electrons are easily moved and may follow the alternating field up to the frequencies of visible light.
- Ionic polarization occurs when there is a relative change of the barycenter of anions and cations from their equilibrium position in the lattice, for instance, in alkali halides. The ionic vibration depends on the thermal energy. Thus, their polarization is in phase with the alternating field and does not affect MW heating.
- Dipolar polarization results from intermolecular inertia, where the already existing dipoles tend to align towards the alternating electric field. In MW, the dipole rotation cannot adequately follow the rate of change in direction of the electric field. This leads to a phase difference, which is translated in dissipative interactions and, hence, in heat generation.
- Interfacial polarization occurs when free charges accumulate at the interfaces within a material. In this case, the applied electric field displaces mobile charges, which are accumulated in the discontinuous region, that is, the phase boundaries. This movement and charges occur at low frequencies, under the RF and MW region of the electromagnetic spectrum.

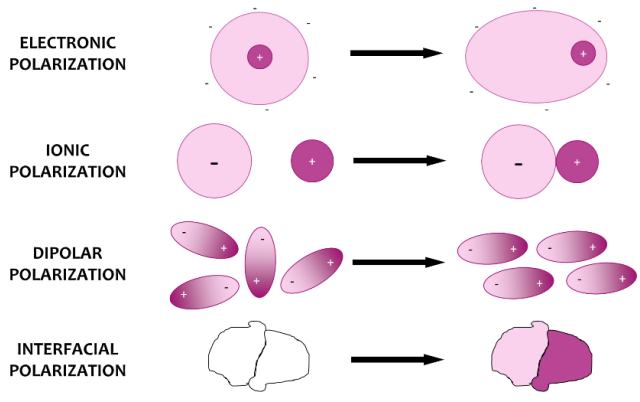

Figure 1.7. Polarization mechanisms [79].

In dielectric heat applications, the degree of interaction can be macroscopically described with the complex relative permittivity [93]. This is a measure of how an electric field affects a dielectric medium. It can be expressed as:

$$\varepsilon_d^* = \varepsilon' - j\varepsilon_d'' = \varepsilon_0(\varepsilon_r' - j\varepsilon_d'') \quad \text{Eq. 2}$$

Where:

$j = \sqrt{-1}$;

$\varepsilon_0 = 8.86 \cdot 10^{-12}$ F·m^{-1}, empty space permittivity;

ε_r': relative dielectric constant;

ε_d'': loss factor for dipolar loss mechanism.

When measuring the permittivity of a certain load is not practical, the effective loss factor, ε_{eff}'', is introduced:

$$\varepsilon^* = \varepsilon' - j\varepsilon_{eff}'' = \varepsilon' - j\left(\varepsilon_d'' + \frac{\sigma}{\omega\varepsilon_0}\right) \quad \text{Eq. 3}$$

Where:

σ: electrical conductivity

$\omega = 2\pi f$, and f is the frequency of the electromagnetic field.

Also, the dielectric properties of matter can be expressed in terms of the dielectric constant and another parameter, tan δ, the loss tangent, which is the ratio of the imaginary to the real part of the complex dielectric constant:

$$\tan\delta = \varepsilon_{eff}''/\varepsilon' \quad \text{Eq. 4}$$

This loss tangent allows to classify materials in relation to their behavior against MW, as depicted in Figure 1.8. Metals are opaque or MW reflectors, high tan δ are characteristic of MW absorbing materials, like distilled water (tan δ = 0.12) [94], whereas low values for tan δ correspond to transparent materials, as PTFE (tan δ = $2.48 \cdot 10^{-4}$) [95].

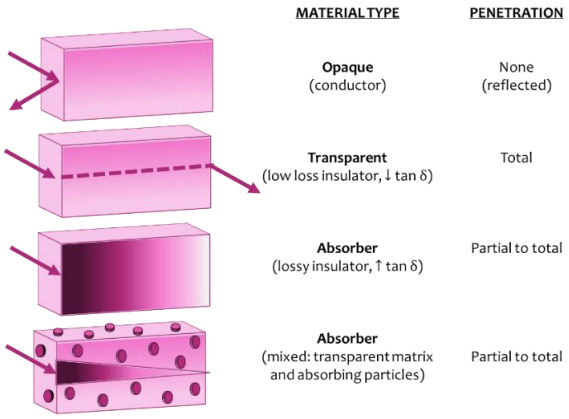

Figure 1.8. Material classification in relation to MW [96].

In general, when coupling MW to catalytic processes, the selectivity, conversion and reaction rate are greatly enhanced, shortening the reaction time and therefore, the operating costs. This improvement is mainly due to the selective heating and the non-thermal effects of MW heating, also known as **hot spots**.

In heterogeneous systems, when using materials with different dielectric properties, especially when heating MW absorbers, an uneven heating can occur, giving rise to hot spots [97]. These are micro plasma regions where the local temperature can rise above 1200ºC.

In heterogeneous catalytic reactions, if the support is a MW absorber, it will gain a higher temperature than the metallic phase, but due to heat transmission phenomena, the active phase will be heated, augmenting the reaction rate [98]. Hot spot formation can also take place when using metallic unsupported catalysts, but only if the particle diameter is in the nanometric range. When the reagents reach the hot spot, they react. Afterwards, they immediately migrate to a lower temperature region in the bulk reaction, avoiding secondary parasitic reactions. Thus, even though hot spots are undesired in fine chemicals synthesis, if controlled, they can be an interesting feature for certain MW applications.

1.2.2. Microwave assisted Advanced Oxidation Processes

Since 2000, there is an increasing scientific interest on MW-assisted processes for wastewater treatment, as may be seen in Figure 1.9. Various processes have been reported in literature, including induced-MW degradation, MW-H_2O_2, MW-Fenton and MW-CWPO.

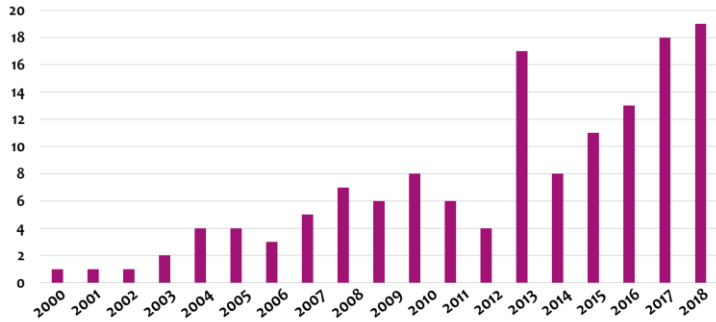

Figure1.9. Publication evolution on MW-assisted wastewater treatments. Source: Web of Knowledge.

INDUCED MW DEGRADATION

Induced-MW degradation of organic pollutants without oxidant addition employs solid metal oxides or metals supported on activated carbon, as collected in Table 1.4. The key to pollutant degradation in this kind of processes relies on hot spot formation, which can be produced on MW absorbers, but also in the surface of metallic nanoparticles. Shen et al. [99] described the degradation mechanism through $HO^{\bullet}$ generation from H_2O on the hot spots, in a similar way to that of photocatalysis.

Despite the high pollutant removal, there is not relevant information about catalyst stability. Furthermore, these studies lack of catalyst characterization after reaction to evaluate metal leaching and adsorption contribution to the overall contaminant depletion, which could be especially high when using AC as support.

Table 1.4. MW-induced degradation applications.

Catalyst	Pollutant	Operating conditions	Results	Remarks	Ref.
$NiFeO_4$/clay	Azo Fuchsine (AF)	$C_{AF,0}$: 10 mg·L^{-1}, C_{cat}: 3.2 g·L^{-1} t: 5 min, pH_0: 6 T: not reported, P: 750 W	X_{AF}: 98%	HO• generation upon hot spots	[99]
NiO_2	Crystal violet (CV)	$C_{CV,0}$: 100 mg·L^{-1}, C_{cat}: 0.8 g·L^{-1} t: 30 min, pH_0: 9 T: not reported, P: 750 W	X_{CV}: 97% X_{TOC}: 90%	Catalyst stability not tested	[100]
NiO_x	4-Nitrophenol (4-NP)	$C_{4\text{-}NP,0}$: 300 mg·L^{-1}, C_{cat}: 2 g·L^{-1} t: 10 min, pH_0:not reported T: 70°C, P: 7 W	$X_{4\text{-}NP}$: 92%	Catalyst stability is maintained over 5 cycles	[101]
$CoFe_2O_4$	Brilliant Green (BG)	$C_{BG,0}$: 20 mg·L^{-1}, C_{cat}: 1 g·L^{-1} t: 10 min, pH_0: 9 T: not reported, P: 900 W	X_{BG}: 95%	Second cycle X_{BG}: 20% Third cycle X_{BG}: 5%	[102]
Pt/AC	Pentachlorophenol (PCP)	$C_{PCP,0}$: 1,450 mg·L^{-1}, C_{cat}: 3 g t: 240 min, pH_0: not reported T: not reported, P: 400 W	X_{PCP}: 90% X_{TOC}: 71%	Fixed bed reactor Catalyst stability not tested	[103]
Cu/AC	*p*-nitrophenol (PNP)	$C_{PNP,0}$: 1,150 mg·L^{-1}, C_{cat}: 3 g t: 300 min, pH_0: not reported T: 150°C, P: 400 W	X_{PNP}: 92% X_{TOC}: 88%	Fixed bed reactor Catalyst stability not tested	[104]
Fe@Fe_2O_3/AC	Dimethyl phthalate (DMP)	$C_{DMP,0}$: 12 mg·L^{-1}, C_{cat}: 20 g·L^{-1} t: 8 min, pH_0: not reported T: 100°C, P_{MAX}: 400 W	X_{DMP}: 96% X_{TOC}: 91%	Catalyst stability not tested	[105]

MW-H_2O_2

MW radiation can generate HO• radicals by H_2O_2 homolytic rupture:

$$H_2O_2 \xrightarrow{MW} 2\,HO^{\bullet} \qquad \text{Eq. 5}$$

Nonetheless, there is a series of parasitic reactions (Eqs 6-8) which diminish the process efficiency.

$$HO^{\bullet} + H_2O_2 \rightarrow HOO^{\bullet} + H_2O \qquad \text{Eq. 6}$$

$$2\,HOO^{\bullet} \rightarrow H_2O_2 + O_2 \qquad \text{Eq. 7}$$

$$H_2O_2 \xrightarrow{\uparrow T} H_2O + \frac{1}{2}O_2 \qquad \text{Eq. 8}$$

Given the inefficient thermal decomposition of H_2O_2 in absence of a catalyst (Eq.8), high oxidant doses are required to achieve an almost complete pollutant removal, as seen in Table 1.5. It should be noted that despite the great amount of H_2O_2 employed, the reported mineralization degrees are very low. Thus, given the high expense in reagents and low efficiency, the MW-H_2O_2 process cannot be implemented for wastewater treatment.

Table 1.5. MW-H_2O_2 applications.

Pollutant	Operating conditions	Results	Ref.
Rhodamine B (RhB)	$C_{RhB,0}$: 300 mg·L^{-1}, C_{H2O2}: 16.6 g·L^{-1} t: 14 min, pH_0: 12 T: 100°C, P: not reported	X_{RhB}: 98% X_{COD}: 43%	[106]
Malachite green (MG)	$C_{MG,0}$: 100mg·L^{-1}, C_{H2O2}: 10.2 g·L^{-1} t: 5 min, pH_0: not reported T: 100°C, P: 900 W	X_{MG}: 95%	[107]
4-chlorophenol (4-CP)	$C_{4\text{-}CP,0}$: 1000 mg·L^{-1}, C_{H2O2}: 11 g·L^{-1} t: 10 min, pH_0: 6 T: 180°C, P: 400 W	$X_{4\text{-}CP}$: 64% X_{COD}: 26%	[108]
Nitrobenzene (NB)	$C_{NB,0}$: 0.3 mg·L^{-1}, C_{H2O2}: 20 mg·L^{-1} t: 35 min, pH_0: not reported T: 50°C, P: 300 W	X_{NB}: 90%	[109]

MW-FENTON

In order to enhance $HO^{\bullet}$ generation upon H_2O_2 decomposition, iron and other metallic cations have been employed in the MW-Fenton process (Table 1.6). Sanz et al. [110] performed the first experiments comparing high-temperature Fenton (HTF) and MW-Fenton simulating the temperature profile obtained in the MW. Results showed a 40% greater phenol degradation in the MW system. Nonetheless, H_2O_2 evolution, TOC and intermediates were not followed during reaction. Hence, despite having an evident enhancement on pollutant removal, there is no explanation to how MW radiation boosts the process.

Wang et al. [113] developed a pilot scale system using a 5.5 L PTFE tubular reactor in a custom-made MW furnace. A PID controlled the MW radiation to avoid $\Delta T>20^{o}C$ in the reactor. Under the selected conditions, with 12 min hydraulic retention time, 93.2% *p*-nitrophenol was eliminated. However, total Fe precipitation after 10 min reaction lead to an incomplete H_2O_2 decomposition (X_{H2O2}: 70%). Furthermore, there is no data on the mineralization degree.

There is a general lack of information on TOC or COD removal, except for the work of Li et al. [112], which compared the performance of Fe^{2+} and Mn^{2+} as catalysts in the MW-Fenton degradation of bisphenol A (BPA). Nonetheless, it should be noted that the reported mineralization achieved is way higher than that expected when using a 13% of the theoretical stoichiometric amount of H_2O_2 for complete BPA mineralization.

There are significant differences on the operating mode. Those whose temperature rose up to $100^{o}C$ [110, 111] work at fixed MW power using a condenser coupled to the reaction flask to avoid evaporation. On the other hand, experiments at fixed temperature [113, 114] usually work with intermittent MW radiation and air flow to chill the reaction vessel. Also, some authors do not specify the operating temperature of the system. Thus, it is really complicated to compare the results obtained by different research groups.

Table 1.6. MW-Fenton applications.

Catalyst	Pollutant	Operating conditions	Results	Remarks	Ref.
Fe^{2+}	Phenol (Ph)	$C_{Ph,0}$: 100 mg·L^{-1}, C_{cat}: 10 mg·L^{-1}, C_{H2O2}: 290 mg·L^{-1}, t: 60 min, pH_0: 3 T_{MAX}: 100ºC, P: 250 W	X_{Ph}: 99%	Comparison between HTF and MW-Fenton HTF, X_{Ph}:60%	[110]
Fe^{2+}	Amoxicillin (AMX)	$C_{AMX,0}$: 0.45 mg·L^{-1}, C_{cat}: 0.095 mg·L^{-1}, C_{H2O2}: 2.35 mg·L^{-1}, t: 5 min, pH_0: 3.5 T_{MAX}: 100ºC, P: 427 W	X_{AMX}: 100%	MW-Fenton is proposed to reduce Fe^{2+} in relation to UV-Fenton	[111]
Fe^{2+}	Methylene blue (MB)	$C_{MB,0}$: 50 mg·L^{-1}, C_{cat}: 20 mg·L^{-1}, C_{H2O2}: 200 mg·L^{-1}, t: 6 min, pH_0: 3 T: not reported, P: 700 W	X_{MB}: 95%	Ambient T Fenton, same conditions, t:70 min: X_{MB}: 92%	[112]
Fe^{2+}	*p*-nitrophenol (PNP)	$C_{PNP,0}$: 100 mg·L^{-1}, C_{cat}: 6.9 mg·L^{-1}, C_{H2O2}: 340 mg·L^{-1}, t: 15 min, pH_0: 3.3 T: 30ºC, P: 2000 W	X_{PNP}: 93.2% X_{H2O2}: 70%	Pilot scale 5.5 L PTFE reactor. Total Fe precipitation after 10 min.	[113]
Fe^{2+} + Cu^{2+}	3-nitroaniline (3NA)	$C_{3NA,0}$: 100 mg·L^{-1}, C_{Fe2+}: 11.3 mg·L^{-1}, C_{Cu2+}: 0.5 mg·L^{-1}, C_{H2O2}: 440 mg·L^{-1}, t: 8.5 min, pH_0: 5.3 T: 84ºC, P: 200 W	X_{3NA}: 92%	Temperature control with intermittent MW and air flow to chill	[114]
Fe^{2+} / Mn^{2+}	Bisphenol A (BPA)	$C_{BPA,0}$: 100 mg·L^{-1}, C_{cat}: 5.6 mg·L^{-1}, C_{H2O2}: 68 mg·L^{-1}, t: 6 min, pH_0: 4 T: not reported, P: 300 W	$\underline{Mn^{2+}}$: X_{BPA}: 99% X_{TOC}: 53% $\underline{Fe^{2+}}$: X_{BPA}: 59% X_{TOC}: 50%	Mn^{2+} showed a better performance than Fe^{2+}. X_{TOC} too high in relation to H_2O_2	[115]

MW-CWPO

A wide variety of catalysts have been used in MW-CWPO, including metal oxides, metal organic frameworks (MOF), supported metals and AC (Table 1.7).

In relation to the MW-induced process, Ahmed et al.[116] reported an increased oxidation rate of phenol when adding H_2O_2 to the system. Nevertheless, metal leaching was also enhanced, being this a key issue in MW-CWPO. Li et al. found a serious activity loss with Fe and Bi leaching up to 60 and 40 $mg \cdot L^{-1}$, respectively, when using $BiFeO_3$ nanoparticles in the MW-CWPO degradation of Rhodamine B [117]. These values are way above the discharge limit and compromise the feasibility of the process. To overcome this issue, they supported their metallic nanoparticles on reduced graphene oxide (rGO), which augmented notoriously their stability, with less than 0.1 $mg \cdot L^{-1}$ dissolved metal in the effluent [124].

Regarding the use of metal-free catalysts in MW-CWPO, there are few works in literature, and the existing ones do not consider the adsorption capacity of AC, which seems to be responsible for a great part of the pollutant removal [129, 130]. This happens as well for the traditional catalysts supported onto AC.

Most of the studies gathered in Table 1.7 attribute the high degradation rates to hot spot formation on the catalyst surface. Still, despite the numerous catalysts employed, there is no comparison between MW absorbers and transparent materials or between CWPO and MW-CWPO to measure the effect of hot spots on the depollution efficiency. Besides, there is little information on H_2O_2 decomposition and carbon balance along the reaction.

Similarly to MW-Fenton, the diverse operating conditions applied in each work makes difficult to compare the existing research and understand the intrinsic mechanisms of MW-CWPO. Thus, this thesis aims to gain depth into the MW hot spot effect in order to develop an efficient process. Furthermore, we seek for an active and stable metal-free catalyst.

Table 1.7. MW-CWPO applications.

Catalyst	Pollutant	Operating conditions	Results	Remarks	Ref.
$BiFeO_3$	Rhodamine B (RhB)	C_{RhB}: 30 mg·L^{-1}, C_{cat}: 1 g·L^{-1}, C_{H2O2}: 44 mg·L^{-1}, t: 6 min, pH_0: 4 T_{MAX}: 170-190ºC, P: 300 W	X_{RhB}: 94.8%	Fe $_{leaching}$: 60 mg·L^{-1} Bi $_{leaching}$: 40 mg·L^{-1}	[117]
$NiFeMnO_4$	Methyl Orange (MO)	$C_{MO,0}$: 30 mg·L^{-1}, C_{cat}: 1 g·L^{-1}, C_{H2O2}: 30 mg·L^{-1}, t: 6 min, pH_0: 2.5 T: 50ºC, P: 750 W	X_{MO}: 99%	Adsorption contribution X_{MO}:43%	[118]
Fe_3O_4 nanoparticles	Rhodamine B (RhB)	$C_{RhB,0}$: 100 mg·L^{-1}, C_{cat}: 1.25 g·L^{-1}, C_{H2O2}: 1650 mg·L^{-1}, t: 5 min, pH_0: 4 T: 80ºC, P: 300 W	X_{RhB}: 100%	Catalyst stability is maintained over 6 cycles	[119]
Fe ore tailings (66% Fe_2O_3)	Tri(2-chloroethyl) phosphate (TCEP)	$C_{TCEP,0}$: 10 mg·L^{-1}, C_{cat}: 0.25 g·L^{-1}, C_{H2O2}: 67 mg·L^{-1}, t: 35 min, pH_0: 3 T: not reported, P: 800 W	X_{TCEP}: 100% X_{TOC}: 98.8%	Catalyst stability is maintained over 8 cycles Adsorption contribution not reported	[120]
Fe_3O_4 (MOF)	Methyl Orange (MO)	$C_{MO,0}$: 100 mg·L^{-1}, C_{cat}: 0.4 g·L^{-1}, C_{H2O2}: 40 mg·L^{-1}, t: 6 min, pH_0: 3 T: not reported, P: 500 W	X_{MO}: 90%	Catalyst stability is maintained over 10 cycles	[121]
$CuNi/Al_2O_3/TiO_2$	Quinoline (Qui)	$C_{Qui,0}$: 100 mg·L^{-1}, C_{cat}: 4 g·L^{-1} C_{H2O2}: 775 mg·L^{-1}, t: 20 min, pH_0: 7 T: 60ºC, P: 500 W	X_{Quin}: 100% X_{TOC}: 81% X_{H2O2}: 70%	Cu $_{leaching}$: 71 µg·L^{-1} Ni $_{leaching}$: 23 µg·L^{-1}	[122]
CuO/Al_2O_3	*p*-nitrophenol (PNP)	$C_{PNP,0}$: 50 mg·L^{-1}, C_{cat}: 40 g·L^{-1}, C_{H2O2}: 850 mg·L^{-1}, t: 6 min, pH_0: 6 T: 70ºC, P: 100 W	X_{PNP}: 100%	Stability test: activity loss due to intermediates chemisorption	[123]

Table 1.7, continuation.

Catalyst	Pollutant	Operating conditions	Results	Remarks	Ref.
Pb-$BiFeO_3$/rGO	Perfluoroctanoic acid (PFOA)	$C_{PFOA,0}$: 50 mg·L^{-1}, C_{cat}: 1 g·L^{-1}, C_{H2O2}: 44 mg·L^{-1}, t: 5 min, pH_0: 5 T: not reported, P: 500 W	X_{PFOA}: 87% X_{TOC}: 52%	Metal $_{leaching}$ <0.1 mg·L^{-1} Adsorption contribution not reported	[124]
CuO-Co_3O_4/AC	Humic Acids (HA)	$C_{HA,0}$: 100 mg·L^{-1}, C_{cat}: 0.5 g·L^{-1}, C_{H2O2}: 315 mg·L^{-1}, t: 60 min, pH_0: 47 T: 80ºC, P: 800 W	X_{HA}: 90%	HCO_3^- and Cl^- ↓efficiency C_{cat}>0.5 g·L^{-1}, ↓efficiency Low HA adsorption	[125]
CuO_X/AC	Phenol (Ph)	$C_{Ph,0}$: 100 mg·L^{-1}, C_{cat}: 3 g·L^{-1}, C_{H2O2}: 600 mg·L^{-1}, t: 5 min, pH_0: 4 T: not reported, P: 400 W	X_{Ph}: 100% X_{COD}:90%	Cu $_{leaching}$: 21 mg·L^{-1} Adsorption, X_{COD}:21%	[126]
CuO/CeO/AC	Pharmaceutical wastewater	$C_{TOC,0}$: 155.9 mg·L^{-1}, C_{cat}: 40 g·L^{-1}, C_{H2O2}: 9900 mg·L^{-1}, t: 6 min, pH_0: 6.54 T: not reported, P: 400 W	X_{TOC}: 65%	↑C_{cat}, ↑X_{TOC}, adsorption. After 5th cycle ↓X_{TOC}	[127]
$CuFe_2O_4$/AC	Reactive yellow 3 (RY3)	$C_{RY3,0}$: 200 mg·L^{-1}, C_{cat}: 1 g·L^{-1} C_{H2O2}: 285 mg·L^{-1}, t: 5 min, pH_0: 6.5 T: not reported, P: 800 W	X_{RY3}: 75% X_{TOC}: 49%	Adsorption contribution X_{RY3}:30%	[128]
AC	Methyl Orange (MO)	$C_{MO,0}$: 50 mg·L^{-1}, C_{cat}: 0.2 g·L^{-1}, C_{H2O2}: 68 mg·L^{-1}, t: 10 min, pH_0: 2.5 T: 100ºC, P: 750 W	X_{MO}: 92%	Similar results with and without MW due to MO adsorption onto AC.	[129]
AC	Nitrobenzene (NB)	$C_{NB,0}$: 0.2 mg·L^{-1}, C_{cat}: 4 g·L^{-1}, C_{H2O2}: 10 mg·L^{-1}, t: 21 min, pH_0: 6.85 T: 60ºC, P: 300 W	X_{NB}: 72%	MW-AC system, in absence of H_2O_2 achieves X_{NB}:66%. Large adsorption contribution.	[130]

1.3. References

[1] UN, Water in a changing world: the United Nations world water development report 3, (2009).

[2] INE, Agua adquirida y suministrada a otras unidades por comunidad autónoma, tipos de usos y periodo, (2018).

[3] UN, Water in the 2030 Agenda for Sustainable Development, (2017).

[4] S. Alvarez-Torrellas, J.A. Peres, V. Gil-Alvarez, G. Ovejero, J. Garcia, Effective adsorption of non-biodegradable pharmaceuticals from hospital wastewater with different carbon materials, Chem. Eng. J. 320 (2017) 319-329.

[5] S. Alvarez-Torrellas, R.S. Ribeiro, H.T. Gomes, G. Ovejero, J. Garcia, Removal of antibiotic compounds by adsorption using glycerol-based carbon materials, Chem. Eng. J. 296 (2016) 277-288.

[6] M. Kraus, U. Trommler, F. Holzer, F.-D. Kopinke, U. Roland, Competing adsorption of toluene and water on various zeolites, Chem. Eng. J. 351 (2018) 356-363.

[7] J. Yang, M. Yang, H. Gui, G. Li, H. Wang, Dynamic and static adsorption of phosphate in water on the zirconium oxychloride modified zeolite, Desalin. Water Treat. 135 (2018) 408-417.

[8] E. Rosales, D. Anasie, M. Pazos, I. Lazar, M.A. Sanroman, Kaolinite adsorption-regeneration system for dyestuff treatment by Fenton based processes, Sci. Total Environ. 622 (2018) 556-562.

[9] J.-R. Li, L. Xu, M.-M. He, H. Xiao, Enhancement of Kaolin Adsorption Affinity Toward Phosphate by Sequestrating Naturally Abundant Ca/Mg From Seawater, Clean-Soil Air Water 46 (2018).

[10] B. Hatimi, H. Nasrellah, I. Yassine, M. Joudi, M.A. El Mhammedi, I.T. Lancar, M. Bakasse, Low cost MF ceramic support prepared from natural phosphate and titania: application for the filtration of Disperse Blue 79 azo dye solution, Desalin. Water Treat. 136 (2018) 433-440.

[11] I.G. Sandoval-Olvera, P. Gonzalez-Munoz, L. Palacio, A. Hernandez, M. Avila-Rodriguez, P. Pradanos, Ultrafiltration membranes modified by PSS deposition and plasma treatment for Cr(VI) removal, Sep. Purif. Technol. 210 (2019) 371-381.

[12] D. Zhou, G. Rong, S. Huang, J. Pang, Preparation of a novel sulfonated polyphenlene sulfone with flexible side chain for ultrafiltration membrane application, Sep. Purif. Technol. 210 (2019) 817-823.

[13] P. Ortiz-Albo, R. Ibanez, A. Urtiaga, I. Ortiz, Phenomenological prediction of desalination brines nanofiltration through the indirect determination of zeta potential, Sep. Purif. Technol. 210 (2019) 746-753.

[14] I. Owusu-Agyeman, M. Reinwald, A. Jeihanipour, A.I. Schafer, Removal of fluoride and natural organic matter from natural tropical brackish waters by nanofiltration/reverse osmosis with varying water chemistry, Chemosphere 217 (2019) 47-58.

[15] S.P. Azerrad, M. Isaacs, C.G. Dosoretz, Integrated treatment of reverse osmosis brines coupling electrocoagulation with advanced oxidation processes, Chem. Eng. J. 356 (2019) 771-780.

[16] R. Ibanez, A. Perez-Gonzalez, P. Gomez, A.M. Urtiaga, I. Ortiz, Acid and base recovery from softened reverse osmosis (RO) brines. Experimental assessment using model concentrates, Desalination 309 (2013) 165-170.

[17] C.-f. Xue, Y.-z. Liu, W.-z. Jiao, Mass transfer of acrylonitrile wastewater treatment by high gravity air stripping technology, Desalin. Water Treat. 57 (2016) 12424-12432.

[18] M.E. Abdullahi, M.A. Abu Hassan, Z.Z. Noor, R.K.R. Ibrahim, Temperature and air-water ratio influence on the air stripping of benzene, toluene and xylene, Desalin. Water Treat. 54 (2015) 2832-2839.

[19] Y. Sheng, X. Zhang, X. Zhai, F. Zhang, G. Li, D. Zhang, A mobile, modular and rapidly-acting treatment system for optimizing and improving the removal of

non-aqueous phase liquids (NAPLs) in groundwater, J. Hazard. Mater. 360 (2018) 639-650.

[20] A.V. Padalkar, R. Kumar, Removal mechanisms of volatile organic compounds (VOCs) from effluent of common effluent treatment plant (CETP), Chemosphere 199 (2018) 569-584.

[21] F.E. Hancock, Catalytic strategies for industrial water re-use, Catal. Today 53 (1999) 3-9.

[22] J. Nieto-Sandoval, M. Munoz, Z.M. de Pedro, J.A. Casas, Fast degradation of diclofenac by catalytic hydrodechlorination, Chemosphere 213 (2018) 141-148.

[23] M. Munoz, V. Kolb, A. Lamolda, Z.M. de Pedro, A. Modrow, B.J.M. Etzold, J.J. Rodriguez, J.A. Casas, Polymer-based spherical activated carbon as catalytic support for hydrodechlorination reactions, Appl. Catal. B-Environ. 218 (2017) 498-505.

[24] H. Wang, G.J. Xu, Z. Qiu, Y. Zhou, Y. Liu, NOB suppression in pilot-scale mainstream nitritation-denitritation system coupled with MBR for municipal wastewater treatment, Chemosphere 216 (2019) 633-639.

[25] M.J. Moya-Llamas, A. Trapote, D. Prats, Removal of micropollutants from urban wastewater using a UASB reactor coupled to a MBR at different organic loading rates, Urban Water J. 15 (2018) 437-444.

[26] V.M. Monsalvo, P. Shanmugam, N.J. Horan, Application of microbial indices to assess the performance of a sequencing batch reactor and membrane bioreactor treating municipal wastewater, Environ. Technol. 33 (2012) 2143-2148.

[27] M.M. Ren, S.Z. Wang, C. Yang, H.T. Xu, Y. Guo, D. Roekaerts, Supercritical water oxidation of quinoline with moderate preheat temperature and initial concentration, Fuel 236 (2019) 1408-1414.

[28] B.W. Yang, Z.W. Cheng, T. Yuan, X.P. Gao, Y.J. Tan, Y.N. Ma, Z.M. Shen, Temperature sensitivity of nitrogen-containing compounds decomposition

during supercritical water oxidation (SCWO), J. Taiwan Inst. Chem. Eng. 93 (2018) 31-41.

[29] B.W. Yang, Z.W. Cheng, M.H. Fan, J.P. Jia, T. Yuan, Z.M. Shen, Supercritical water oxidation of 2-, 3-and 4-nitroaniline: A study on nitrogen transformation mechanism, Chemosphere 205 (2018) 426-432.

[30] A. Sharma, A. Ghosh, R.A. Pandey, S.N. Mudliar, Wet Air Oxidation Pretreatment of Mixed Lignocellulosic Biomass to Enhance Enzymatic Convertibility, Korean Chem. Eng. Res. 53 (2015) 216-223.

[31] L.B. Zhou, H.B. Cao, C. Descorme, H. Zhao, Y.B. Xie, Wet air oxidation of indole, benzopyrazole, and benzotriazole: Effects of operating conditions and reaction mechanisms, Chem. Eng. J. 338 (2018) 496-503.

[32] A. Rodríguez, P. Letón, R. Rosal, M. Dorado, S. Villar, J.M. Sanz, Tratamientos avanzados de aguas residuales industriales. Informe de vigilancia tecnológica VT2., Madri+d 2006. www.madrimasd.org. (2009).

[33] D. Davies, S. Golunski, P. Johnston, G. Lalev, S.H. Taylor, Dominant Effect of Support Wettability on the Reaction Pathway for Catalytic Wet Air Oxidation over Pt and Ru Nanoparticle Catalysts, ACS Catal. 8 (2018) 2730-2734.

[34] A.E. de los Monteros, G. Lafaye, A. Cervantes, G. Del Angel, J. Barbier, G. Torres, Catalytic wet air oxidation of phenol over metal catalyst (Ru,Pt) supported on TiO2-CeO2 oxides, Catal. Today 258 (2015) 564-569.

[35] A. Quintanilla, J.A. Casas, A.F. Mohedano, J.J. Rodriguez, Reaction pathway of the catalytic wet air oxidation of phenol with a Fe/activated carbon catalyst, Appl. Catal. B-Environ. 67 (2006) 206-216.

[36] W.H. Glaze, J.W. Kang, Advanced Oxidation Processes for treating groundwater contaminated with TCE and PCE - laboratory studies, J. Am. Water Work Assoc. 80 (1988) 57-63.

[37] D.A. Armstrong, R.E. Huie, W.H. Koppenol, S.V. Lymar, G. Merenyi, P. Neta, B. Ruscic, D.M. Stanbury, S. Steenken, P. Wardman, Standard electrode potentials

involving radicals in aqueous solution: inorganic radicals (IUPAC Technical Report), Pure Appl. Chem. 87 (2015) 1139-1150.

[38] R. Munter, Advanced oxidation processes – current status and prospects, Proc. Estonian Acad. Sci. Chem. 50 (2001) 59-80.

[39] J. McCallum, Standard aqueous electrode potentials and temperature coefficients at 25 degrees, J. Chem. Educ. 42 (1965) A496-&.

[40] X.D. Duan, T. Sanan, A. de la Cruz, X.X. He, M.H. Kong, D.D. Dionysiou, Susceptibility of the Algal Toxin Microcystin-LR to UV/Chlorine Process: Comparison with Chlorination, Environ. Sci. Technol. 52 (2018) 8252-8262.

[41] J.E. Silveira, T.O. Cardoso, M. Barreto-Rodrigues, J.A. Zazo, J.A. Casas, Electro activation of persulfate using iron sheet as low-cost electrode: the role of the operating conditions, Environ. Technol. 39 (2018) 1208-1216.

[42] J.E. Silveira, A.L. Garcia-Costa, T.O. Cardoso, J.A. Zazo, J.A. Casas, Indirect decolorization of azo dye Disperse Blue 3 by electro-activated persulfate, Electrochim. Acta 258 (2017) 927-932.

[43] J.A. Zazo, J.A. Casas, C.B. Molina, A. Quintanilla, J.J. Rodriguez, Evolution of ecotoxicity upon Fenton's oxidation of phenol in water, Environ. Sci. Technol. 41 (2007) 7164-7170.

[44] H.J.H. Fenton, Oxidation of tartaric acid in presence of iron, J. Chem. Soc. Trans. 65 (1894) 899-910

[45] G.M.S. ElShafei, F.Z. Yehia, G. Eshaq, A.E. ElMetwally, Enhanced degradation of nonylphenol at neutral pH by ultrasonic assisted-heterogeneous Fenton using nano zero valent metals, Sep. Purif. Technol. 178 (2017) 122-129.

[46] W.Z. Tang, C.P. Huang, 2,4-dichlorophenol oxidation kinetics by Fenton's reagent, Environ. Technol. 17 (1996) 1371-1378.

[47] L. Szpyrkowicz, C. Juzzolino, S.N. Kaul, A comparative study on oxidation of disperse dyes by electrochemical process, ozone, hypochlorite and Fenton reagent, Water Res. 35 (2001) 2129-2136.

[48] C.M. Dominguez, A. Quintanilla, J.A. Casas, J.J. Rodriguez, Kinetics of wet peroxide oxidation of phenol with a gold/activated carbon catalyst, Chem. Eng. J. 253 (2014) 486-492.

[49] P. Bautista, A.F. Mohedano, J.A. Casas, J.A. Zazo, J.J. Rodriguez, Highly stable Fe/gamma-Al2O3 catalyst for catalytic wet peroxide oxidation, J. Chem. Technol. Biotechnol. 86 (2011) 497-504.

[50] E. Guelou, J.M. Tatibouet, J. Barrault, Fe-Al-Pillared Clays: Catalysts for Wet Peroxide Oxidation of Phenol, Springer, New York, 2010.

[51] K.M. Valkaj, A. Katovic, V. Tomasic, S. Zrncevic, Characterization and activity of Cu/ZSM5 catalysts for the oxidation of phenol with hydrogen peroxide, Chem. Eng. Technol. 31 (2008) 398-403.

[52] J.A. Zazo, J.A. Casas, A.F. Mohedano, J.J. Rodriguez, Catalytic wet peroxide oxidation of phenol with a Fe/active carbon catalyst, Appl. Catal. B-Environ. 65 (2006) 261-268.

[53] E. Serrano, M. Munoz, Z.M. De Pedro, J.A. Casas, Efficient removal of the pharmaceutical pollutants included in the EU Watch List (Decision 2015/495) by modified magnetite/H2O2, Chem. Eng. J. In press (2018).

[54] C. Pizarro, M. Escudey, M. Gacitua, J.D. Fabris, Iron-bearing minerals from soils developing on volcanic materials from Southern Chile: Application in heterogeneous catalysis, J. Soil Sci. Plant Nutr. 18 (2018) 668-693.

[55] M. Munoz, P. Dominguez, Z.M. de Pedro, J.A. Casas, J.J. Rodriguez, Naturally-occurring iron minerals as inexpensive catalysts for CWPO, Appl. Catal. B-Environ. 203 (2017) 166-173.

[56] T.D. Augusto, P. Chagas, D.L. Sangiorge, T.C.D. Mac Leod, L.C.A. Oliveira, C.S. de Castro, Iron ore tailings as catalysts for oxidation of the drug paracetamol and dyes by heterogeneous Fenton, J. Environ. Chem. Eng. 6 (2018) 6545-6553.

[57] F.F. Dias, A.A.S. Oliveira, A.P. Arcanjo, F.C.C. Moura, J.G.A. Pacheco, Residue-based iron catalyst for the degradation of textile dye via heterogeneous photo-Fenton, Appl. Catal. B-Environ. 186 (2016) 136-142.

[58] J.L.D. de Tuesta, A. Quintanilla, J.A. Casas, J.J. Rodriguez, P-, B- and N-doped carbon black for the catalytic wet peroxide oxidation of phenol: Activity, stability and kinetic studies, Catal. Commun. 102 (2017) 131-135.

[59] J.C. Espinosa, S. Navalon, A. Primo, M. Moral, J.F. Sanz, M. Alvaro, H. Garcia, Graphenes as Efficient Metal-Free Fenton Catalysts, Chem.-Eur. J. 21 (2015) 11966-11971.

[60] C.M. Dominguez, P. Ocon, A. Quintanilla, J.A. Casas, J.J. Rodriguez, Graphite and carbon black materials as catalysts for wet peroxide oxidation, Appl. Catal. B-Environ. 144 (2014) 599-606.

[61] C.M. Dominguez, P. Ocon, A. Quintanilla, J.A. Casas, J.J. Rodriguez, Highly efficient application of activated carbon as catalyst for wet peroxide oxidation, Appl. Catal. B-Environ. 140 (2013) 663-670.

[62] A.I. Stankiewicz, J.A. Moulijn, Process intensification: Transforming chemical engineering, Chem. Eng. Prog. 96 (2000) 22-34.

[63] E. Brillas, C.A. Martinez-Huitle, Decontamination of wastewaters containing synthetic organic dyes by electrochemical methods. An updated review, Appl. Catal. B-Environ. 166 (2015) 603-643.

[64] A. Anglada, A. Urtiaga, I. Ortiz, Contributions of electrochemical oxidation to waste-water treatment: fundamentals and review of applications, J. Chem. Technol. Biotechnol. 84 (2009) 1747-1755.

[65] L. Gherardini, C. Comninellis, N. Vatistas, Electrochemical oxidation of para-chlorophenol on Ti/SnO2-PbO2 electrodes: Introduction of a parameter for the estimation of their efficiency, Ann. Chim. 91 (2001) 161-168.

[66] I. Yahiaoui, F. Aissani-Benissad, F. Fourcade, A. Amrane, Removal of tetracycline hydrochloride from water based on direct anodic oxidation (Pb/PbO2 electrode) coupled to activated sludge culture, Chem. Eng. J. 221 (2013) 418-425.

[67] R.C. Burgos-Castillo, I. Sires, M. Sillanpaa, E. Brillas, Application of electrochemical advanced oxidation to bisphenol A degradation in water. Effect of sulfate and chloride ions, Chemosphere 194 (2018) 812-820.

[68] F.C. Moreira, R.A.R. Boaventura, E. Brillas, V.J.P. Vilar, Electrochemical advanced oxidation processes: A review on their application to synthetic and real wastewaters, Appl. Catal. B-Environ. 202 (2017) 217-261.

[69] G. Pliego, J.A. Zazo, S. Blasco, J.A. Casas, J.J. Rodriguez, Treatment of Highly Polluted Hazardous Industrial Wastewaters by Combined Coagulation-Adsorption and High-Temperature Fenton Oxidation, Ind. Eng. Chem. Res. 51 (2012) 2888-2896.

[70] G. Pliego, J.A. Zazo, J.A. Casas, J.J. Rodriguez, Case study of the application of Fenton process to highly polluted wastewater from power plant, J. Hazard. Mater. 252 (2013) 180-185.

[71] J.L. Diaz de Tuesta, C. Garcia-Figueruelo, A. Quintanilla, J.A. Casas, J.J. Rodriguez, Application of high-temperature Fenton oxidation for the treatment of sulfonation plant wastewater, J. Chem. Technol. Biotechnol. 90 (2015) 1839-1846.

[72] C.M. Dominguez, A. Quintanilla, J.A. Casas, J.J. Rodriguez, Treatment of real winery wastewater by wet oxidation at mild temperature, Sep. Purif. Technol. 129 (2014) 121-128.

[73] G. Pliego, P. Garcia-Munoz, J.A. Zazo, J.A. Casas, J.J. Rodriguez, Improving the Fenton process by visible LED irradiation, Environ. Sci. Pollut. Res. 23 (2016) 23449-23455.

[74] L.M. Pastrana-Martinez, S. Morales-Torres, S.A.C. Carabineiro, J.G. Buijnsters, J.L. Figueiredo, A.M.T. Silva, J.L. Faria, Photocatalytic activity of functionalized nanodiamond-TiO2 composites towards water pollutants degradation under UV/Vis irradiation, Appl. Surf. Sci. 458 (2018) 839-848.

[75] P. Garcia-Munoz, G. Pliego, J.A. Zazo, A. Bahamonde, J.A. Casas, Ilmenite (FeTiO3) as low cost catalyst for advanced oxidation processes, J. Environ. Chem. Eng. 4 (2016) 542-548.

[76] J.A. Zazo, G. Pliego, P. Garcia-Munoz, J.A. Casas, J.J. Rodriguez, UV-LED assisted catalytic wet peroxide oxidation with a Fe(II)-Fe(III)/activated carbon catalyst, Appl. Catal. B-Environ. 192 (2016) 350-356.

[77] S.G. Babu, M. Ashokkumar, B. Neppolian, The Role of Ultrasound on Advanced Oxidation Processes, Top. Curr. Chem. 374 (2016) 32.

[78] G. Harichandran, S. Prasad, SonoFenton degradation of an azo dye, Direct Red, Ultrason. Sonochem. 29 (2016) 178-185.

[79] G. Cravotto, D. Carnaroglio, Microwave Chemistry, De Gruyter (2017).

[80] N.N. Wang, P. Wang, Study and application status of microwave in organic wastewater treatment - A review, Chem. Eng. J. 283 (2016) 193-214.

[81] P.L. Spencer, Method of treating foodstuffs., US Patent 2495429A (1950).

[82] A.R. Zhang, H. Wang, P.F. Zha, M.L. Wang, H.F. Wang, B.Q. Fan, D.H. Ren, Y.X. Han, S.T. Gao, Microwave-induced combustion of graphene for further determination of elemental impurities using ICP-OES and TXRF, J. Anal. At. Spectrom. 33 (2018) 1910-1916.

[83] P.S. Barela, J.P. Souza, J.S.F. Pereira, J.C. Marques, E.I. Muller, D.P. Moraes, Development of a microwave-assisted ultraviolet digestion method for biodiesel and subsequent trace elements determination by SF-ICP-MS, J. Anal. At. Spectrom. 33 (2018) 1049-1056.

[84] M. Levi, C. Hjelm, F. Harari, M. Vahter, ICP-MS measurement of toxic and essential elements in human breast milk. A comparison of alkali dilution and acid digestion sample preparation methods, Clin. Biochem. 53 (2018) 81-87.

[85] R.M. Jiang, M.Y. Liu, H.Y. Huang, L. Huang, Q. Huang, Y.Q. Wen, Q.Y. Cao, J.W. Tian, X.Y. Zhang, Y. Wei, Microwave-assisted multicomponent tandem polymerization for rapid preparation of biodegradable fluorescent organic

nanoparticles with aggregation-induced emission feature and their biological imaging applications, Dyes Pigment. 149 (2018) 581-587.

[86] R. Wang, J.W. Ye, A. Rauf, X.M. Wu, H.X. Liu, G.L. Ning, H. Jiang, Microwave-induced synthesis of pyrophosphate Zr1-xTixP2O7 and TiP(2)O7 with enhanced sorption capacity for uranium (VI), J. Hazard. Mater. 315 (2016) 76-85.

[87] E. Burgaz, A. Erciyes, M. Andac, O. Andac, Synthesis and characterization of nano-sized metal organic framework-5 (MOF-5) by using consecutive combination of ultrasound and microwave irradiation methods, Inorg. Chim. Acta 485 (2019) 118-124.

[88] G.H. Elgemeie, R.A. Mohamed, Microwave synthesis of fluorescent and luminescent dyes (1990-2017), J. Mol. Struct. 1173 (2018) 707-742.

[89] E. Koyama, N. Ito, J. Sugiyama, J.P. Barham, Y. Norikane, R. Azumi, N. Ohneda, Y. Ohno, T. Yoshimura, H. Odajima, T. Okamoto, A continuous-flow resonator-type microwave reactor for high-efficiency organic synthesis and Claisen rearrangement as a model reaction, J. Flow Chem. 8 (2018) 147-156.

[90] P.P. Falciglia, P. Roccaro, L. Bonanno, G. De Guidi, F.G.A. Vagliasindi, S. Romano, A review on the microwave heating as a sustainable technique for environmental remediation/detoxification applications, Renew. Sust. Energ. Rev. 95 (2018) 147-170.

[91] H. Hidaka, A. Saitou, H. Honjou, K. Hosoda, M. Moriya, N. Serpone, Microwave-assisted dechlorination of polychlorobenzenes by hypophosphite anions in aqueous alkaline media in the presence of Pd-loaded active carbon, J. Hazard. Mater. 148 (2007) 22-28.

[92] U.M. Nascimento, E.B. Azevedo, Microwaves and their coupling to advanced oxidation processes: Enhanced performance in pollutants degradation, J. Environ. Sci. Health Part A-Toxic/Hazard. Subst. Environ. Eng. 48 (2013) 1056-1072.

[93] J.K.S. Wan, Microwaves and chemistry - the catalysis of an exciting marriage, Res. Chem. Intermed. 19 (1993) 147-158.

[94] O.P.N. Calla, S.K. Mishra, D. Bohra, N. Khandelwal, P. Kalla, C. Sharma, N. Gathania, N. Bohra, S. Shukla, Design a tunable cavity resonator for complex permittivity measurement of low-loss material at L band, Indian J. Pure Appl. Phys. 46 (2008) 134-138.

[95] N. Li, P. Wang, C. Zuo, H.L. Cao, Q.S. Liu, Microwave-Enhanced Fenton Process for DMSO-Containing Wastewater, Environ. Eng. Sci. 27 (2010) 271-280.

[96] N. Remya, J.G. Lin, Current status of microwave application in wastewater treatment-A review, Chem. Eng. J. 166 (2011) 797-813.

[97] J.A. Menendez, A.H. Moreno, Aplicaciones industriales del calentamiento con energía microondas, Editorial Universidad Técnica de Cotopaxi (2017) 315.

[98] V. Hessel, A. Anastasopoulou, Q. Wang, G. Kolb, J. Lang, Energy, catalyst and reactor considerations for (near)-industrial plasma processing and learning for nitrogen-fixation reactions, Catal. Today 211 (2013) 9-28.

[99] M.L. Shen, L. Fu, J.H. Tang, M.Y. Liu, Y.T. Song, F.Y. Tian, Z.G. Zhao, Z.H. Zhang, D.D. Dionysiou, Microwave hydrothermal-assisted preparation of novel spinel-NiFe2O4/natural mineral composites as microwave catalysts for degradation of aquatic organic pollutants, J. Hazard. Mater. 350 (2018) 1-9.

[100] H. He, S.G. Yang, K. Yu, Y.M. Ju, C. Sun, L.H. Wang, Microwave induced catalytic degradation of crystal violet in nano-nickel dioxide suspensions, J. Hazard. Mater. 173 (2010) 393-400.

[101] C.W. Tang, T.C. Liu, R.C. Wu, Y.Y. Shu, C.B. Wang, Efficient microwave enhanced degradation of 4-nitrophenol in water over coupled nickel oxide and solid acid catalysts, Sustain. Chem. Pharm. 8 (2018) 10-15.

[102] Y.M. Ju, X.Y. Wang, J.Q. Qiao, G.H. Li, Y. Wu, Y. Li, X.Y. Zhang, Z.C. Xu, J.Y. Qi, J.D. Fang, D.D. Dionysiou, Could microwave induced catalytic oxidation (MICO)

process over CoFe2O4 effectively eliminate brilliant green in aqueous solution?, J. Hazard. Mater. 263 (2013) 600-609.

[103] L.L. Bo, X. Quan, X.C. Wang, S. Chen, Preparation and characteristics of carbon-supported platinum catalyst and its application in the removal of phenolic pollutants in aqueous solution by microwave-assisted catalytic oxidation, J. Hazard. Mater. 157 (2008) 179-186.

[104] L.L. Bo, Y.B. Zhang, X. Quan, B. Zhao, Microwave assisted catalytic oxidation of p-nitrophenol in aqueous solution using carbon-supported copper catalyst, J. Hazard. Mater. 153 (2008) 1201-1206.

[105] Y.L. Chen, Z.H. Ai, L.Z. Zhang, Enhanced decomposition of dimethyl phthalate via molecular oxygen activated by Fe@Fe2O3/AC under microwave irradiation, J. Hazard. Mater. 235 (2012) 92-100.

[106] J. Hong, N.N. Yuan, Y.X. Wang, S.H. Qi, Efficient degradation of Rhodamine B in microwave-H2O2 system at alkaline pH, Chem. Eng. J. 191 (2012) 364-368.

[107] Y.M. Ju, S.G. Yang, Y.C. Ding, C. Sun, C.G. Gu, Z. He, C. Qin, H. He, B. Xu, Microwave-enhanced H2O2-based process for treating aqueous malachite green solutions: Intermediates and degradation mechanism, J. Hazard. Mater. 171 (2009) 123-132.

[108] H. Milh, K. Van Eyck, R. Dewil, Degradation of 4-Chlorophenol by Microwave-Enhanced Advanced Oxidation Processes: Kinetics and Influential Process Parameters, Water 10 (2018) 12.

[109] H.H. Zeng, L.J. Lu, M.N. Liang, J. Liu, Y.H. Li, Degradation of trace nitrobenzene in water by microwave-enhanced H2O2-based process, Front. Env. Sci. Eng. 6 (2012) 477-483.

[110] J. Sanz, J.I. Lombrana, A.M. De Luis, M. Ortueta, F. Varona, Microwave and Fenton's reagent oxidation of wastewater, Environ. Chem. Lett. 1 (2003) 45-50.

[111] V. Homem, A. Alves, L. Santos, Microwave-assisted Fenton's oxidation of amoxicillin, Chem. Eng. J. 220 (2013) 35-44.

[112] S.T. Liu, J. Huang, Y. Ye, A.B. Zhang, L. Pan, X.G. Chen, Microwave enhanced Fenton process for the removal of methylene blue from aqueous solution, Chem. Eng. J. 215 (2013) 586-590.

[113] N.N. Wang, T. Zheng, J.P. Jiang, W.S. Lung, X.J. Miao, P. Wang, Pilot-scale treatment of p-Nitrophenol wastewater by microwave-enhanced Fenton oxidation process: Effects of system parameters and kinetics study, Chem. Eng. J. 239 (2014) 351-359.

[114] N.N. Wang, T. Zheng, J.P. Jiang, P. Wang, Cu(II)-Fe(II)-H2O2 oxidative removal of 3-nitroaniline in water under microwave irradiation, Chem. Eng. J. 260 (2015) 386-392.

[115] S. Li, G.S. Zhang, P. Wang, H.S. Zheng, Y.J. Zheng, Microwave-enhanced Mn-Fenton process for the removal of BPA in water, Chem. Eng. J. 294 (2016) 371-379.

[116] A.B. Ahmed, B. Jibril, S. Danwittayakul, J. Dutta, Microwave-enhanced degradation of phenol over Ni-loaded ZnO nanorods catalyst, Appl. Catal. B-Environ. 156 (2014) 456-465.

[117] S. Li, G.S. Zhang, H.S. Zheng, N.N. Wang, Y.J. Zheng, P. Wang, Microwave-assisted synthesis of BiFeO3 nanoparticles with high catalytic performance in microwave-enhanced Fenton-like process, RSC Adv. 6 (2016) 82439-82446.

[118] Y.L. Lei, X.Y. Lin, H.W. Liao, New insights on microwave induced rapid degradation of methyl orange based on the joint reaction with acceleration effect between electron hopping and Fe2+-H2O2 reaction of NiFeMnO4 nanocomposites, Sep. Purif. Technol. 192 (2018) 220-229.

[119] P. Yan, L.B. Gao, W.T. Li, Microwave-Enhanced Fenton-Like System, Fe3O4/H2O2 for Rhodamine B Wastewater Degradation, Applied Mechanics and Materials 448-453 (2014) 834-837.

[120] L.Z. Du, X.L. Wang, J.F. Wu, Degradation of tri(2-chloroethyl)phosphate by a microwave enhanced heterogeneous Fenton process using iron oxide containing waste, RSC Adv. 8 (2018) 18139-18145.

[121] S.E. Moradi, S. Dadfarnia, A.M.H. Shabani, S. Emami, Microwave-enhanced Fenton-like degradation by surface-modified metal-organic frameworks as a promising method for removal of dye from aqueous samples, Turk. J. Chem. 41 (2017) 426-439.

[122] B. Zhang, H. You, Z.Z. Yang, F. Wang, A highly active bimetallic oxide catalyst supported on gamma-Al2O3/TiO2 for catalytic wet peroxide oxidation of quinoline solutions under microwave irradiation, RSC Adv. 6 (2016) 66027-66036.

[123] W.Q. Pan, G.S. Zhang, T. Zheng, P. Wang, Degradation of p-nitrophenol using CuO/Al2O3 as a Fenton-like catalyst under microwave irradiation, RSC Adv. 5 (2015) 27043-27051.

[124] S. Li, G.S. Zhang, W. Zhang, H.S. Zheng, W.Y. Zhu, N. Sun, Y.J. Zheng, P. Wang, Microwave enhanced Fenton-like process for degradation of perfluorooctanoic acid (PFOA) using Pb-BiFeO3/rGO as heterogeneous catalyst, Chem. Eng. J. 326 (2017) 756-764.

[125] X.S. Yao, Q.T. Lin, L.Z. Zeng, J.X. Xiang, G.C. Yin, Q.J. Liu, Degradation of humic acid using hydrogen peroxide activated by CuO-Co3O4@AC under microwave irradiation, Chem. Eng. J. 330 (2017) 783-791.

[126] Z.L. Liu, H.L. Meng, H. Zhang, J.S. Cao, K. Zhou, J.J. Lian, Highly efficient degradation of phenol wastewater by microwave induced H2O2-CuOx/GAC catalytic oxidation process, Sep. Purif. Technol. 193 (2018) 49-57.

[127] X.D. Qi, Z.H. Li, Efficiency Optimization of Pharmaceutical Wastewater Treatment by a Microwave-Assisted Fenton-Like Process Using Special Supported Catalysts, Pol. J. Environ. Stud. 25 (2016) 1205-1214.

[128] J. Xiao, X. Fang, S.G. Yang, H. He, C. Sun, Microwave-assisted heterogeneous catalytic oxidation of high-concentration Reactive yellow 3 with CuFe2O4/PAC, J. Chem. Technol. Biotechnol. 90 (2015) 1861-1868.

[129] A. Veksha, P. Pandya, J.M. Hill, The removal of methyl orange from aqueous solution by biochar and activated carbon under microwave irradiation and in the presence of hydrogen peroxide, J. Environ. Chem. Eng. 3 (2015) 1452-1458.

[130] D.N. Tani, H.H. Zeng, J. Liu, X.Z. Yu, Y.P. Liang, L.J. Lu, Degradation kinetics and mechanism of trace nitrobenzene by granular activated carbon enhanced microwave/hydrogen peroxide system, J. Environ. Sci. 25 (2013) 1492-1499.

2. AIM AND SCOPUS

The main objective of this Thesis is the study and development of an active and cost-efficient microwave-assisted advanced oxidation process for wastewater treatment.

High-temperature AOPs have shown to be effective in wastewater treatment, with enhanced reaction rates and higher removal of recalcitrant species. Besides, as described in literature, the use of MW radiation as heating source seems to enhance these processes by the unique feature of MW non-thermal effects, or hot spots, which are punctual zones of high temperature generated due to MW selective absorption phenomena. Thus, different iron catalysts and metal-free materials will be evaluated in the microwave-assisted catalytic wet peroxide oxidation (MW-CWPO) of synthetic wastewaters containing as target pollutants phenol, benzene, toluene, xylene and naphthalene, as representative and widely studied pollutants present in chemical industry wastewaters.

Iron and other transition metals are commonly used as catalytic active phase in this kind of technologies. Nonetheless, the usual operating conditions, which imply an acidic pH, lead to metal lixiviation resulting in activity loss, low stability and additional water pollution. In order to overcome these problems, different carbonaceous materials will be used as a metal-free, non-expensive and efficient alternative to the traditional catalysts.

In the first stages of investigation, MW-CWPO will be studied at constant temperature to compare its effect in relation to the non-assisted process and to evaluate the contribution of the non-thermal effects. Furthermore, two different materials will be used as catalytic support for iron oxides, a transparent material (γ-Al_2O_3) and a MW-absorbing material (activated carbon). Both supported catalysts have been widely employed for CWPO. Afterwards, different materials without metals, as carbon materials, will be employed. Attending to the results, once selected an optimum reactive catalyst, the process will be optimized in terms of efficiency and energy consumption.

In order to determine which catalyst is the most suitable for this process, we will focus our attention in the following issues:

i. Catalytic activity in terms of H_2O_2 consumption and pollutant depletion, considering both pollutant adsorption and the oxidation reactions until complete mineralization.
ii. H_2O_2 efficiency, measured as the ratio between the depleted organic matter (TOC) and the amount of employed H_2O_2.
iii. Oxidation pathway, paying special attention to the reaction byproducts, in particular condensed oligomers which are known to interfere with the catalytic activity and stability in traditional CWPO.
iv. Catalyst stability and reusability.

For the consecution of the main objective, the Thesis has been divided in four different tasks, which have led to the publication of four articles which analyze:

1. Influence of the non-thermal effects and dielectric properties of catalytic supports on MW-CWPO.
2. Use of activated carbon as metal-free catalyst in the MW-CWPO degradation of petrochemical pollutants.
3. Activity and stability of commercial carbon materials in MW-CWPO of phenol.
4. Energy optimization.

3. ABSTRACT / RESUMEN

ABSTRACT

Catalytic decomposition of hydrogen peroxide to generate hydroxyl ($HO^{\bullet}$) and hydroperoxyl ($HOO^{\bullet}$) radicals is a well-known process (CWPO) for wastewater treatment. Nowadays, the research is focused on the intensification of this technology, aiming to reach higher reaction rates and efficiencies to treat polluted effluents. Against the general belief that H_2O_2 thermal decomposition towards water and oxygen prevails over the catalytic redox cycle of CWPO, previous research within our group demonstrated that increasing the temperature (T: 90-130ºC), the $HO_X^{\bullet}$ generation rate was greatly enhanced. Moreover, these radicals were efficiently employed, reacting at a higher rate with the pollutants than between themselves. Hence, the auto-scavenging reactions were minimized, favoring the oxidation process with high Total Organic Carbon (TOC) and H_2O_2 conversions.

Based in these results, this doctoral Thesis explores the use of various heating techniques, comparing the traditional conduction/convection mechanism with a different heating system based in the dipolar rotation caused by microwaves (MW). Besides a quick and homogeneous heating, MW can generate local overheated regions, also known as hot spots, that may favor the H_2O_2 decomposition and pollutant degradation, achieving a further intensification of CWPO.

The first work of this Thesis, published in Applied Catalysis B, explores the application of microwaves with a double aim, to intensify the CWPO process by increasing the temperature but also to analyze the interaction of MW with Fe catalysts supported onto alumina (Fe/Al_2O_3) and activated carbon (Fe/AC). CWPO runs at 120ºC were performed with and without MW to study the heating rate and oxidation mechanism. We found significant differences in the H_2O_2 decomposition rate and mineralization degree between the traditional and MW-assisted systems, as may be seen in Figure 3.1.

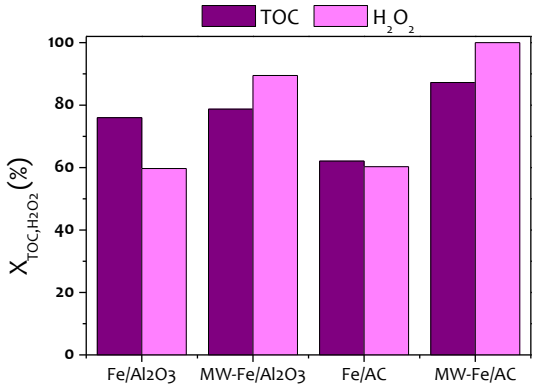

Figure 3.1. Comparison between Fe/AC and Fe/Al_2O_3 in CWPO and MW-CWPO of phenol. $C_{Phenol,0}$: 100 mg·L^{-1}, $C_{Catalyst}$: 100 mg·L^{-1}, $C_{H2O2,0}$: 500 mg·L^{-1}, T: 120ºC, pH_0:3, t:60 min

H_2O_2 decomposition rate increased for both MW systems due to the MW-mediated H_2O_2 homolytic rupture in conjunction with the H_2O_2 redox catalytic decomposition. In these conditions, a very high TOC conversion was observed, faster than conventional thermal CWPO. This effect depends strongly on the type of catalyst employed. When using Al_2O_3 as support, there was a minimal difference between the CWPO and the MW-CWPO processes. On the other hand, MW radiation greatly boosted the Fe/AC activity, increasing TOC removal around 25% in relation to the non-assisted process. This was ascribed to the action of hot spots generated on the surface of AC, which is a **MW absorber**. The mechanisms for H_2O_2 decomposition are outlined in Figure 3.2, in which the green arrows correspond to the CWPO redox cycle and the pink arrows to the MW-mediated reactions.

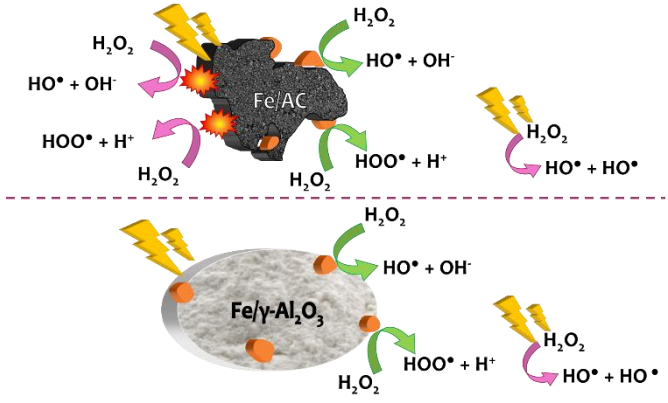

Figure 3.2. H_2O_2 decomposition over Fe/AC and Fe/Al_2O_3 catalysts in MW-CWPO.

Based on these results, the degradation pathway for phenol was also analyzed, also finding a great impact of MW radiation. In the MW-Fe/AC process, the aromatic ring opening was very fast. This favored a lower generation of condensation byproducts (CBP) and their complete elimination from the aqueous phase. These CBP are unidentified oligomeric compounds, reported by several authors in phenol and other aromatics oxidation. The results for Fe/Al_2O_3 were very different. In this case, we observed a very high formation of condensed byproducts, along with a change in the catalyst color. Thus, hot spot formation on the catalyst surface seems to have an important contribution to CBP breakdown, resulting in two degradation pathways depending on the catalytic support, as shown in Figure 3.3.

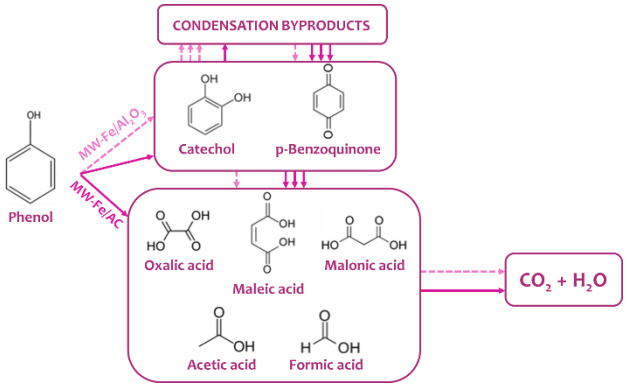

Figure 3.3. Phenol degradation pathway for MW-Fe/Al_2O_3 and MW-Fe/AC

In order to obtain more information on hot spot formation, we performed new MW experiments, comparing the previous results with a no-catalyst run (MW-H_2O_2) and the bare supports as catalysts (Figure 3.4). We could observe that there is practically no difference between the MW-H_2O_2 and MW-Al_2O_3 experiments. This seemed logical, as alumina is a **MW transparent** material. Furthermore, AC presented a similar activity to Fe/AC under MW radiation, with complete H_2O_2 decomposition and a superior TOC conversion than Fe/Al_2O_3.

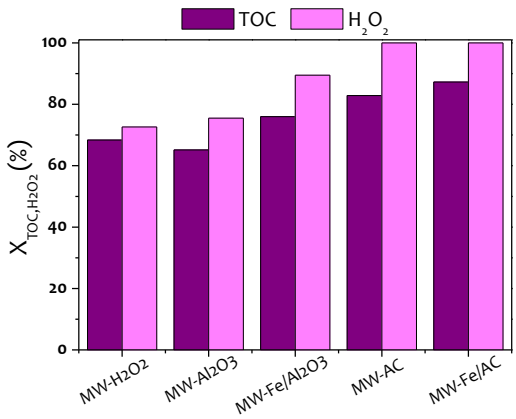

Figure 3.4. MW-CWPO in absence of catalyst (MW-H_2O_2), with bare supports and Fe catalysts.

As main conclusion, we observed that the dielectric properties of the catalyst play a key role in the MW-CWPO process, presenting MW absorbers a greater activity towards phenol mineralization. The full published article is included in Appendix 5.1.

After studying the hot spot generation on the AC surface and its effect on H_2O_2 decomposition and degradation pathway of aromatic compounds, we realized that this MW-assisted technology was the perfect set-up to work on metal-free catalysis using carbon materials. Therefore, we optimized the operating conditions of the MW-AC process (pH, temperature, catalyst load and reaction time) and started a new work using synthetic wastewaters containing benzene (B), toluene (T), o-xylene (X) or naphthalene (N) as representative pollutants from the petrochemical industry. This led to the second article of this Thesis, published in the Environmental Science and Pollution Research as part of a special issue from the 2nd Summer School of the European PhD School on AOPs.

In the selected operating conditions, complete pollutant removal was achieved in 15 minutes. Nonetheless, the quick BTXN and TOC initial decay signaled the presence of two steps in the reaction. First, there is a rapid pollutant adsorption onto AC followed by its oxidation by MW-CWPO. H_2O_2 evolution followed a similar trend, with a noticeable decomposition slowdown after 3 min. However, TOC removal was significantly faster than the H_2O_2 consumption, as may be seen

in Figure 3.5. Working at the stoichiometric dose of H_2O_2, the ideal behavior of the system would follow the diagonal, in which each fraction of decomposed H_2O_2 would efficiently mineralize the same fraction of TOC. Our experiments were way above this situation, confirming the high contribution of contaminant or intermediates adsorption onto the catalyst.

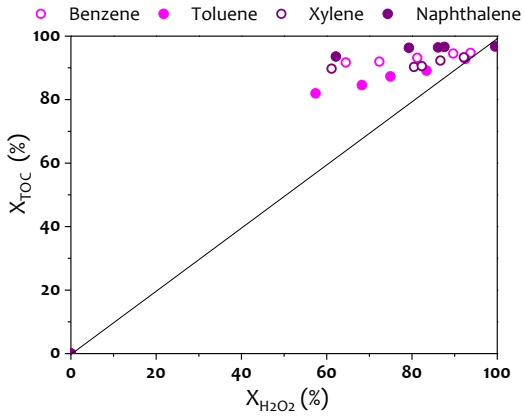

Figure 3.5. H_2O_2 efficiency in MW-CWPO of BTNX. $C_{B,T,X,0}$: 100 mg·L^{-1}, $C_{N,0}$: 30 mg·L^{-1}, C_{AC}: 1 g·L^{-1}, $C_{H2O2,0}$: stoichiometric, pH_0: 3, t_r: 15 min.

Intermediates analyses only showed short chain acids and traces of phenol in the case of benzene oxidation, but no other aromatic intermediates or CBP were detected in the aqueous phase. Thus, we believe that these species may remain adsorbed onto the AC and were not be fully oxidized in the selected operating conditions.

TGA analyses of the AC after reaction confirmed our theory and allowed us to perform an estimation on the carbon balance, as depicted in Figure 3.6. This carbon balance has been performed assuming a similar carbon content in the adsorbed species (aromatics and CBP) in relation to the starting pollutants. The results are given as C in gas phase (CO_2), C adsorbed on AC and C in the liquid phase (TOC). The mineralization degree of the starting pollutant varies from 70% in the case of B to only 30% for N.

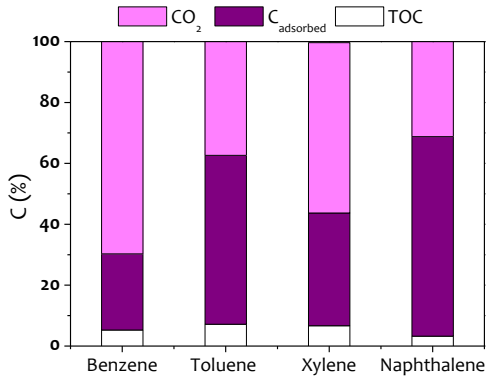

Figure 3.6. Carbon balance after 15 min.

To sum things up, the results showed that despite having a total benzene, toluene, xylene and naphthalene removal from the aqueous phase, an important fraction of the pollutants and reaction intermediates remained adsorbed onto the AC, following the reaction a two-step mechanism with an initial adsorption followed by H_2O_2 catalyzed oxidation, as shown in Figure 3.7. This article on aromatic hydrocarbons oxidation can be found in Appendix 5.2.

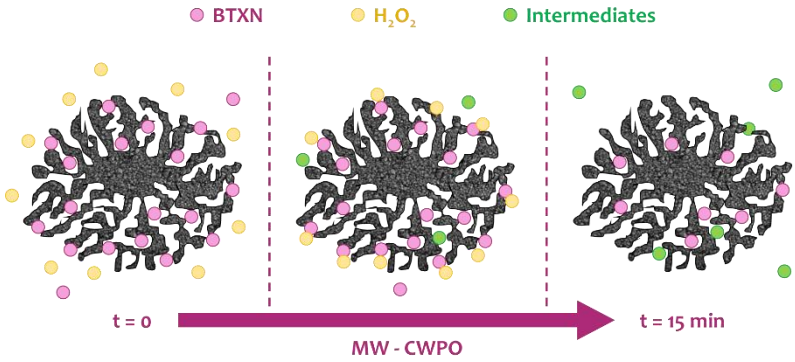

Figure 3.7. MW-CWPO reaction mechanism for BTXN working at: $C_{B,T,X,0}$: 100 mg·L^{-1}, $C_{N,0}$: 30 mg·L^{-1}, C_{AC}: 1 g·L^{-1}, $C_{H2O2,0}$: stoichiometric, pH_0: 3, t_r: 15 min.

In the third work, we focused our attention on the effect of the carbon nature in the catalytic process. For this purpose, different carbon materials were selected: activated carbons (AC), graphites (G), carbon blacks (CB) and silicon carbide (SiC). All of them were tested in phenol degradation. Mineralization degree and H_2O_2 decomposition for these materials can be found in Figure 3.8. Analyzing the results, we could corroborate that carbon materials are active in MW-CWPO,

thanks to both their MW-absorbing and redox properties, generating $HO_X^{\bullet}$ at a high rate. Nonetheless, the activity of carbon blacks was very limited in relation to other materials. Moreover, we observed that the surface chemistry plays an essential role in phenol degradation, especially for graphite, augmenting the mineralization and H_2O_2 decomposition twofold when using a **graphite (G-S)**, which presents an acid behavior.

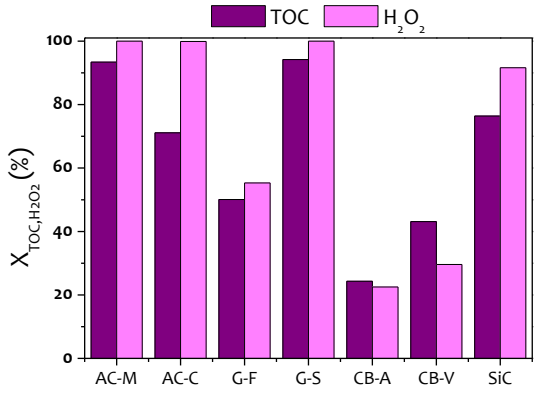

Figure 3.8. Activity of carbon materials in MW-CWPO of phenol.
$C_{Phenol,0}$: 100 mg·L^{-1}, $C_{Catalyst}$: 500 mg·L^{-1}, $C_{H2O2,0}$: 500 mg·L^{-1}, T: 120ºC, pH_0:3, t:60 min

The most active materials (AC-M and G-S) were used in 5 consecutive cycles in order to test their stability. TOC removal results are shown in Figure 3.9. As may be seen, G-S maintained its activity, with TOC removal above 90% for all runs. On the contrary, AC-M suffered a progressive deactivation due to the loss of its textural properties.

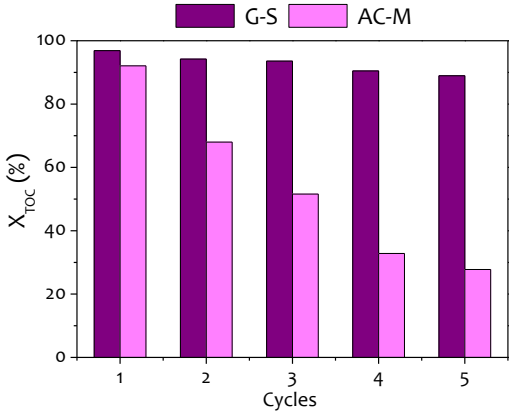

Figure 3.9. G-S and AC-M stability upon 5 cycles of MW-CWPO.

This different behavior between catalysts was related to their structure and, especially to the effect of hot spots. AC is a porous material, when hot spots are generated inside the micropores, confined vapor is generated. Pression builds up in these points and the catalysts crumbles in the so-called **popcorn effect**. This micro-explosion collapses the catalyst structure and results in a progressive catalyst deactivation, transforming AC into a very fine powder, difficult to separate from the treated effluent. On the other hand, graphite, which is a layered ordered material, can dissipate the heat generated in the hot spots more easily, maintaining its structure and catalytic activity intact. These phenomena are outlined in Figure 3.10.

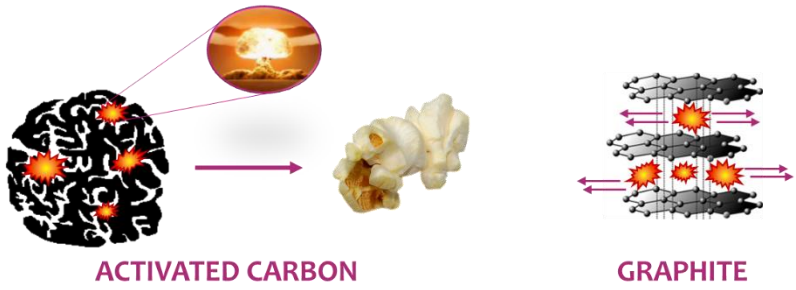

Figure 3.10. Hot-spot formation and catalysts structure.

Results for activity and stability of carbon materials in MW-CWPO were published in the Separation and Purification Technology journal, as the third work of this Thesis, which can be found in Appendix 5.3.

Once obtained an active and stable catalyst, we could propose a MW-intensified CWPO process, but first we had to launch an economical study in order to optimize the MW radiation usage. This was the aim of the fourth work included in this doctoral Thesis, in which we compared the usual operating modes found in literature, fixed MW power and fixed temperature. The latter, which was the one employed in our previous studies, means that we set the MW to heat our samples from room temperature to 120ºC in 90 seconds, concentrating the MW radiation at 1800 W in that short period of time. Afterwards the reactor is radiated to maintain the temperature, but at a much lower power. The MW-CWPO process is efficient because of hot spot formation and hot spots are

related to MW radiation. Thus, it seemed we were not taking full advantage of MW radiation working at controlled temperature. In order to test this theory and aiming to optimize the energy consumption, we set up different runs working at fixed temperature, fixed continuous MW power and fixed pulsated MW power. Results are collected in Figure 3.11.

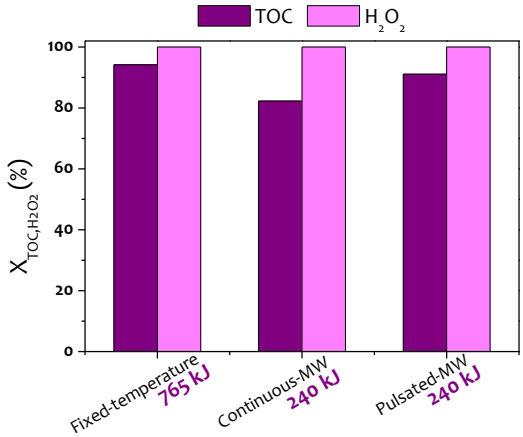

Figure 3.11. Radiation influence on MW-CWPO.
$C_{Phenol,0}$: 100 mg·L^{-1}, $C_{G\text{-}S}$: 500 mg·L^{-1}, $C_{H2O2,0}$: 500 mg·L^{-1}, pH$_0$:3.

We could observe that the radiation mode also plays a key role in MW-CWPO. **MW pulsation** reached a higher mineralization degree and better H_2O_2 exploitation than the continuous MW thanks to the relaxation periods, where the heat generated by the hot spots could be dissipated.

Analyzing the system's requirements, energy consumption was reduced to one third in relation to the controlled-temperature run. Additionally, the energy consumption per TOC mass at the end of reaction (EC_{TOC}) was significantly lower compared to other intensified AOPs, as depicted in Figure 3.12. Thus, MW-CWPO is a feasible cost-efficient alternative.

In this work we also studied the kinetic model, fining that it follows a pseudo-second order for TOC and a pseudo-first order in the case of H_2O_2. Activation energy for both reactions, H_2O_2 decomposition and TOC removal, were calculated. $E_{A,\,TOC}$ was significantly lower than that reported in literature for phenol degradation by CWPO. On the other hand, $E_{A,\,H2O2}$ presented similar values than those previously reported. Thus, hot spot formation has a greater

influence on organic pollutants depletion rather than H_2O_2 decomposition. The full article, published in the Separation and Purification Technology journal, is included in Appendix 5.4.

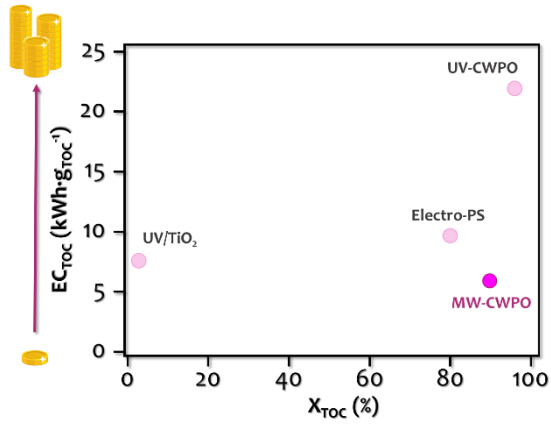

Figure 3.12. Cost-efficiency relation for different intensified AOPs.

In short, this dissertation shows that the use of MW substantially improves the well-known CWPO process in which H_2O_2 is used as $HO_X^{\bullet}$ promoter. MW-absorption can generate hot spots on the surface of carbon materials. When these are of graphitic nature, the heat excess produced in these areas can be dissipated without losing their mechanical properties. Furthermore, the nature of its surface plays an important role, similar to that of hot spots formation. Finally, the operation mode concerning MW-radiation has also a major impact on the promotion of hot spots and, therefore, on the catalytic activity.

RESUMEN

La descomposición catalítica de peróxido de hidrógeno para generar radicales hidroxilo ($HO^{\bullet}$) e hidroperoxilo ($HOO^{\bullet}$) es un proceso conocido (CWPO) para el tratamiento de aguas residuales. Actualmente la investigación se centra en la intensificación de esta tecnología, con el fin de alcanzar un aumento en la velocidad de reacción y en su rendimiento para tratar efluentes contaminados. Tradicionalmente se ha venido pensando que el aumento de la temperatura en este tipo de procesos favorece la descomposición térmica del H_2O_2 en agua y oxígeno. Sin embargo, trabajos previos del grupo de investigación han demostrado que el aumento de la temperatura entre 90-130ºC conlleva un aumento en la velocidad de producción de radicales $HO_X^{\bullet}$. Se puso de manifiesto la eficiencia de este tipo de intensificación, ya que los radicales reaccionan más rápido con los contaminantes que entre ellos, minimizando las reacciones de autosecuestro, favoreciendo el proceso de oxidación y, por lo tanto, el tratamiento del agua.

En base a estos resultados, la presente Tesis doctoral estudia el uso de diferentes técnicas de calentamiento, comparando el sistema tradicional basado en mecanismos de conducción/convección con un nuevo sistema basado en la rotación de dipolos por acción de microondas (MW). Además de un calentamiento rápido y homogéneo, los MW pueden dar lugar a regiones localizadas de sobrecalentamiento, también conocidas como puntos calientes, que pueden favorecer la descomposición del peróxido y la degradación de contaminantes, logrando una intensificación adicional del proceso CWPO.

El primer trabajo de esta Tesis, publicado en *Applied Catalysis B*, estudia la aplicación de microondas con un doble propósito, intensificar el proceso CWPO mediante el aumento de la temperatura y analizar la interacción de las MW con catalizadores de Fe soportados en alúmina (Fe/Al_2O_3) y sobre carbón activado (Fe/CA). Estos experimentos se hicieron a temperatura constante (120ºC) con y sin microondas (MW), para estudiar la velocidad de calentamiento y el mecanismo de oxidación. Encontramos diferencias significativas en el consumo

de H_2O_2 y el grado de mineralización entre el proceso tradicional y el asistido por MW, como se puede observar en la Figura 3.1.

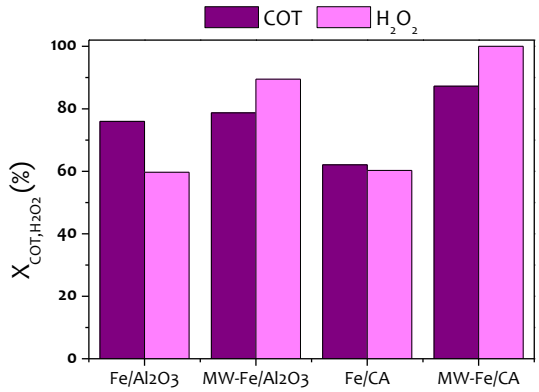

Figura 3.1. Comparativa entre Fe/CA y Fe/Al_2O_3 en CWPO y MW-CWPO de fenol. $C_{Fenol,0}$: 100 mg·L^{-1}, $C_{Catalizador}$: 100 mg·L^{-1}, $C_{H2O2,0}$: 500 mg·L^{-1}, T: 120ºC, pH_0:3, t:60 min

La velocidad de descomposición de H_2O_2 aumentó significativamente en ambos sistemas. Esto se debe a que, además del ciclo redox de descomposición de peróxido del CWPO, se produce la ruptura homolítica del H_2O_2 por acción de las microondas. En estas condiciones se alcanzó una alta conversión del Carbono Orgánico Total (COT), más rápida que la del proceso CWPO convencional. Este efecto se ve fuertemente influenciado por el tipo de catalizador utilizado. Cuando se empleó Al_2O_3 como soporte, la diferencia entre los procesos CWPO y MW-CWPO fue mínima. Sin embargo, la radiación MW potenció notablemente la actividad del Fe/AC, aumentando el grado de mineralización en torno a un 25% en relación al proceso no irradiado. Esto se debe al efecto de los puntos calientes generados en la superficie del CA, que es un material **absorbedor de MW**. Los mecanismos descritos para descomposición de H_2O_2 con ambos catalizadores está esquematizado en la Figura 3.2, en la que las flechas verdes corresponden al ciclo redox del CWPO y las flechas rosas a las reacciones mediadas por MW.

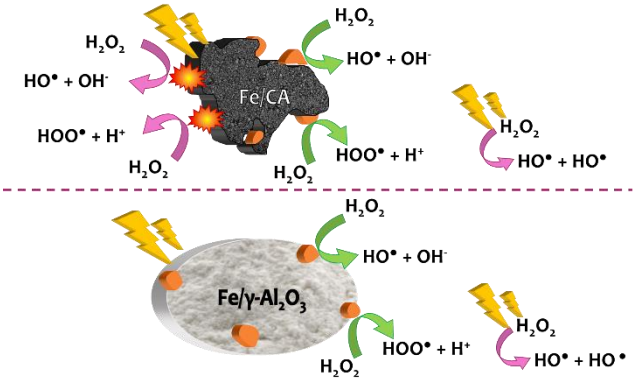

Figura 3.2. Descomposición de H_2O_2 sobre catalizadores Fe/CA y Fe/Al_2O_3 en MW-CWPO.

En base a estos resultados, también se analizó la ruta de degradación del fenol, encontrando una gran influencia de la radiación MW. En el proceso MW-Fe/CA, la apertura del anillo aromático fue muy rápida. Esto favorece una menor generación de subproductos de condensación (CBP) y su completa eliminación en fase acuosa. Estos CBP son oligómeros no identificados, descritos en bibliografía en la oxidación de fenol y otros compuestos aromáticos. Los resultados con Fe/Al_2O_3 fueron muy diferentes. En este caso se observó una producción muy alta de CBP, además del cambio de color en el catalizador. Por tanto, la formación de puntos calientes en la superficie del catalizador parece tener una contribución importante en la degradación de los CBP. De esta forma, se describieron dos rutas de degradación en base al catalizador empleado, como se muestra en la Figura 3.3.

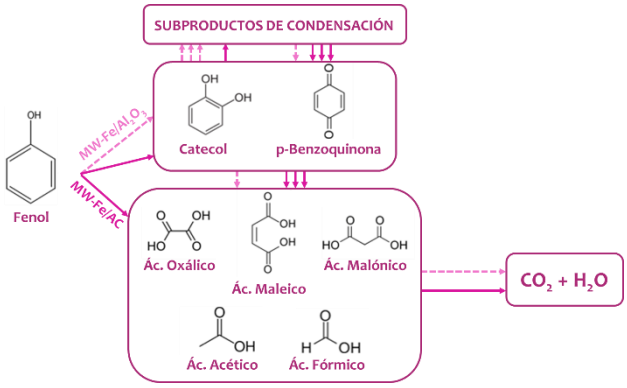

Figura 3.3. Ruta de degradación del fenol en los sistemas MW-Fe/Al_2O_3 y MW-Fe/AC.

Para obtener más información sobre la generación de puntos calientes, realizamos nuevos experimentos, comparando los resultados obtenidos con un ensayo en ausencia de catalizador (MW-H_2O_2) y los soportes por sí mismos, como se recoge en la Figura 3.4. Pudimos observar que prácticamente no había diferencia entre los procesos MW-H_2O_2 y MW-Al_2O_3. Esto parece lógico, ya que la alúmina es un **material transparente** a las microondas. Por otra parte, el CA presentó una actividad catalítica similar al Fe/CA bajo radiación MW, con una completa descomposición de H_2O_2 y una mineralización superior a la alcanzada con el catalizador Fe/Al_2O_3.

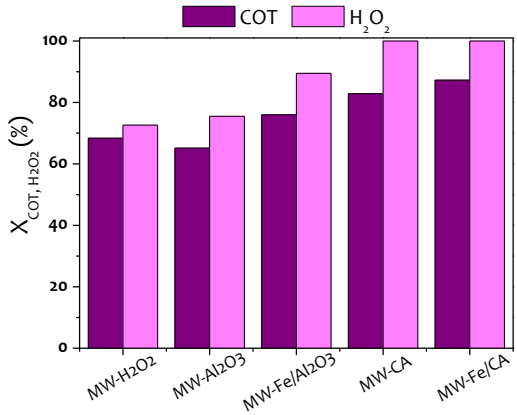

Figura 3.4. Proceso MW-CWPO en ausencia de catalizador (MW-H_2O_2) y con catalizadores con y sin Fe.

Como conclusión principal, observamos que las propiedades dieléctricas del catalizador tienen un rol clave en el proceso MW-CWPO, presentando los materiales absorbedores de MW una actividad significativamente mayor en la mineralización de fenol. El artículo completo se encuentra en el Apéndice 5.1. del presente documento.

Después de estudiar la generación de puntos calientes en la superficie del CA y su efecto en la descomposición de H_2O_2 y ruta de degradación de compuestos aromáticos, vimos la oportunidad de aplicar la tecnología MW con catalizadores libres de metales. Para ello optimizamos las condiciones de operación del proceso MW-CA (pH, temperatura, carga de catalizador y tiempo de reacción) y empezamos un nuevo trabajo utilizando aguas sintéticas con benceno (B),

tolueno (T), o-xyleno (X) y naftaleno (N), como contaminantes representativos de la industria petroquímica. Esto llevó a la publicación del segundo artículo de la Tesis, publicado en la revista *Environmental Science and Pollution Research* como parte de un número especial derivado de la 2ª escuela de verano de la Escuela Europea de doctorado en AOPs.

En las condiciones de operación ensayadas, se alcanzó la completa eliminación de los contaminantes en 15 minutos. No obstante, la rápida caída inicial de BTXN y COT indicaba la presencia de dos etapas en la reacción. Primero se da una rápida adsorción de los contaminantes en la superficie del CA, seguida por su oxidación mediante MW-CWPO. La descomposición de H_2O_2 siguió una tendencia similar, con un descenso notable en la velocidad de reacción tras los primeros 3 minutos. No obstante, la eliminación de COT fue significativamente más rápida que el consumo de peróxido, como se puede apreciar en la Figura 3.5. Trabajando con la dosis estequiométrica de H_2O_2 para cada contaminante, el comportamiento ideal del sistema sería el marcado por la diagonal, en la que cada fracción de H_2O_2 consumido es empleada en la mineralización de la misma cantidad de COT. Nuestros experimentos se sitúan muy por encima de esta diagonal, confirmando una alta contribución de la adsorción del contaminante sobre el catalizador.

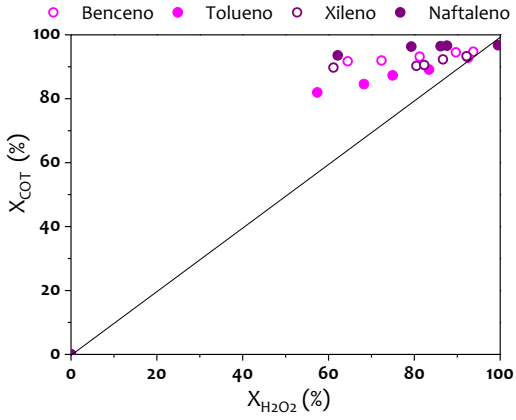

Figura 3.5. Eficiencia de consumo de H_2O_2 en MW-CWPO de BTNX. $C_{B,\,T,\,X,\,0}$: 100 mg·L^{-1}, $C_{N,0}$: 30 mg·L^{-1}, C_{CA}: 1 g·L^{-1}, $C_{H2O2,0}$: estequiométrica, pH_0: 3, t_r: 15 min.

En el análisis de intermedios solo se detectaron ácidos de cadena corta y trazas de fenol en el caso de la oxidación de benceno. Sin embargo, no se detectaron otros compuestos aromáticos ni CBP en la fase acuosa. Por tanto, pensamos que estas especies quedaron retenidas sobre el catalizador y no fueron completamente oxidadas en las condiciones de operación ensayadas.

Análisis termogravimétricos (TGA) del catalizador después de reacción confirmaron esta teoría y nos permitieron estimar el balance de carbono, como se muestra en la Figura 3.6. Este balance de carbono se realizó asumiendo un contenido en C similar en las especies adsorbidas en relación con los contaminantes de partida. Los resultados se muestran como C en la fase gas (CO_2), C adsorbido en el CA y C en fase acuosa (COT). Se puede observar que el grado de mineralización varía en función del contaminante, desde el 70% para benceno, hasta tan solo un 30% en el caso del naftaleno.

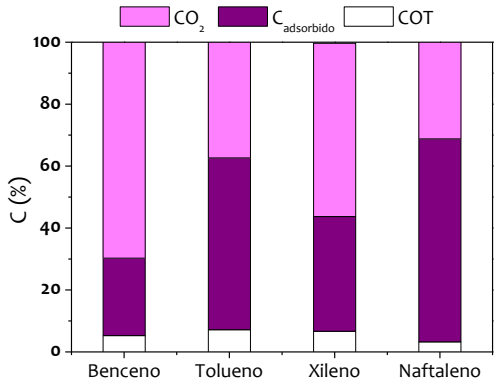

Figura 3.6. Balance de C tras 15 min.

En resumen, los resultados mostraron que, pese a lograr una completa eliminación de BTXN en la fase acuosa, una fracción importante de los mismos permanece adsorbida en el CA. La reacción sigue un mecanismo en dos etapas con una rápida adsorción inicial, seguida por la oxidación catalítica, tal y como se muestra de forma esquematizada en la Figura 3.7. El artículo completo sobre oxidación de hidrocarburos aromáticos mediante MW-CWPO se encuentra en el Apéndice 5.2 de la presente Tesis doctoral.

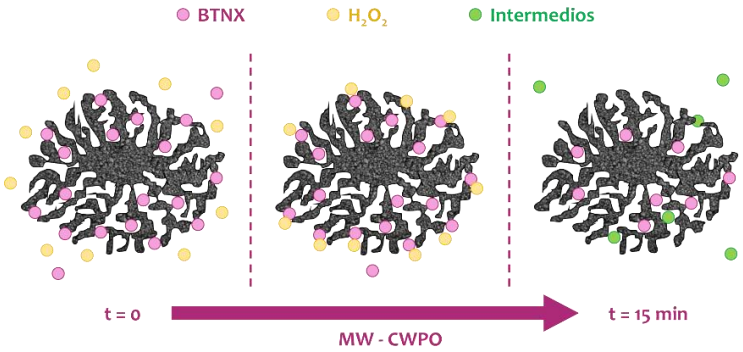

Figura 3.7. Mecanismo de reacción en MW-CWPO de BTXN a: $C_{B,T,X,0}$: 100 mg·L^{-1}, $C_{N,0}$: 30 mg·L^{-1}, C_{CA}: 1 g·L^{-1}, $C_{H2O2,0}$: estequiométrica, pH_0: 3, t_r: 15 min.

En el tercer trabajo, centramos nuestra atención en el efecto de la naturaleza de los materiales carbonosos en el proceso catalítico. Para ello, seleccionamos diferentes materiales: carbones activados (CA), grafitos (G), negros de humo (NH) y carburo de silicio (SiC). Todos ellos fueron probados en la degradación de fenol. La Figura 3.8. recoge los resultados de COT y H_2O_2, que confirman que los materiales carbonosos son activos en MW-CWPO, gracias a la combinación de sus propiedades de absorción de MW y sus propiedades redox, que permiten la generación de $HO_X^{\bullet}$ a gran velocidad. No obstante, la actividad de los NH es muy limitada en comparación con el resto de materiales. Además, observamos que la química superficial tiene un papel muy importante el proceso, especialmente en el caso del grafito, aumentando la actividad el doble cuando se emplea un **grafito** de carácter ácido, el **G-S**.

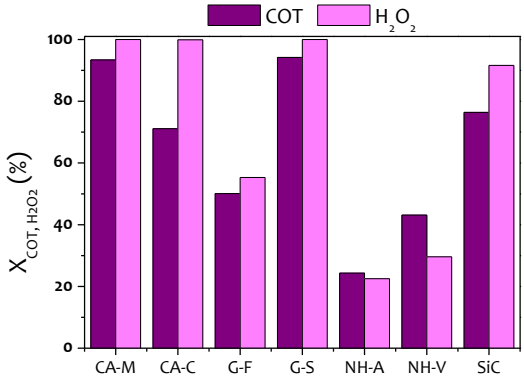

Figura 3.8. Actividad de materiales carbonosos en MW-CWPO de fenol. $C_{Fenol,0}$: 100 mg·L^{-1}, $C_{Catalizador}$: 500 mg·L^{-1}, $C_{H2O2,0}$: 500 mg·L^{-1}, T: 120ºC, pH_0:3, t:60 min

Los materiales más activos (CA-M y G-S) fueron sometidos a 5 ciclos consecutivos de reacción para probar su estabilidad. La conversión de COT se muestra en la Figura 3.9. Como se puede observar, el G-S mantuvo su actividad, con una mineralización superior al 90% en todos los ensayos. Por el contrario, el CA-M sufrió una desactivación progresiva debido a la pérdida de sus propiedades texturales.

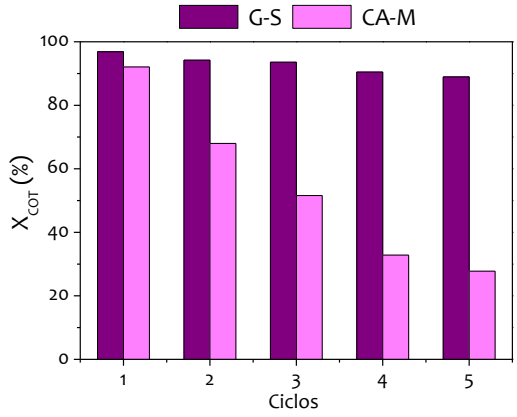

Figura 3.9. Estabilidad de G-S y CA-M en 5 ciclos consecutivos de MW-CWPO.

Este comportamiento tan dispar entre catalizadores fue relacionado con su estructura y, en especial, al efecto de los puntos calientes. El carbón activado es un material poroso. De esta forma, cuando se producen los puntos calientes en el interior de los microporos, se genera vapor confinado. En esos puntos la presión aumenta de forma local y el catalizador acaba desmoronándose en lo que hemos denominado **efecto palomita de maíz**. Estas micro explosiones colapsan la estructura del catalizador, lo que conlleva su desactivación progresiva, transformando el catalizador en un polvo difícil de separar del efluente tratado.

Por otra parte, el grafito es un material laminar y ordenado. Esta estructura permite disipar el calor generado en los puntos calientes con mayor facilidad, manteniendo el grafito su estructura y su actividad catalítica intactas. Estos fenómenos están detallados en la Figura 3.10.

Figura 3.10. Formación de puntos calientes y estructura de los catalizadores.

Los resultados del estudio de actividad y estabilidad de materiales carbonosos en MW-CWPO fueron publicados en la revista *Separation and Purification Technology,* como el tercer trabajo de esta Tesis, recogido en el Apéndice 5.3.

Tras obtener un catalizador activo y estable, ya podíamos proponer un proceso CWPO intensificado mediante microondas, pero antes teníamos que realizar un estudio económico con tal de optimizar el uso de las microondas. Este es el objetivo del cuarto trabajo de esta Tesis doctoral, en la que se comparan los diferentes métodos de operación posibles y descritos en bibliografía, potencia MW fija y temperatura fija. Este último, que es el empleado en los trabajos previos, implica programar el microondas para calentar las muestras desde temperatura ambiente hasta 120ºC en 90 segundos, concentrando la radiación MW a 1800W en ese corto período de tiempo. Después los reactores son irradiados para mantener la temperatura, pero a una potencia mucho menor. El proceso MW-CWPO es eficiente debido a la formación de puntos calientes y estos están relacionados con la radiación MW. Por tanto, parecía que no estábamos aprovechando al máximo el potencial de esta tecnología trabajando a temperatura fija. Para probar esta teoría y optimizar el consumo energético en el sistema, se llevaron a cabo diferentes experimentos trabajando a temperatura fija, potencia MW fija con radiación en continuo y potencia MW fija con radiación a pulsos. Los resultados se recogen en la Figura 3.11.

Pudimos observar que el modo de radiación también tiene un papel importante en el proceso MW-CWPO. Los **pulsos de MW** lograron una mayor mineralización y una mejor utilización del H_2O_2 que el uso de MW continuas.

Esto se atribuye a la disipación del calor generado en los puntos calientes en los periodos de relajación del material.

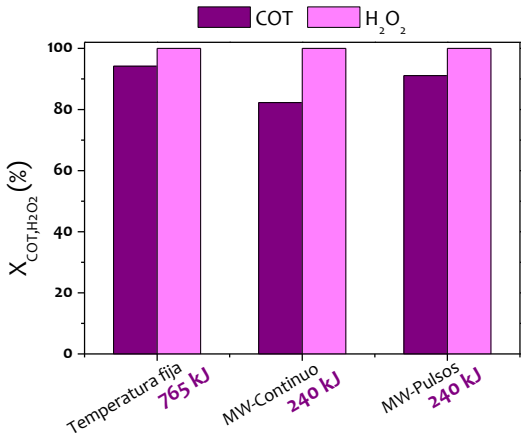

Figura 3.11. Influencia del modo de radiación en MW-CWPO. $C_{Fenol,0}$: 100 mg·L^{-1}, $C_{G\text{-}S}$: 500 mg·L^{-1}, $C_{H2O2,0}$: 500 mg·L^{-1}, pH_0:3.

Analizando los requisitos del sistema, el consumo energético se redujo a un tercio con relación al experimento a temperatura controlada. Además, el consumo energético por masa de COT eliminada al final de la reacción (EC_{COT}) fue significativamente menor en comparación con otros procesos de oxidación avanzada intensificados, como se muestra en la Figura 3.12. Por tanto, el proceso MW-CWPO se presenta como una alternativa competitiva desde el punto de vista económico.

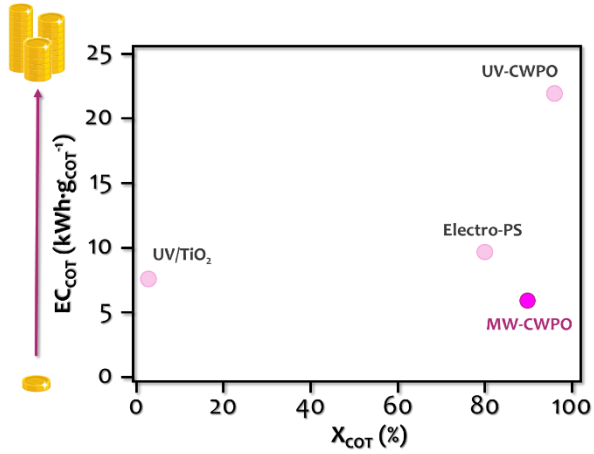

Figura 3.12. Relación coste-eficiencia de diversos AOP intensificados.

En este trabajo también se estudió el modelo cinético, encontrando que sigue un pseudo-segundo orden para el COT y un pseudo-primer orden en el caso del peróxido. También se calcularon las energías de activación E_A para ambas reacciones. La $E_{A,\ COT}$ fue significativamente menor que las reportadas en bilbiografía para la oxidación de fenol. Sin embargo, la $E_{A,\ H2O2}$ presentaba valores similares a los previamente encontrados. Por tanto, la formación de puntos calientes tiene un impacto mayor en la degradación de contaminantes orgánicos que en la descomposición del H_2O_2. El artículo completo, publicado en la revista *Separation and Purufication Technology*, está recogido en el Apéndice 5.4.

En resumen, esta Tesis doctoral muestra que el uso de radiación microondas mejora substancialmente el conocido proceso CWPO, en el que se emplea H_2O_2 como promotor de $HO_X^{\bullet}$. La absorción de MW puede generar puntos calientes en la superficie de materiales carbonosos. Cuando estos son de naturaleza grafítica, el calor generado en estas áreas puede ser disipado, manteniendo el catalizador sus propiedades. Además, la química superficial tiene un rol importante, tanto como la formación de puntos calientes. Finalmente, el modo de operación, en lo que concierne al procedimiento de irradiación también tiene un impacto importante en la formación de puntos calientes y, por tanto, en la actividad catalítica.

4. CONCLUSIONS / CONCLUSIONES

CONCLUSIONS

The main conclusions obtained throughout this dissertation, in which the Catalytic Wet Peroxide Oxidation process has been intensified by means of microwave radiation are:

- Hydrogen peroxide decomposition is sensitive to MW radiation. Due to its high loss factor, which is higher than that of water, H_2O_2 is affected by the electromagnetic field induced by microwaves. This produces its homolytic rupture, giving rise to free radicals which are able to oxidize the pollutants.

- H_2O_2 decomposition process is also favored by the presence of redox catalysts, which increase considerably the $HO_X^{\bullet}$ radicals generation rate and, therefore, the efficiency of the oxidation process.

- Dielectric properties of the catalyst play a key role in MW-CWPO, due to hot-spot formation on their structure. Hence, MW-absorbing materials, such as carbon materials, accelerate the $HO_X^{\bullet}$ production rate and minimize the generation of intermediates, especially oligomers, common in CWPO processes. Thus, a higher mineralization degree is reached at higher rate.

- In conventional CWPO processes, carbon materials have shown a moderate activity. Nonetheless, in MW-CWPO their activity is noticeably enhanced due to hot spot formation. It should be noted that:

    - Carbon blacks present a relatively low activity in relation to other carbon materials.
    - Silicon carbide presents a high initial activity, followed by a quick deactivation caused by a loss of its crystalline structure.
    - Activated carbons present a high activity with a low H_2O_2 consumption efficiency in relation to other materials.

- Activity in graphites is high, but it can be conditioned by their superficial chemistry. In this sense, G-S, which has an acidic character, is more active in terms of mineralization and H_2O_2 decomposition tan G-F, which has a basic pH_{Slurry}.

- The MW-CWPO process follows a pseudo-second order kinetic for TOC and pseudo-first order in relation to H_2O_2, with a lower activation energy tan the non-assisted process due to the contribution of hot spots.

- Stability in carbon materials is related to their structure. All these materials absorb MW radiation and generate hot spots, although the heat dissipation is different, which affects their stability. In this sense, AC presents a quick deactivation due to collapse upon the so-called popcorn effect. On the other hand, the laminar structure of G-S eases the heat dissipation, enhancing its stability.

- Radiation mode in terms of intensity and MW duration has an important role in the MW-CWPO process. MW application by pulses results in a high mineralization degree with an efficient H_2O_2 consumption, minimizing the energy requirements per unit of eliminated TOC and turning MW into a competitive option in relation to other intensification techniques.

- Pulsated MW-CWPO presents a lower energy consumption by unit of removed TOC in relation to other assisted AOP, making this process a competitive alternative.

CONCLUSIONES

Las principales conclusiones obtenidas durante el desarrollo de la presente Tesis Doctoral, en la que se ha intensificado el proceso CWPO mediante radiación microondas son:

- La descomposición del peróxido de hidrógeno es sensible a la radiación microondas. Debido a su alto factor de pérdida, que dobla al del agua, el H_2O_2 se ve afectado por el campo electromagnético inducido por las MW, dando lugar a su ruptura homolítica para generar radicales libres, que son capaces de oxidar los compuestos presentes en disolución.

- Este proceso de descomposición de H_2O_2 se encuentra igualmente favorecido por la presencia de catalizadores redox, aumentando significativamente la velocidad de producción de radicales $HO_x^{\bullet}$ y, por tanto, la eficiencia global del proceso de oxidación.

- Las propiedades dieléctricas del catalizador presentan un papel importante en el proceso MW-CWPO, debido a la generación de puntos calientes en su estructura. Así, los materiales absorbedores de microondas, como son los materiales carbonosos, aceleran la generación de radicales $HO_x^{\bullet}$ y minimizan la formación de intermedios, especialmente oligómeros frecuentes en procesos CWPO, alcanzando un mayor grado de mineralización a una mayor velocidad.

- La actividad catalítica de los materiales carbonosos en el proceso MW-CWPO está íntimamente relacionada con sus propiedades superficiales. Cabe destacar que:
    - Los negros de humo presentan una actividad relativamente baja en comparación con el resto de materiales carbonosos empleados.
    - El carburo de silicio presenta una alta actividad inicial, aunque una muy baja estabilidad.

- Los carbones activos presentan una alta actividad, con un consumo de H_2O_2 menos eficiente que otros materiales.
- La actividad de los grafitos es alta, aunque puede estar muy condicionada por su química superficial. Así, el G-S, de carácter ácido, es más activo en la oxidación y descomposición de H_2O_2 que el G-F, con un pH_{Slurry} de carácter básico.

- El proceso MW-CWPO sigue una cinética de pseudo-segundo orden respecto al COT y pseudo-primer orden con relación al H_2O_2, presentando una energía de activación inferior al proceso no asistido debido a la contribución de los puntos calientes.

- La estabilidad de los materiales carbonosos en MW-CWPO está relacionada con su estructura tridimensional. Todos ellos adsorben las microondas y generan puntos calientes, aunque la disipación del calor es diferente, lo que afecta a su estabilidad. Así, el CA se desactiva rápidamente al desmoronarse mediante el mecanismo al que hemos denominado como efecto palomita de maíz. La estructura laminar del G-S permite una mayor disipación del calor generado en los puntos calientes, mejorando su estabilidad.

- El modo de irradiación en cuanto a intensidad y duración de las microondas tiene un papel clave en el proceso MW-CWPO. La irradiación por pulsos permite alcanzar un alto grado de mineralización con un consumo eficiente de H_2O_2, minimizando las necesidades energéticas por unidad de COT eliminado y convirtiéndolo en una opción competitiva frente a otras alternativas de intensificación.

5. APPENDIX

5.1. Microwave-assisted Catalytic Wet Peroxide Oxidation. Comparison of Fe catalysts supported on activated carbon and γ-alumina

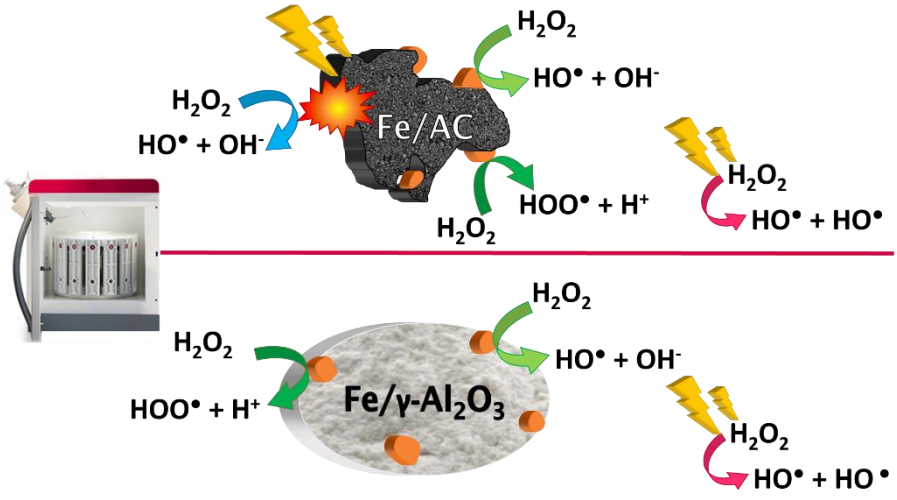

Applied Catalysis B: Environmental 218 (2017) 637–642

Contents lists available at ScienceDirect

Applied Catalysis B: Environmental

journal homepage: www.elsevier.com/locate/apcatb

Microwave-assisted catalytic wet peroxide oxidation. Comparison of Fe catalysts supported on activated carbon and γ-alumina

Alicia L. Garcia-Costa*, Juan A. Zazo, Juan J. Rodriguez, Jose A. Casas

Chemical Engineering, Faculty of Science, Universidad Autonoma de Madrid, Ctra. Colmenar Viejo km. 15, 28049, Madrid, Spain

ARTICLE INFO

Article history:
Received 7 April 2017
Received in revised form 15 June 2017
Accepted 20 June 2017
Available online 8 July 2017

Keywords:
CWPO
Microwave
Fe/AC
Fe/γ-Al_2O_3
Hot spot

ABSTRACT

This paper studies the role of the catalytic support on microwave-assisted catalytic wet peroxide oxidation (MW-CWPO) with Fe as active phase. Experiments were carried out with and without MW using catalysts of Fe on activated carbon (Fe/AC) and gamma alumina (Fe/γ-Al_2O_3). Phenol (100 mg·L^{-1}) was used as target pollutant, operating at pH 3, 120 °C, 100 mg·L^{-1} catalyst concentration and the theoretical stoichiometric amount of H_2O_2 (500 mg·L^{-1}). MW radiation promotes hot spot formation on the surface of AC, enhancing HO_X• generation, so that the rate of mineralization is significantly increased with respect to non-assisted CWPO. Under these conditions, phenol oxidation proceeded essentially through direct aromatic ring breakdown, yielding carboxylic acids, while the formation of the highly toxic intermediates hydroquinone and p-benzoquinone were barely detected. The Fe/AC catalyst showed a better performance than the Fe/γ-Al_2O_3 one, which can be explained by the much higher MW absorption on AC, which, in fact, showed to be a good MW-CWPO catalyst by itself. Meanwhile, the results proved that γ-Al_2O_3 was basically transparent to MW, and deposition of condensation byproducts on the surface hindered the activity of the Fe/γ-Al_2O_3 catalyst.

1. Introduction

Environmental policies, with increasingly stringent discharge limits, demand new or enhanced technologies for wastewater treatment, capable to deal with bio-refractory pollutants. Advanced Oxidation Processes (AOPs) have been widely used for this purpose. Among them, Catalytic Wet Peroxide Oxidation (CWPO) is one of the most investigated in the last decade. This AOP uses H_2O_2 as a source of HO_X• radicals (HO• and HOO•) for the abatement of pollutants in water at mild or moderate working conditions (T: 25–120 °C; P: 1–5 bar) [1].

The main points of concern in CWPO are efficient H_2O_2 consumption and catalyst stability. Metals supported on activated carbon (AC) [2–7] or alumina (γ-Al_2O_3) [8–11], or even carbon materials themselves [1,12–15], have been tested for this process. Activated carbon-based catalysts have shown higher activity but lower stability than alumina catalysts, mainly due to active phase leaching [9]. On the other hand, activated carbon by itself gives a lower oxidation rate despite its higher stability [15]. All these catalysts have shown to be highly efficient when working well above ambient-like temperature.

Microwave (MW) radiation has been used for water treatment intensification, since it provides rapid heating and improves energy efficiency [16,17]. MW heating depends on the electric loss tangent (tan δ), defined as the quotient between ε", the relative loss factor (which represents the dissipation of the absorbed energy as heat) and ε', the relative dielectric constant (which is the relative measure of the MW energy density in a given material). Thereby, a lossy material with a high ε" is easily heated by MW [17].

$$tan\delta = \frac{\varepsilon''}{\varepsilon'} \quad (1)$$

Materials can be classified as opaque, transparent or absorbers, depending on the penetration of MW. Therefore, materials presenting high tan δ values are considered MW absorbers, whereas lower values correspond to transparent materials [18].

Table 1 lists those values for different materials. According to them, AC is a MW absorber, whereas Al_2O_3 is transparent to MW. When supporting iron on these materials, tan δ increases, being more noticeable this effect for Al_2O_3.

MW- assisted CWPO has been used to treat different synthetic and real wastewaters (Table 2). However, so far there is a lack of reliable and conclusive studies. Even though $CuFe_2O_4$ and Fe_3O_4 have shown to be effective for Rhodamine B removal in short reac-

* Corresponding author.
E-mail address: alicial.garcia@uam.es (A.L. Garcia-Costa).

http://dx.doi.org/10.1016/j.apcatb.2017.06.058
0926-3373/

Table 1
Dielectric properties of different materials at 25 °C.

Material	tan δ	MW interaction	Reference
PTFE[a]	$2.48{\cdot}10^{-4}$	Transparent	[19]
Distilled H_2O[a]	0.123	Absorber	[20]
AC[a]	0.57–0.80	Absorber	[21]
AC[a]	0.22–2.95	Absorber	[22]
Carbon nanotubes[b]	1.06	Absorber	[23]
Fe/carbon nanotubes[b]	2	Absorber	[23]
Al_2O_3[c]	$3{\cdot}10^{-5}$–$4{\cdot}10^{-2}$	Transparent	[24]
Al_2O_3 (99,5%)[d]	$8{\cdot}10^{-5}$	Transparent	[25]
Fe/Al_2O_3 [d]	$8{\cdot}10^{-4}$	Transparent	[25]

tan δ measured at [a]2,45 GHz, [b]8 GHz, [c]9 GHz, [d]1 GHz.

tion time [26,27], no specific data on mineralization were reported. On the other hand, supported Cu leaches when working in acidic media [35] giving rise to rapid deactivation and turning these catalysts into potential pollutants. Despite using the same active phase [29–31], the role of the support has not yet been analyzed, while it can be a key issue in MW-CWPO. Besides, no studies have been conducted working at high temperature (above 100 °C). Therefore, further research is needed to learn more on the potential application of this technology.

Two well-known catalysts, already used in CWPO of phenol as target pollutant have been tested: (i) Fe on activated carbon (Fe/AC) and (ii) Fe on γ-Al_2O_3 (Fe/γ-Al_2O_3) [2,11]. The aim of this research is to learn on the potential advantage of associating MW radiation to CWPO and analyze the behavior of those two commonly used different supports in the MW-CWPO approach investigated.

2. Materials and methods

2.1. Reagents and materials

Phenol was supplied by Sigma-Aldrich and H_2O_2 (30% w/v) by Panreac. The respective aqueous solutions were prepared at pH 3 using HCl (Panreac). The catalysts were synthesized with $Fe(NO_3)_3{\cdot}9H_2O$ (98 wt.%) purchased from Sigma-Aldrich and γ-Al_2O_3 and AC supplied by Merck. Working standard solutions of phenol, catechol, resorcinol, hydroquinone, *p*-benzoquinone, and organic acids (fumaric, malonic, maleic, acetic and formic from Sigma-Aldrich and oxalic from Panreac) were prepared for equipment calibration. H_2SO_4 (96 wt.%; Panreac), $NaHCO_3$ (Merck), Na_2CO_3 (Panreac) and H_3PO_4 (85 wt.%; Sigma-Aldrich) were also used for the analysis. All reagents were of analytical grade and were used as received without further purification. Milli-Q water was always used.

2.2. Catalysts preparation

The preparation of Fe/AC and Fe/γ-Al_2O_3 catalysts was described elsewhere [2,8,11,36]. Briefly, they were prepared by incipient wetness impregnation of AC or γ-Al_2O_3 with an aqueous solution of $Fe(NO_3)_3{\cdot}9H_2O$ in order to obtain a 4% Fe wt.% nominal load. Afterwards, the AC-supported catalyst was calcined at 200 °C for 2 h, while for the γ-Al_2O_3 300 °C and 4 h were used. Under those conditions, Fe_2O_3 was the main iron species in both catalysts.

Table 3
Porous texture and Fe content of the supports and catalysts.

	S_{BET} (m^2/g)	A_{ext} (m^2/g)	Fe (%)
AC	1018	175	0.04
Fe/AC	951	73	4.2
γ-Al_2O_3	142	140	–
Fe/γ-Al_2O_3	133	120	4.1

2.3. Catalyst characterization

The porous texture of the supports and catalysts was characterized by 77 K N_2 adsorption/desorption using a Micromeritics Tristar apparatus. The specific surface area (S_{BET}) and the external or non-microporous area (A_{ext}) were calculated by the BET method and t-method, respectively. The total iron content of the catalyst was determined by inductively coupled plasma mass spectrometry (ICP-MS) using an ICP-MS Elan 6000 Perkin-Elmer Sciex instrument. Additional characterization of these catalysts can be found elsewhere [2,9].

2.4. CWPO and MW-CWPO experiments

All the experiments were carried out at 120 °C and $pH_0 = 3$ with 100 mg·L^{-1} of aqueous phenol solution and 100 mg·L^{-1} of catalyst (particle size < 100 μm). H_2O_2 was added at 500 mg·L^{-1}, corresponding to the theoretical stoichiometric amount for complete mineralization of phenol. Stirring was fixed at 400 rpm, which allowed maintaining the catalyst in suspension and avoiding mass-transfer limitations. All the experiments were done by triplicate, being the standard deviation always less than 5%.

CWPO tests were carried out for 1 h in a batch stainless steel pressurized reactor (BR-300, Berghof) with a 500 mL PTFE insert reaction vessel equipped with backpressure and temperature controllers. When the temperature was equilibrated at 120 °C, hydrogen peroxide solution was injected.

MW-CWPO runs were performed in high pressure 100 mL PTFE reaction vessels in a microwave oven (FlexiWAVE, Milestone) equipped with temperature controller. The reactors were initially loaded with phenol, H_2O_2 and the catalyst and the heating rate was set at 80 °C/min (P_{max}: 1800 W) to reach the reaction temperature (120 °C), which was maintained for 1 h. During reaction, the system pressure rose up to 2.4 bar.

2.5. Analytical methods

Samples were periodically withdrawn from the reactors and immediately analyzed after filtration through fiber glass filters (Albet FV-C). Phenol and aromatic intermediates were identified and quantified by means of an Ultra HPLC (Thermo Scientific Ulti-

Table 2
Application of MW-assisted CWPO.

	Catalyst	Pollutant	Operating conditions	Results	Ref
Metals	$CuFe_2O_4$	Rhodamine B (RhB)	T = 80 °C, [RhB] = 100 mg·L^{-1}, t = 5 min, P = 300 W	X_{RhB} = 100%	[26]
	Fe_3O_4	Rhodamine B	T = 80 °C, [RhB] = 100 mg·L^{-1}, t = 2 min, P = 300 W	X_{RhB} = 99%	[27]
	Iron tailings	Landfill leachate	T = 25 °C, [COD] = 12 g·L^{-1}, t = 3 min, P = 480 W	X_{COD} = 45.1%	[28]
Al_2O_3	CuO/Al_2O_3	P-Nitrophenol (NP)	T = 70 °C, [2NP] = 50 mg·L^{-1}, t = 6 min, P = 100 W	X_{PNP} = 93%	[29]
	CuO/Al_2O_3	2-Nitrophenol	T = 60 °C, [2NP] = 200 mg·L^{-1}, t = 5 min, P = 300 W	X_{2NP} = 97%, X_{TOC} = 79%	[30]
AC	CuO/AC	P-Chlorophenol (PCP)	T = 70 °C, [PCP] = 100 mg·L^{-1}, t = 30 min, P = 400 W	X_{TOC} = 90%	[31]
	Ferrihydrite/AC	Methyl Orange (MO)	[MO] = 20 mg·L^{-1}, t = 4 min, P = 700 W	X_{MO} = 99.1%	[32]
	Cu-Ce/AC	Pharmaceutical wastewater	[TOC] = 158 mg·L^{-1}, t = 6 min, P = 539 W	X_{TOC} = 65.9%	[33]
	Fe/AC	Landfill leachate	t = 30 min, P = 720 W	X_{COD} = 93%	[34]

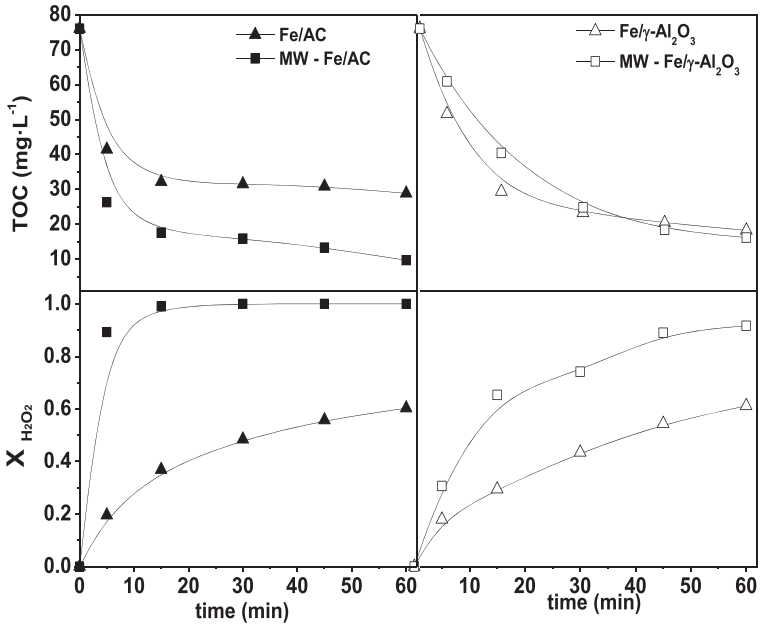

Fig. 1. TOC and H_2O_2 evolution upon CWPO of phenol with and without MW radiation with the catalysts tested. ($[Ph]_0$: 100 mg·L^{-1}; $[H_2O_2]_0$: 500 mg·L^{-1}; [cat]: 100 mg·L^{-1}; T: 120 °C and pH_0: 3).

mate 3000) with a Diode Array detector (Dionex Ultimate 3000). A C18 column (ZORBAX Eclipse Plus C18, 100 mm, 1.8 μm) was used as stationary phase and a 4 mM H_2SO_4 aqueous solution at 1 mL/min as mobile phase. UV detector at 210 nm wavelength was used for phenol, resorcinol, catechol and hydroquinone and at 246 nm for *p*-benzoquinone. Short-chain organic acids were analyzed in an ion chromatograph with chemical suppression (Metrohm 790 IC) using a conductivity detector. A Metrosep A supp 5–250 column (25 cm long, 4 mm diameter) was used as stationary phase and 0.7 mL/min of a 3.2 mM/1 mM aqueous solution of Na_2CO_3 and $NaHCO_3$, respectively, as mobile phase. Total Organic Carbon was measured using a TOC analyzer (Shimadzu TOC-VSCH). Residual H_2O_2 in the liquid phase was determined by colorimetric titration with an Agilent spectrophotometer using the $TiOSO_4$ method [37].

3. Results and discussion

Table 3 summarizes the BET and external area of the supports and catalysts. AC and Fe/AC have a high developed porosity, corresponding mainly to microporosity, whereas fresh alumina and its catalyst are essentially mesoporous solids with much lower values of surface area. AC has a high adsorption capacity, related to the surface area. Thus, phenol adsorption should be considered. In this terms, previous to the oxidation runs, blank runs were carried out with the catalysts and phenol (no H_2O_2 added to the solution). TOC did not vary when using either Fe/AC or Fe/γ-Al_2O_3 at 120 °C, thus, phenol adsorption is unlikely to occur in the tested conditions. The iron content was around 4 wt.% for the home-made catalysts.

A set of experiments were carried out with and without MW to learn on the effect of this energy source on CWPO. The results are shown in Fig. 1, where it can be seen that MW affects quite differently to the activity of the catalysts tested. In the case of Fe/AC, mineralization was significantly improved, consistently with the enhanced H_2O_2 decomposition rate. This effect is attributed to hot spot formation on the surface of AC. Meanwhile, when using Fe/γ-Al_2O_3, the rate of H_2O_2 decomposition was also increased but in a lower extent and the effect of MW on the CWPO process was irrelevant in terms of mineralization.

The normalized H_2O_2 yield ε, defined as the amount of TOC removed per unit weight of H_2O_2 fed in relation to the maximum theoretical TOC removal at that H_2O_2 dosage, has been used to evaluate the efficiency of H_2O_2 [38]. MW heating allowed increasing this value from 0.77 to 0.88 after 60 min with Fe/AC, whereas with Fe/γ-Al_2O_3, ε remained practically unchanged ($\varepsilon \approx 0.82$). Therefore, H_2O_2 was somewhat more efficient in CWPO with the Fe/γ-Al_2O_3 catalyst, whereas in the MW-assisted process, the AC-supported catalyst showed a significantly improved behavior.

Table 4
Byproducts distribution from MW-assisted and non-assisted CWPO of phenol with the catalyst tested.

Time	CWPO Fe/AC		MW-CWPO Fe/AC		CWPO Fe/γ-Al_2O_3		MW-CWPO Fe/γ-Al_2O_3	
(min)	Acids %	Arom %	Acids %	Arom %	Acids %	Arom %	Acids %	Arom %
5	86.6	13.4	99.5	0.5	63.6	36.4	42.2	57.8
15	98.6	1.4	99.8	0.2	74.6	25.4	63.4	36.6
30	98.5	1.5	100	0	78.3	21.7	77.2	22.8
45	98.4	1.6	100	0	91.3	8.7	89.7	10.3
60	98.2	1.8	100	0	97.2	2.7	94.8	5.2

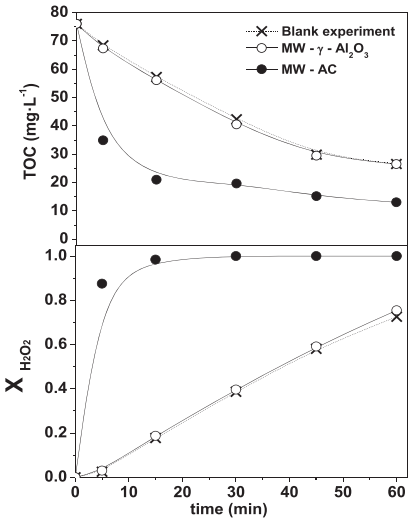

Fig. 2. TOC and H_2O_2 evolution in MW-CWPO of phenol with the bare supports tested and blank experiment with no catalyst. Operating conditions: $[Ph]_0$: 100 mg·L^{-1}; $[H_2O_2]_0$:500 mg·L^{-1}; [cat]: 100 mg·L^{-1}; T: 120 °C and pH_0: 3.

Table 5
Byproducts distribution from MW-CWPO of phenol with the bare supports.

Time	MW AC		MW γ-Al_2O_3	
(min)	Acids %	Arom %	Acids %	Arom %
5	70.5	29.5	29.8	70.2
15	90.6	9.4	23.7	76.3
30	100	0	54.5	45.5
45	100	0	82.6	17.4
60	100	0	91.1	8.9

The distribution of intermediates was followed by means of Ion Chromatography to quantify short chain organic acids, such as acetic, formic, malonic, maleic and oxalic and Ultra HPLC to analyze aromatic compounds, being only detected catechol and *p*-benzoquinone. Byproducts distribution as short chain organic acids and aromatic compounds is shown in Table 4. These results correspond in all cases to complete conversion of phenol, since it was always achieved in less than 5 min.

Under MW-CWPO with the Fe/AC catalyst, phenol disappearance proceeded at a high rate and after 15 min only organic acids were detected, while in the non-assisted process some remaining amounts of aromatic byproducts were still detected even after 1 h reaction time. The highly toxic benzoquinone is of particular concern and in that respect the beneficial effect of MW was very important. With the Fe/γ-Al_2O_3 catalyst, the residual amounts of aromatic byproducts after 1 h reaction time were still quite significant, being that even more pronounced in the MW-assisted CWPO. To learn more on the specific effect of the support, MW-CWPO experiments with the bare AC and γ-Al_2O_3 were carried out under the same conditions than the previous ones performed with the Fe catalysts. The results are depicted in Fig. 2 in terms of mineralization and H_2O_2 conversion. The evolution of reaction byproducts is given in Table 5, where it can be seen the dramatically different behavior of both supports. The lossy character of AC allows a high MW absorption giving rise to the formation of hot spots on its surface [17,39,40], enhancing wet peroxide oxidation. This phenomenon does not take place, or represents a much less significant contribution, in the case of Fe/γ-Al_2O_3 since it is a MW insulator,

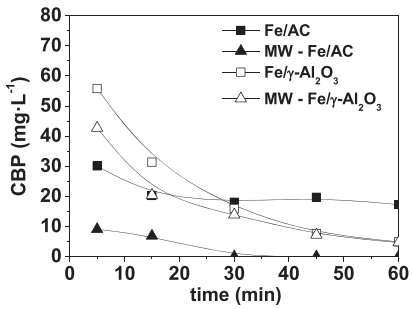

Fig. 3. Condensation byproducts (CBP) upon CWPO with and without MW with the catalysts tested.

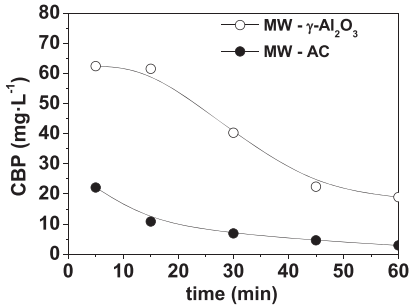

Fig. 4. Condensation byproducts (CBP) upon MW-CWPO with the bare supports.

essentially transparent to MW radiation. Fig. 2 includes the results of a blank experiment performed under MW radiation and the same amount of H_2O_2, but without any catalyst or support. As can be seen, the γ-Al_2O_3 support does not provoke any significant enhancement on the MW-assisted wet peroxide oxidation. Comparing Fig. 1 and Fig. 2, it can be observed that the dielectric properties of the support play a key role on MW-CWPO. When working with AC as support under MW, iron has a minor contribution in the reaction, since hot spot formation upon the AC surface greatly enhances $HO_X^{\bullet}$ generation. On the other hand, when working with a MW-transparent support such as Al_2O_3, the activity of Fe/Al_2O_3 relies exclusively on the active phase.

It was observed a more or less pronounced difference between the measured TOC and the amount of C associated to the identified species, as can be seen in Figs. 3 and 4 for the catalysts and bare supports, respectively. That difference has been ascribed to oligomeric condensation byproducts (CBP), whose formation has been reported in homogeneous Fenton [41] as well as in CWPO of phenol [1,2,15,42,43]. This refers to CBP in the liquid phase, but those species can be also deposited on the surface of the catalysts. In the case of γ-Al_2O_3 this was confirmed by the dark brown color observed in the solid after use (Fig. 1. of Supporting Information). This darkening of the catalyst was evidenced since the earlier stages of reaction. As can be seen in Fig. 3, the amount of unidentified organic carbon in the liquid phase was significantly higher with the Fe/γ-Al_2O_3 catalyst and became almost negligible in the MW-assisted CWPO with the Fe/AC catalyst after 30 min reaction time. Fig. 3 also reveals the influence of MW on CBP stability. Hot spot formation on the surface of Fe/AC lead to a complete CBP removal, whereas for Fe/Al_2O_3, MW radiation had no effect on the fate of CBP, which are adsorbed on its surface. The results with the bare supports (Fig. 4), show the significantly better performance of AC in that respect.

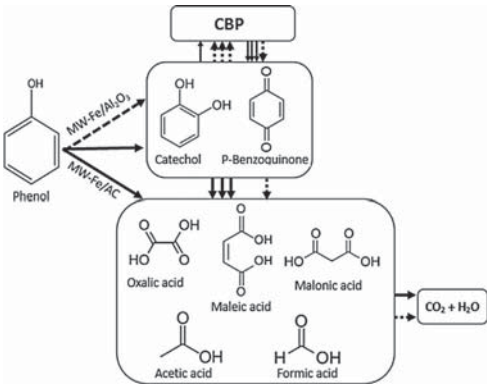

Fig. 5. Reaction pathway of MW-CWPO of phenol with the tested catalysts.

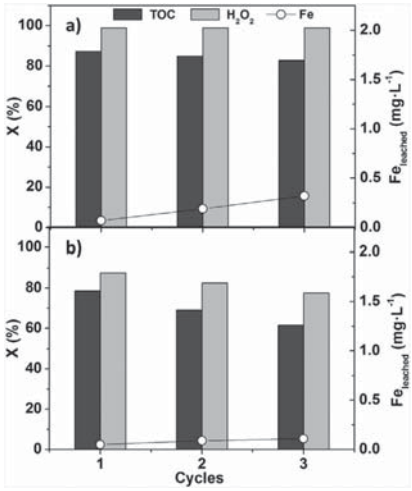

Fig. 6. Stability of a) Fe/AC and b) Fe/Al_2O_3 in MW-CWPO through three reaction cycles. ($[Ph]_0$: 100 mg·L^{-1}; $[H_2O_2]_0$: 500 mg·L^{-1}; [cat]: 100 mg·L^{-1}; T: 120 °C and pH_0: 3).

With the results obtained so far, the oxidation route depicted in Fig. 5 is proposed for MW-CWPO of phenol. Starting with phenol, the reaction byproducts are divided in three blocks: aromatic intermediates, short chain organic acids and condensation byproducts. This scheme is consistent with the well-known breakdown routes proposed for Fenton-like oxidation of phenol in the literature [2,41]. As indicated before, with MW-Fe/AC there is a much less formation of CBP, whereas with Fe/γ-Al_2O_3 those species appear in significant amounts since the earlier stages of the process.

Stability of Fe/AC and Fe/Al_2O_3 under MW-CWPO was tested in 3 consecutive cycles. Results are shown in Fig. 6. Fe/AC remained active under the selected operating conditions, since it allowed complete H_2O_2 decomposition in all runs and mineralization degree was always above 80%. Iron leaching was measured after each run. There was a progressive iron leaching ascribed to the action of oxalic acid. Nevertheless, this active phase loss was always below 10%, being this amount negligible regarding homogeneous Fenton contribution. On the other hand, Fe/Al_2O_3 presented a deeply pronounced deactivation due to CBP deposition on the surface of the catalyst, which lead to active sites blockage, hindering the efficiency of the process for the decomposition of H_2O_2 as well as for TOC removal.

4. Conclusions

The dielectric properties of the catalyst support play a crucial role on MW-assisted CWPO. With a MW absorber such as AC, formation of hot spots on the surface of the catalyst enhances the oxidative breakdown of the target pollutants. In this particular case, phenol mineralization upon CWPO was significantly improved under MW-radiation with the Fe/AC catalyst. The efficiency of H_2O_2 consumption was also improved and the highly toxic aromatic intermediates were barely detected and completely removed at around 15 min reaction time, working at 120 °C with 100 mg·L^{-1} catalyst and the stoichiometric dose of H_2O_2 (500 mg·L^{-1} for the 100 mg·L^{-1} phenol solution). The formation of oligomeric condensation byproducts was also reduced with respect to the non-assisted process, and their presence in the liquid phase became almost negligible after 30 min reaction time.

In contrast, γ-Al_2O_3, being essentially transparent to MW radiation, did not show any significant enhancing effect in the MW-assisted process and even a lower efficiency of the Fe/γ-Al_2O_3 catalyst was observed compared to the non-assisted CWPO. This can be due to a higher formation of CBP covering active Fe sites.

Acknowledgements

This study is funded by the Spanish MINECO through projects CTQ2013-41963-R and CTM2016-76454-R. A.L. Garcia-Costa would like to thank the Spanish MINECO and the European Social Fund for their support through the PhD. grant BES-2014-067598.

Appendix A. Supplementary data

Supplementary data associated with this article can be found, in the online version, at http://dx.doi.org/10.1016/j.apcatb.2017.06.058.

References

[1] C.M. Dominguez, P. Ocon, A. Quintanilla, J.A. Casas, J.J. Rodriguez, Appl. Catal. B-Environ. 144 (2014) 599–606.
[2] J.A. Zazo, J.A. Casas, A.F. Mohedano, J.J. Rodriguez, Appl. Catal. B-Environ. 65 (2006) 261–268.
[3] H.S. Park, J.R. Koduru, K.H. Choo, B. Lee, J. Hazard. Mater. 286 (2015) 315–324.
[4] S.A. Messele, O. Soares, J.J.M. Orfao, F. Stuber, C. Bengoa, A. Fortuny, A. Fabregat, J. Font, Appl. Catal. B-Environ. 154 (2014) 329–338.
[5] A. Rey, A.B. Hungria, C.J. Duran-Valle, M. Faraldos, A. Bahamonde, J.A. Casas, J.J. Rodriguez, Appl. Catal. B-Environ. 181 (1) (2016) 249–259.
[6] F. Duarte, F.J. Maldonado-Hodar, L.M. Madeira, Appl. Catal. B-Environ. 129 (2013) 264–272.
[7] F. Duarte, V. Morais, F.J. Maldonado-Hodar, L.M. Madeira, Chem. Eng. J. 232 (2013) 34–41.
[8] P. Bautista, A.F. Mohedano, J.A. Casas, J.A. Zazo, J.J. Rodriguez, Water Sci. Tech. 61 (2010) 1631–1636.
[9] P. Bautista, A.F. Mohedano, N. Menendez, J.A. Casas, J.J. Rodriguez, Catal. Today 151 (2010) 148–152.
[10] M. Munoz, Z.M. de Pedro, J.A. Casas, J.J. Rodriguez, Water Res. 47 (2013) 3070–3080.
[11] M. Munoz, Z.M. de Pedro, N. Menendez, J.A. Casas, J.J. Rodriguez, Appl. Catal. B-Environ. 136 (2013) 218–224.
[12] R.S. Ribeiro, A.M.T. Silva, J.L. Figueiredo, J.L. Faria, H.T. Gomes, Appl. Catal. B-Environ. 140 (2013) 356–362.
[13] F. Martinez, I. Pariente, C. Brebou, R. Molina, J.A. Melero, D. Bremner, D. Mantzavinos, J. Chem. Technol. Biotechnol. 89 (2014) 1182–1188.
[14] F. Lucking, H. Koser, M. Jank, A. Ritter, Water Res. 32 (1998) 2607–2614.
[15] C.M. Dominguez, P. Ocon, A. Quintanilla, J.A. Casas, J.J. Rodriguez, Appl. Catal. B-Environ. 140 (2013) 663–670.
[16] N. Remya, J.-G. Lin, Chem. Eng. J. 166 (2011) 797–813.
[17] N. Wang, P. Wang, Chem. Eng. J. 283 (2016) 193–214.
[18] W.H. Sutton, Am. Ceram. Soc. Bull. 68 (1989) 376–386.
[19] O.P.N. Calla, S.K. Mishra, D. Bohra, N. Khandelwal, P. Kalla, C. Sharma, N. Gathania, N. Bohra, S. Shukla, Indian J. Pure Appl. Phys. 46 (2008) 134–138.

[20] N. Li, P. Wang, C. Zuo, H.L. Cao, Q.S. Liu, Environ. Eng. Sci. 27 (2010) 271–280.
[21] E.A. Dawson, G.M.B. Parkes, P.A. Barnes, G. Bond, R. Mao, Carbon 46 (2008) 220–228.
[22] X.F. Zhang, J.W. Wang, Z.J. Yu, R.S. Wang, H.M. Xie, Mater. Lett. 63 (2009) 2523–2525.
[23] H. Lin, H. Zhu, H. Guo, L. Yu, Mater. Lett. 61 (2007) 3547–3550.
[24] S.J. Penn, N.M. Alford, A. Templeton, X.R. Wang, M.S. Xu, M. Reece, K. Schrapel, J. Am. Ceram. Soc. 80 (1997) 1885–1888.
[25] R. Vila, M. Gonzalez, J. Molla, A. Ibarra, J. Nucl. Mater. 253 (1998) 141–148.
[26] P. Yan, D. Bai, in: Z. Liu, X. Dong, Z. Liu, Q. Liu (Eds.) Environ. Prot. Res. Expl. (Pts 1–3) (2013) 1384–1387.
[27] L.B.G.P. Yan, W.T. Li, Appl. Mech. Mat. 448–453 (2014) 834–837.
[28] B.H. Jiang, Y. Zhao, Y. Jin, X.M. Hu, L. Jiang, X.M. Li, in: R. Chen, W.P. Sung (Eds.) Biotech. Chem. Mat. Eng. (Pts 1–3) (2012) 1443–1446.
[29] W. Pan, G. Zhang, T. Zheng, P. Wang, RSC Adv. 5 (2015) 27043–27051.
[30] A.Y. Atta, B.Y. Jibril, T.K. Al-Waheibi, Y.M. Al-Waheibi, Catal. Comm. 26 (2012) 112–116.
[31] G.H. Zhao, B.Y. Lv, Y. Jin, D.M. Li, Water Environ. Res. 82 (2010) 120–127.
[32] D.Y. Xu, Y.S. Zhang, F. Cheng, P. Dai, J. Taiwan Inst. Chem. Eng. 60 (2016) 376–382.
[33] X.D. Qi, Z.H. Li, Pol. J. Environ. Stud. 25 (2016) 1205–1214.
[34] Z. Ding, W.S. Guan, J. Test. Eval. 41 (2013) 693–700.
[35] A. Santos, P. Yustos, A. Quintanilla, G. Ruiz, F. Garcia-Ochoa, Appl. Catal. B-Environ. 61 (2005) 323–333.
[36] J.A. Zazo, A.F. Fraile, A. Rey, A. Bahamonde, J.A. Casas, J.J. Rodriguez, Catal. Today 143 (2009) 341–346.
[37] G.M. Eisenberg, Ind. Eng. Chem.-Anal. (1943) 327–328, Edition 15.
[38] J.A. Zazo, G. Pliego, S. Blasco, J.A. Casas, J.J. Rodriguez, Ind. Eng. Chem. Res. 50 (2011) 866–870.
[39] J.A. Menéndez, A. Arenillas, B. Fidalgo, Y. Fernández, L. Zubizarreta, E.G. Calvo, J.M. Bermúdez, Fuel Process. Technol. 91 (2010) 1–8.
[40] Z.H. Zhang, Y. Xu, M.L. Shen, D.D. Dionysiou, D. Wu, Z.L. Chen, F.Y. Li, D.N. Liu, F.Q. Zhang, Environ. Prog. Sustain. Energy 32 (2013) 181–186.
[41] J.A. Zazo, J.A. Casas, A.F. Mohedano, M.A. Gilarranz, J.J. Rodriguez, Environ. Sci. Tech. 39 (2005) 9295–9302.
[42] J.L.D. de Tuesta, A. Quintanilla, J.A. Casas, J.J. Rodriguez, Appl. Catal. B-Environ. 209 (2017) 701–710.
[43] M.E. Suarez-Ojeda, F. Stuber, A. Fortuny, A. Fabregat, J. Carrera, J. Font, Appl. Catal. B-Environ. 58 (2005) 105–114.

Supporting information.

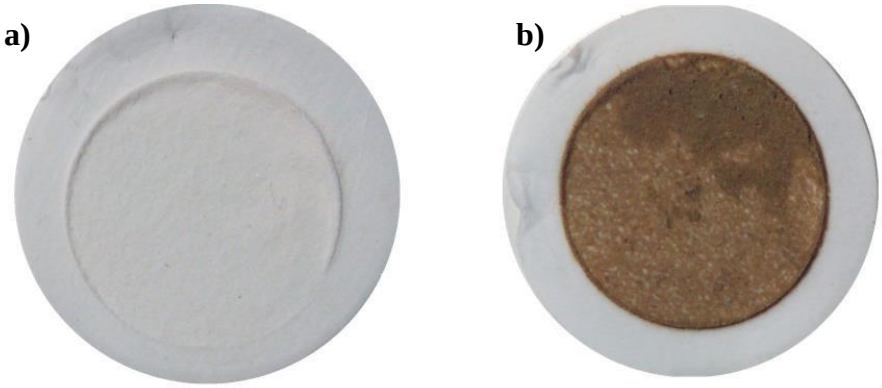

Figure 1 - a) Fresh and b) used γ-Al_2O_3 samples.

5.2. Activated carbon as catalyst for Microwave-assisted Wet Peroxide Oxidation of aromatic hydrocarbons

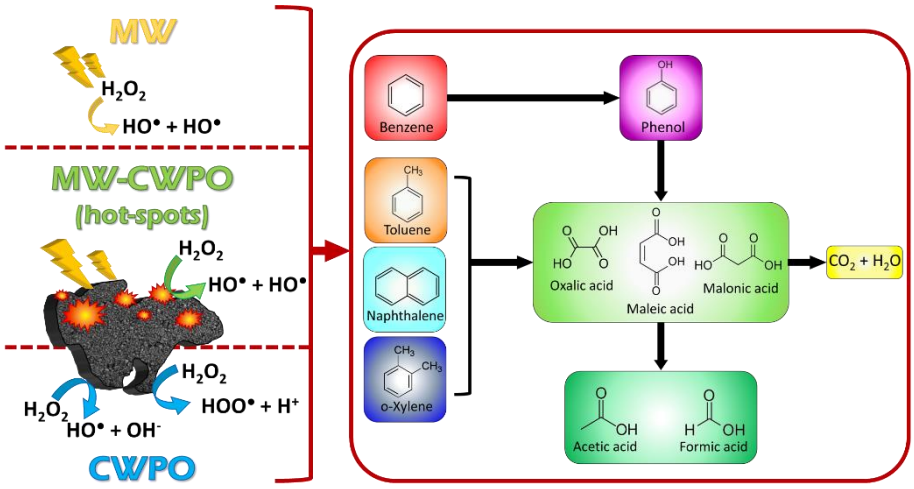

Environmental Science and Pollution Research
https://doi.org/10.1007/s11356-018-2291-9

NEW CHALLENGES IN THE APPLICATION OF ADVANCED OXIDATION PROCESSES

Activated carbon as catalyst for microwave-assisted wet peroxide oxidation of aromatic hydrocarbons

Alicia L. Garcia-Costa[1] · Lucia Lopez-Perela[1] · Xiyan Xu[1] · Juan A. Zazo[1] · Juan J. Rodriguez[1] · Jose A. Casas[1]

Received: 24 October 2017 / Accepted: 9 May 2018

Abstract
This paper addresses the removal of four aromatic hydrocarbons typically found in petrochemical wastewater: benzene (*B*), toluene (*T*), o-xylene (*X*), and naphthalene (*N*), by microwave-assisted catalytic wet peroxide oxidation (MW-CWPO) using activated carbon (AC) as catalyst. Under the studied conditions, complete pollutant elimination (*B*, 1.28 mM; *T*, 1.09 mM; *X*, 0.94 mM; and *N*, 0.78 mM) was achieved, with more than 90% TOC removal after only 15-min reaction time, working at 120 °C, $pH_0 = 3$, AC at 1 g L^{-1}, and H_2O_2 at the stoichiometric dose. Furthermore, in the case of toluene, naphthalene, and xylene, the hydroxylation and breakdown of the ring is very rapid and toxic intermediates were not detected. The process follows two steps: (i) pollutant adsorption onto AC followed by (ii) adsorbed compounds oxidation. Thus, MW-CWPO with AC as catalyst appears a promising way for a fast and effective process for *B*, *T*, *X*, and *N* removal in aqueous phase.

Keywords Microwave · CWPO · Activated carbon · BTXN · Mineralization · AOP

Introduction

Nowadays, there is an increasing concern on water quality due to the scarcity of this resource. Aromatic hydrocarbons such as benzene (*B*), toluene (*T*), o-xylene (*X*), and naphthalene (*N*) are potential water pollutants from the petrochemical industry. These species imply a high risk for human health and the environment due to their highly toxic and non-readily biodegradable character (Kang et al. 2014).

Their removal from water has been studied by physical or physicochemical methods including coagulation (Steliga et al. 2015), electrocoagulation (Gong et al. 2017), adsorption (Lutynski and Suponik 2014; Qi et al. 2017; Valderrama et al. 2008), and filtration (Smol et al. 2017). Nonetheless, this kind of treatments only transfers the pollutants into another phase. In the past few years, surfactant-enhanced biological remediation of these contaminants has gained attention. This technique consists in the addition of surfactants to increase the solubility of these compounds making them bioavailable (Lamichhane et al. 2017; Wei et al. 2016). Nevertheless, surfactants can inhibit microbial activity besides introducing additional contamination.

In this scenario, advanced oxidation processes (AOP) can provide a feasible solution (Mota 2008). These are based on the generation of strong oxidizing agents, mainly hydroxyl radicals (HO·), highly reactive species. Among the AOPs, catalytic wet peroxide oxidation (CWPO) has gained attention in the past two decades. This process is based in the redox decomposition of H_2O_2 under mild or moderate working conditions (*T*, 25–120 °C; *P*, 1–5 bar) with a solid catalyst giving rise to both hydroxyl and hydroperoxyl (HOO·) radicals (Dominguez et al. 2013; Zazo et al. 2006). A current trend in AOPs is the intensification of the existing techniques (Pliego et al. 2015). This intensification can be accomplished by rising the temperature (Zazo et al. 2011), with electrochemical methods (Yavuz et al. 2010) or applying different kinds of energy sources: UV-light (Mascolo et al. 2008; Zazo et al. 2016), ultrasound (Psillakis et al. 2004; Ramteke and Gogate 2015), or microwaves (Atta et al. 2012; Nascimento and Azevedo 2013; Pan et al. 2015). Microwave (MW)-assisted AOPs represent a rising and promising technology. MW

Responsible editor: Vítor Pais Vilar

Electronic supplementary material The online version of this article (https://doi.org/10.1007/s11356-018-2291-9) contains supplementary material, which is available to authorized users.

✉ Alicia L. Garcia-Costa
alicial.garcia@uam.es

[1] Universidad Autonoma de Madrid, Crta Colmenar Viejo km 15, 28049 Madrid, Spain

Published online: 21 May 2018

provides higher heating rates and thus, higher reaction rates, resulting in an improved energy efficiency (Wang and Wang 2016).

Table 1 summarizes previous intensified oxidation processes used in the treatment of *B*, *T*, *X*, and *N* and petrochemical wastewater containing these compounds. Abussaud et al. (2008) studied the wet air oxidation (WAO) of benzene. Although this is an effective technique, it requires high temperature and pressure in order to solubilize and activate O_2. To decrease the operating costs, different AOP have been developed as cost-efficient alternatives. In this sense, Ramteke and Gogate (2015) studied both Fenton and US/H_2O_2 processes for the removal of *B*, *T*, *X*, and *N* in aqueous phase. Fenton process reached almost complete pollutant removal in all cases but no TOC or COD removal data were provided. On the other hand, US/H_2O_2 presented a very poor performance in the removal of these compounds. Furthermore, the experimental section is not clear with respect to the composition of the treated influents. Those are referred in terms of COD which correspond to concentrations of *B*, *T*, *X*, and *N*, shown in Table 1 that are impossible to be solubilized in water. Tiburtius et al. (2005) achieved complete pollutant removal in UV/Fenton after 90 min. Nonetheless, the mineralization degree was very low. Furthermore, no data on the oxidation by-products was reported. Thus, there could be remaining recalcitrant toxic compounds such as quinones.

Previous work showed that the dielectric properties of the catalyst or support play a crucial role on MW-CWPO (Garcia-Costa 2017). The rapid pollutant degradation in the MW system with an MW-adsorbent, like activated carbon, is mainly due to the hot-spot formation on its surface, which is a unique mechanism for MW. This is essential to speed-up reactions in many processes. Generally, the delocalized π-electrons in the surface of the AC are free to move. During the MW irradiation, the kinetic energy of electrons on the surface of the AC increases, which enables the electrons to jump out of the material resulting in the formation of hot spots by ionizing the surrounding atmosphere (Menéndez et al. 2010). These hot

Table 1 Oxidation processes used for *B*, *T*, *X*, *N* depletion

AOP	Pollutant	Operating conditions	Pollutant removal	TOC/COD removal	Reference
WAO	*B*	*B*, 5.63 mM Temp, 300 °C *P*, 1.72 MPa *t*, 30 min	100%	X_{TOC}, 87%	(Abussaud et al. 2008)
Fenton	*B*, *T*, *X*, *N*	*B*, 28.7 mM *T*, 11.8 mM *X*, 8.3 mM *N*, 6.7 mM Fe^{2+} 3 g/L H_2O_2, 58.82 mM *t*, 40 min	*B*, 97.6% *T*, 97.5% *X*, 98.3% *N*, 93.9%		(Ramteke and Gogate 2015)
US/H_2O_2	*B*, *T*, *X*, *N*	*B*, 28.7 mM *T*, 11.8 mM *X*, 8.3 mM *N*, 6.7 mM US, 22 kHz H_2O_2, 58.82 mM *t*, 40 min	*B*, 34% *T*, 35% *X*, 28% *N*,24%		(Ramteke and Gogate 2015)
UV/Fenton	*B*, *T*, *X*	*B*, 0.26 mM *T*, 0.22 mM *X*, 0.19 mM TiO_2, 50 mg/L Fe^{2+} 10 mg/L H_2O_2, 2.95 mM *t*, 90 min	100%	X_{TOC}, 30%	(Tiburtius et al. 2005)
UV/TiO_2	Petrochem. wastewater	COD, 175 mg/L TiO_2, 100 mg/L *T*, 45 °C *t*, 240 min	–	X_{COD}, 90%	(Saien and Nejati 2007)

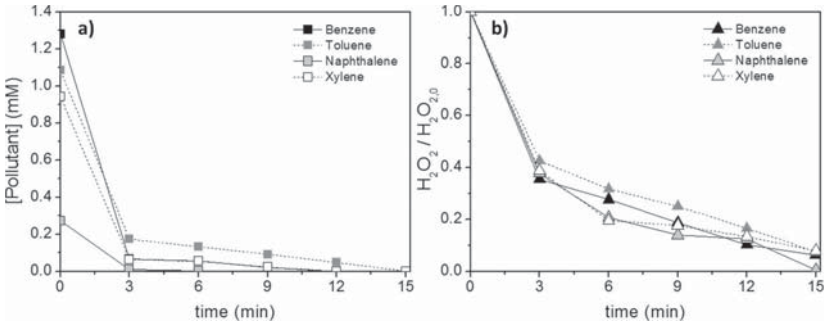

Fig. 1 **a** Pollutant and **b** H_2O_2 evolution upon MW-CWPO of *B*, *T*, *X* and *N*; $C_{B,0}$, 1.28 mM; $C_{T,0}$, 1.09 mM; $C_{X,0}$, 0.94 mM; $C_{N,0}$, 0.78 mM; $C_{H2O2,0}$ stoichiometric; C_{AC}, 1 g L^{-1}; *T*, 120 °C; pH,3

spots, which may reach 1200 °C (Remya and Lin 2011), enhance the oxidation processes boosting both HO_X generation and oxidation rate and degrading the condensed by-products typically found in the oxidation of aromatic compounds (Garcia-Costa 2017). Thus, in this work, we address the degradation of *B*, *T*, *X*, and *N* by MW-CWPO using bare AC as catalyst.

Material and methods

Reactants

Synthetic waters containing known amounts of the contaminants were prepared with benzene (99%, Sigma-Aldrich), toluene (99,99%, Sigma-Aldrich), o-xylene (98%, Sigma-Aldrich) naphthalene (99%, Sigma-Aldrich), and H_2O_2 (30% *w*/*v*; Panreac), respectively, at pH 3 using HCl (37% *w*/*v*; Panreac).

Commercial activated carbon was supplied by Merck (ACM, ref. 102514, granular). Complete analysis of this AC can be found elsewhere (Dominguez et al. 2013). In brief, this material contains 4% ashes in dry basis, 89.3% C, 0.9% H, 0.5% N, 0.6% S, with traces of Cl, Fe, Zn, Pb, and As. It has 991 m^2/g BET surface area, corresponding 17% to external or non-microporous area.

H_2SO_4 (96 wt.%; Panreac), acetonitrile (Sigma-Aldrich), and H_3PO_4 (85 wt.%; Sigma-Aldrich) were used in the analytic procedure. Working standard solutions of phenol, catechol, resorcinol, hydroquinone, p-benzoquinone, and organic acids (fumaric, malonic, maleic, acetic, and formic from Sigma-Aldrich and oxalic from Panreac) were prepared for equipment calibration. All reagents are analytical grade and they were used as received without further purification. Milli-Q water was used throughout the work.

MW-CWPO experiments

MW-CWPO runs were performed in high pressure PTFE reaction vessels located in a microwave furnace (FlexiWAVE, Milestone). The experiments were conducted in batch using 100-mL stoppered PTFE reactors which were initially loaded with aqueous pollutant solution (*B*, 1.28 mM, *T*, 1.09 mM, *X*, 0.94 mM, and *N*, 0.78 mM), activated carbon at 1 g L^{-1} and H_2O_2 (theoretical stoichiometric dose for each pollutant, that is 17.82 mM for *B*, 17.83 mM for *T*, 19.93 mM for *X*, and 7.03 mM for *N*). Right after the H_2O_2 addition, reactors were tightly sealed and placed in the microwave oven. Heating rate was set at 80 °C/min to reach the reaction temperature 120 °C, which was maintained for 15 min. Catalyst is kept in suspension by magnetic stirring at 400 rpm. During reaction pressure rose up to 2.4 bar.

Analytical methods

Samples were periodically withdrawn and placed in an ice bath to reduce the temperature and quench the reaction. Afterwards samples were immediately analyzed after filtration through fiber glass filters (Albet FV-C). *B*, *T*, *X*, *N* and aromatic intermediates were identified and quantified by means of an Ultra HPLC (Thermo Scientific Ultimate 3000) with a diode array detector (Dionex Ultimate 3000). An ion-exclusion column (ZORBAX Eclipse Plus C18, 100 mm, 1.8 μm) was used as stationary phase. As mobile phases, a mix of 50% acetonitrile and 50% 4 mM H_2SO_4 aqueous solution at 1 mL/min was used for *B*, *T*, *X*, and N and only H_2SO_4 aqueous solution at 1 mL/min as mobile phase for aromatic intermediates. UV detector at 210 nm wavelength was used for *B*, *T*, *X*, *N*, phenol, resorcinol, catechol, and hydroquinone and at 246 nm for p-benzoquinone. Short-chain organic acids were analyzed in an ion chromatograph with chemical suppression (Metrohm 790 IC) using a conductivity detector. A Metrosep A supp 5-250 column (25 cm long, 4 mm diameter) was used as stationary phase and 0.7 mL/min of a 3.2 mM/1 mM aqueous solution of Na_2CO_3 and $NaHCO_3$, respectively, as mobile phase. Total organic carbon was measured using a TOC analyzer (Shimadzu TOC-VSCH). Residual H_2O_2 in the liquid phase was determined by colorimetric titration with an Agilent spectrophotometer using the $TiOSO_4$ method (Eisenberg 1943).

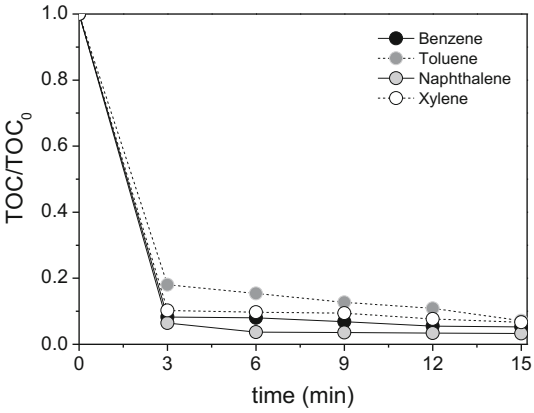

Fig. 2 TOC evolution upon MW-CWPO of $C_{B,0}$, 1.28 mM; $C_{T,0}$, 1.09 mM; $C_{X,0}$, 0.94 mM; $C_{N,0}$, 0.78 mM; $C_{H2O2,0}$, stoichiometric; C_{AC}, 1 g L^{-1}; *T*, 120 °C; pH 3

Thermogravimetric analyses (TGA) of the fresh, used, and pollutant saturated AC were performed in a thermoscale TGA Q500 (TA Instruments). Runs were conducted under N_2 flow at 800 °C, reached at 10 °C/min heating rate.

Results and discussion

The MW/AC/H_2O_2 system is active and capable of eliminating the aromatic species tested in aqueous phase after 15 min of reaction time under the operating conditions described before. All these compounds exhibited a similar behavior, disappearing quite rapidly within 3 min. That covers most of the conversion percentage and then complete disappearance was reached at slower rate but always in less than 15 min. This seems to be related to the adsorption of the target pollutants or a rapid formation of aromatic intermediates including condensation by-products (Dominguez et al. 2014; Garcia-Costa 2017; Suarez-Ojeda et al. 2005; Zazo et al. 2005) which can be adsorbed onto the active centers of the carbon and, therefore, disappear from the medium.

The evolution of H_2O_2 follows a similar trend to that of the pollutants. At the beginning, H_2O_2 is transformed to HO_X· radicals, although their production rate decreases with oligomeric formation and sorption over activated carbon. Its decomposition seems to follow a first order kinetics as H_2O_2 conversion is independent of its initial concentration, as can be seen in Fig. 1b. After the initial stages, H_2O_2 decomposition rate depends on the number of active centers that are covered by the oligomer formed in the initial stages. On the other hand, this oligomer is oxidized and removed from the surface of the catalyst as the time evolves. Almost complete H_2O_2 conversion was achieved at 15 min in all cases. Hence, MW greatly enhances the rate of decomposition compared to traditional CWPO (Garcia-Costa 2017).

Figure 2 shows the evolution of total organic carbon (TOC). It follows a fairly similar pattern to that observed in Fig. 1 for the pollutants conversion. Thus, the disappearance of the target compound seems to be accompanied in all cases by both adsorption and a rapid breakdown towards complete oxidation. The remaining TOC in solution after the initial stage corresponds to short organic acids, more resistant to mineralization. Nevertheless, TOC decay during the first minutes of reaction is not consistent with the H_2O_2 decomposition, which is slower. For the sake of comparison, blank experiments in absence of H_2O_2 were performed. Results, shown in Fig. S1 of the supporting information, reveal an adsorption around 70% of the target pollutants. These results would be in agreement to the combined adsorption-oxidation mechanism proposed in which the pollutants and oligomeric by-products are initially adsorbed onto AC, as previously described by Dominguez et al. (2013). Consequently, there is a higher TOC decrease than the one expected in relation to the oxidant consumption. Therefore, with these active centers occupied, the H_2O_2 decomposition is slowed down. The adsorbed by-products are later mineralized, being the catalyst partially regenerated. The availability of the active sites could explain the different slopes observed in Figs. 1 and 2. It is important to remark the high TOC removal achieved in short term, most in particular of naphthalene, a representative PAH. In this regard, the combined use of AC as adsorbent and MW-

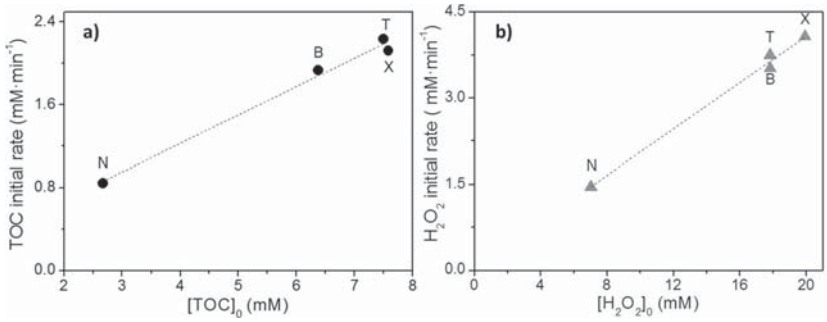

Fig. 3 Initial reaction rates of TOC and H_2O_2 disappearance versus the initial concentrations (R^2_{TOC} = 0.9828, R^2_{H2O2} = 0.9903)

Table 2 Kinetic parameters for TOC and H_2O_2 from minutes 3 to 12 of reaction

	Compound	k_{App} (min^{-1})	R^2
TOC	Benzene	5.1×10^{-2}	0.965
	Toluene	5.7×10^{-2}	0.998
	Naphthalene	9.7×10^{-2}	0.959
	Xylene	3.2×10^{-2}	0.952
H_2O_2	Benzene	1.36×10^{-1}	0.963
	Toluene	1.01×10^{-1}	0.979
	Naphthalene	1.43×10^{-1}	0.957
	Xylene	1.22×10^{-1}	0.989

CWPO catalyst presents a low-cost feasible alternative in relation to the previous AOP studied for *B*, *T*, *X*, and *N* removal.

The TOC and H_2O_2 initial reaction rates were calculated. As can be seen in Fig. 3, there is a relationship between these initial rates and the starting concentration used in each experiment. That confirms an apparent first-order kinetics for both, TOC and H_2O_2.

This model has been used to fit the experimental data and the values of the apparent kinetic constant are collected in Table 1. The corresponding plots can be found in Figs. S2 and S3 of the supporting information. Xylene yielded the slowest mineralization rate, related to its methyl group. These are hydroxylated by HO_X· radicals giving rise to formic and acetic acids, which are highly resistant to further oxidation. On the other hand, the mechanism of H_2O_2 decomposition is the same in all cases, resulting in similar rate constants (Table 2).

Oxidation pathway

The evolution of the reaction by-products identified from MW-CWPO of *B*, *T*, *X*, and *N* is depicted in Fig. 4. The results suggest a similar route than the one previously reported for conventional CWPO of phenol (Dominguez et al. 2013). The starting pollutants and aromatic intermediates can follow two different paths. In the first one, there is rapid hydroxylation, which leads to the opening of the aromatic ring, thus no aromatic intermediates such as catechol, benzoquinone, hydroquinone, or resorcinol were detected in solution. On the other hand, the hydroxylation process can produce aromatic radicals which can give rise to condensation oligomeric species (Zazo et al. 2005). These condensation by-products (CBP), along with the target pollutants, can be quickly adsorbed by the activated carbon and removed from water. Once adsorbed, they are oxidized by HO_X· yielding organic acids that are released to the aqueous medium. Malonic, maleic, oxalic, acetic, and formic acids were detected. Higher acids are oxidized to acetic and formic, which are more resistant to CWPO. The proposed oxidation pathway is illustrated in Fig. 5.

The oxidation by-products identified in solution accounted for more than 98% of the measured TOC, indicating no significant amounts of condensation by-products (CBP) were in the aqueous phase.

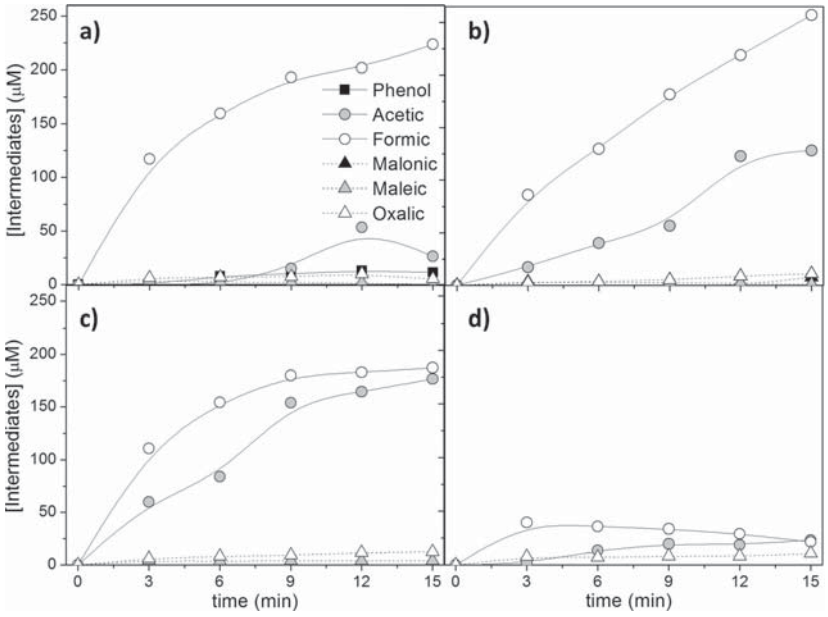

Fig. 4 Time course of intermediates upon MW-CWPO of **a** benzene, **b** toluene, **c** xylene, and **d** naphthalene

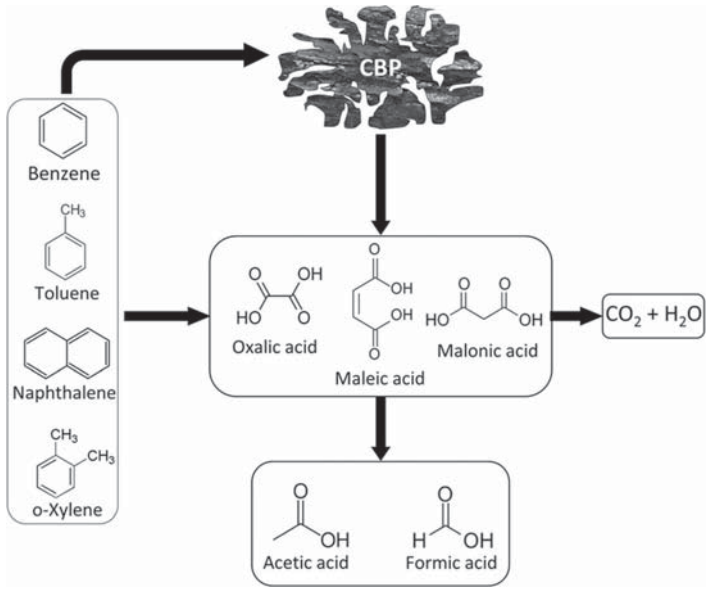

Fig. 5 Reaction pathway

Thermogravimetric analyses (TGA) in inert N_2 atmosphere of the fresh AC, AC after pollutant adsorption in MW-AC and AC after MW-CWPO were carried out. The results are shown in Fig. 6. In all cases adsorbed matter is remaining on the AC after reaction. Starting pollutants and oligomeric by-products remain partially adsorbed onto AC and are not totally oxidized in the studied conditions. Regardless of the target compounds which are desorbed around 300–450 °C, the oligomeric by-products are highly stable, starting its decomposition at 700 °C. It should be remarked that MW-CWPO achieves the degradation of above 50% of the initial adsorbed compounds. Taking into account the adsorbed species and TOC, an estimation of the mineralized carbon has been calculated, as shown in Fig. S4 of the supporting information. In brief,

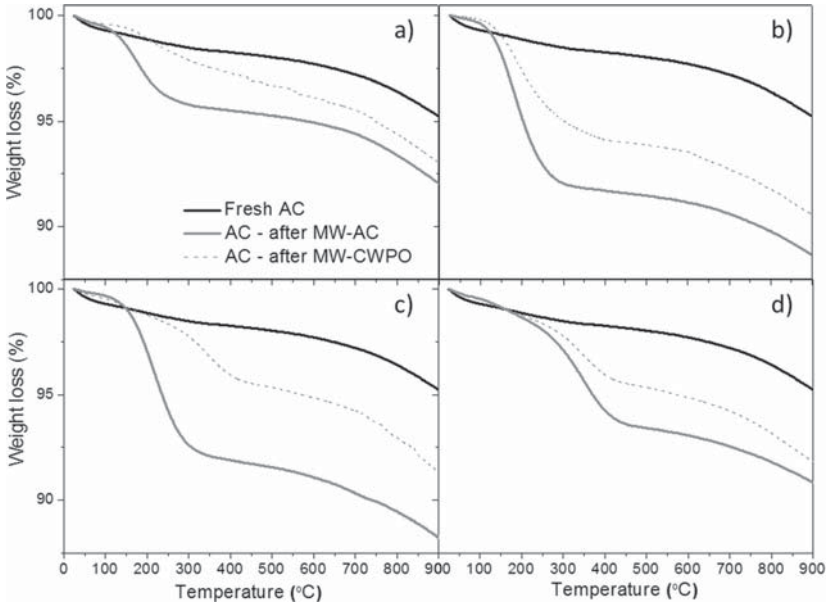

Fig. 6 TGA-N_2 profiles for fresh AC, MW-AC, and used AC in MW-CWPO of **a** benzene, **b** toluene, **c** xylene, and **d** naphthalene

TGA analyses confirm the proposed adsorption-oxidation mechanism in which AC acts as both pollutant adsorbent and MW-CWPO catalyst, reaching complete *B*, *T*, *X*, and *N* removal from water.

Conclusions

MW-CWPO with AC has proven to be effective for the removal of *B*, *T*, *X*, and *N* in aqueous phase. AC acts as both adsorbent and catalyst in a complex mechanism implying the adsorption of the target pollutants or oligomeric by-products. Then, HO_X· achieve both pollutant oxidation and catalyst partial regeneration, upon MW-assisted CWPO. Complete pollutant elimination from the aqueous phase and up to 97% TOC removal was achieved in fairly short time (15 min) under the testing conditions (120 °C, $pH_0 = 3$, H_2O_2 at the stoichiometric dose, and AC at 1 g L^{-1}). The evolution of the reaction by-products suggests a fast oxidation towards non-toxic carboxylic acids with no aromatic intermediates detected in the aqueous phase.

Funding information Authors would like to thank the Spanish *Ministerio de Economía y Competitividad* (MINECO) for financial support through project CTM2016-76454-R. A.L. Garcia-Costa acknowledges the *European Social Fund* and MINECO for PhD grant BES-2014-067598.

References

Abussaud BA, Ulkem N, Berk D, Kubes GJ (2008) Wet air oxidation of benzene. Ind Eng Chem Res 47:4325–4331. https://doi.org/10.1021/ie800162j

Atta AY, Jibril BY, Al-Waheibi TK, Al-Waheibi YM (2012) Microwave-enhanced catalytic degradation of 2-nitrophenol on alumina-supported copper oxides. Catal Commun 26:112–116. https://doi.org/10.1016/j.catcom.2012.04.033

Dominguez CM, Ocon P, Quintanilla A, Casas JA, Rodriguez JJ (2013) Highly efficient application of activated carbon as catalyst for wet peroxide oxidation. Appl Catal B Environ 140:663–670. https://doi.org/10.1016/j.apcatb.2013.04.068

Dominguez CM, Ocon P, Quintanilla A, Casas JA, Rodriguez JJ (2014) Graphite and carbon black materials as catalysts for wet peroxide oxidation. Appl Catal B Environ 144:599–606. https://doi.org/10.1016/j.apcatb.2013.07.069

Eisenberg GM (1943) Colorimetric determination of hydrogen peroxide. Ind Eng Chem Anal Ed 15:327–328. https://doi.org/10.1021/i560117a011

Garcia-Costa AL, Zazo JA, Casas JA, Rodriguez JJ (2017) Microwave-assisted catalytic wet peroxide oxidation. Comparison of Fe catalysts supported on activated carbon and g-alumina. Appl Catal B Environ 218:5–642. https://doi.org/10.1016/j.apcatb.2017.06.058

Gong CH, Shen G, Huang HO, He PR, Zhang ZG, Ma BQ (2017) Removal and transformation of polycyclic aromatic hydrocarbons during electrocoagulation treatment of an industrial wastewater. Chemosphere 168:58–64. https://doi.org/10.1016/j.chemosphere.2016.10.044

Kang HJ, Lee SY, Roh JY, Yim UH, Shim WJ, Kwon JH (2014) Prediction of Ecotoxicity of heavy crude oil: contribution of measured components. Environ Sci Technol 48:2962–2970. https://doi.org/10.1021/es404342k

Lamichhane S, Krishna KCB, Sarukkalige R (2017) Surfactant-enhanced remediation of polycyclic aromatic hydrocarbons: a review. J Environ Manag 199:46–61. https://doi.org/10.1016/j.jenvman.2017.05.037

Lutynski M, Suponik T (2014) Hydrocarbons removal from underground coal gasification water by organic adsorbents. Physicochem Probl Miner Process 50:289–298. https://doi.org/10.5277/ppmp140124

Mascolo G, Ciannarella R, Balest L, Lopez A (2008) Effectiveness of UV-based advanced oxidation processes for the remediation of hydrocarbon pollution in the groundwater: a laboratory investigation. J Hazard Mater 152:1138–1145. https://doi.org/10.1016/j.jhazmat.2007.07.120

Menéndez JA, Arenillas A, Fidalgo B, Fernández Y, Zubizarreta L, Calvo EG, Bermúdez JM (2010) Microwave heating processes involving carbon materials. Fuel Process Technol 91:1–8. https://doi.org/10.1016/j.fuproc.2009.08.021

Mota ALN, Albuquerque LF, Beltrame LTC, Chiavone-Filho O, Machulek A Jr, Nascimento CAO (2008) Advanced oxidation processes and their application in the petroleum industry: a review. Brazilian Journal of Petroleum and Gas 2:20

Nascimento UM, Azevedo EB (2013) Microwaves and their coupling to advanced oxidation processes: enhanced performance in pollutants degradation. J Environ Sci Health A Tox Hazard Subst Environ Eng 48:1056–1072. https://doi.org/10.1080/10934529.2013.773822

Pan W, Zhang G, Zheng T, Wang P (2015) Degradation of p-nitrophenol using CuO/Al2O3as a Fenton-like catalyst under microwave irradiation. RSC Adv 5:27043–27051. https://doi.org/10.1039/c4ra14516j

Pliego G, Zazo JA, Garcia-Munoz P, Munoz M, Casas JA, Rodriguez JJ (2015) Trends in the intensification of the Fenton process for wastewater treatment: an overview. Crit Rev Environ Sci Technol 45:2611–2692. https://doi.org/10.1080/10643389.2015.1025646

Psillakis E, Goula G, Kalogerakis N, Mantzavinos D (2004) Degradation of polycyclic aromatic hydrocarbons in aqueous solutions by ultrasonic irradiation. J Hazard Mater 108:95–102. https://doi.org/10.1016/j.jhazmat.2004.01.004

Qi JW, Li J, Li Y, Fang X, Sun X, Shen J, Han W, Wang L (2017) Synthesis of porous carbon beads with controllable pore structure for volatile organic compounds removal. Chem Eng J 307:989–998. https://doi.org/10.1016/j.cej.2016.09.022

Ramteke LP, Gogate PR (2015) Treatment of toluene, benzene, naphthalene and xylene (BTNXs) containing wastewater using improved biological oxidation with pretreatment using Fenton/ultrasound based processes. J Ind Eng Chem 28:247–260. https://doi.org/10.1016/j.jiec.2015.02.022

Remya N, Lin J-G (2011) Current status of microwave application in wastewater treatment—a review. Chem Eng J 166:797–813. https://doi.org/10.1016/j.cej.2010.11.100

Saien J, Nejati H (2007) Enhanced photocatalytic degradation of pollutants in petroleum refinery wastewater under mild conditions. J Hazard Mater 148:491–495. https://doi.org/10.1016/j.jhazmat.2007.03.001

Smol M, Wlodarczyk-Makula M, Skowron-Grabowska B (2017) PAHs removal from municipal landfill leachate using an integrated membrane system in aspect of legal regulations. Desalin Water Treat 69:335–343. https://doi.org/10.5004/dwt.2017.20241

Steliga T, Jakubowicz P, Kapusta P (2015) Changes in toxicity during treatment of wastewater from oil plant contaminated with petroleum hydrocarbons. J Chem Technol Biotechnol 90:1408–1418. https://doi.org/10.1002/jctb.4442

Suarez-Ojeda ME, Stuber F, Fortuny A, Fabregat A, Carrera J, Font J (2005) Catalytic wet air oxidation of substituted phenols using

activated carbon as catalyst. Appl Catal B Environ 58:105–114. https://doi.org/10.1016/j.apcatb.2004.11.017

Tiburtius ERL, Peralta-Zamora P, Emmel A (2005) Treatment of gasoline-contaminated waters by advanced oxidation processes. J Hazard Mater 126:86–90. https://doi.org/10.1016/j.jhazman.2005.06.003

Valderrama C, Gamisans X, de las Heras X, Farran A, Cortina JL (2008) Sorption kinetics of polycyclic aromatic hydrocarbons removal using granular activated carbon: intraparticle diffusion coefficients. J Hazard Mater 157:386–396. https://doi.org/10.1016/j.jhazmat.2007.12.119

Wang N, Wang P (2016) Study and application status of microwave in organic wastewater treatment—a review. Chem Eng J 283:193–214. https://doi.org/10.1016/j.cej.2015.07.046

Wei J, Li J, Huang GH, Wang XJ, Chen GH, Zhao BH (2016) Adsorptive removal of naphthalene induced by structurally different Gemini surfactants in a soil-water system. Environ Sci Pollut Res 23:18034–18042. https://doi.org/10.1007/s11356-016-6966-9

Yavuz Y, Koparal AS, Ogutveren UB (2010) Treatment of petroleum refinery wastewater by electrochemical methods. Desalination 258:201–205. https://doi.org/10.1016/j.desal.2010.03.013

Zazo JA, Casas JA, Mohedano AF, Gilarranz MA, Rodriguez JJ (2005) Chemical pathway and kinetics of phenol oxidation by Fenton's reagent. Environ Sci Technol 39:9295–9302. https://doi.org/10.1021/es050452h

Zazo JA, Casas JA, Mohedano AF, Rodriguez JJ (2006) Catalytic wet peroxide oxidation of phenol with a Fe/active carbon catalyst. Appl Catal B Environ 65:261–268. https://doi.org/10.1016/j.apcatb.2006.02.008

Zazo JA, Pliego G, Blasco S, Casas JA, Rodriguez JJ (2011) Intensification of the Fenton process by increasing the temperature. Ind Eng Chem Res 50:866–870. https://doi.org/10.1021/ie101963k

Zazo JA, Pliego G, García-Muñoz P, Casas JA, Rodriguez JJ (2016) UV-LED assisted catalytic wet peroxide oxidation with a Fe(II)-Fe(III)/activated carbon catalyst. Appl Catal B Environ 192:350–356. https://doi.org/10.1016/j.apcatb.2016.04.010

Supporting information

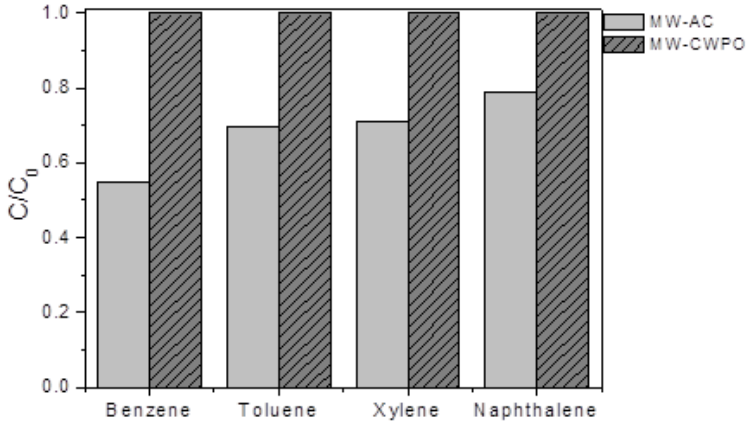

Figure S1. B, T, X and N removal in MW-AC and MW-CWPO for $C_{B,0}$: 1.28 mM, $C_{T,0}$: 1.09 mM, $C_{X,0}$: 0.94 mM, $C_{N,0}$: 0.78 mM, $C_{H2O2,0}$: MW-AC: 0, MW-CWPO: stoichiometric, C_{AC}: 1 g·L^{-1}, t: 15 min, T: 120ºC, pH_0:3

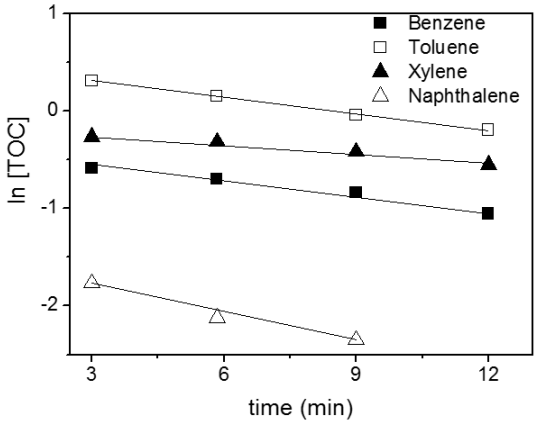

Figure S2. Pseudo-first order plot for TOC in MW-CWPO for $C_{B,0}$: 1.28 mM, $C_{T,0}$: 1.09 mM, $C_{X,0}$: 0.94 mM, $C_{N,0}$: 0.78 mM, $C_{H2O2,0}$: stoichiometric, C_{AC}: 1 g·L^{-1}, T: 120ºC, pH_0:3

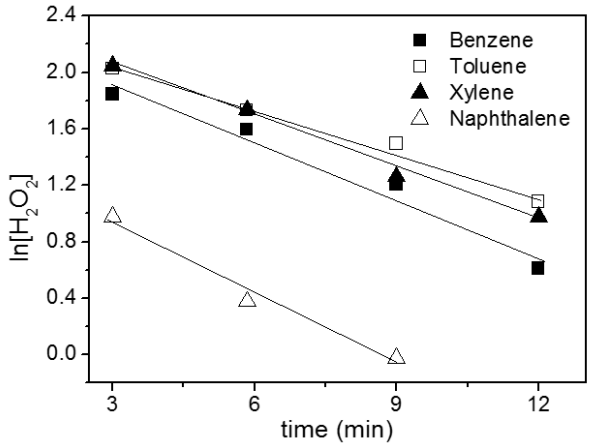

Figure S3. Pseudo-first order plot for H_2O_2 in MW-CWPO for $C_{B,0}$: 1.28 mM, $C_{T,0}$: 1.09 mM, $C_{X,0}$: 0.94 mM, $C_{N,0}$: 0.78 mM, $C_{H2O2,0}$: stoichiometric, C_{AC}: 1 g·L^{-1}, T: 120°C, pH_0:3

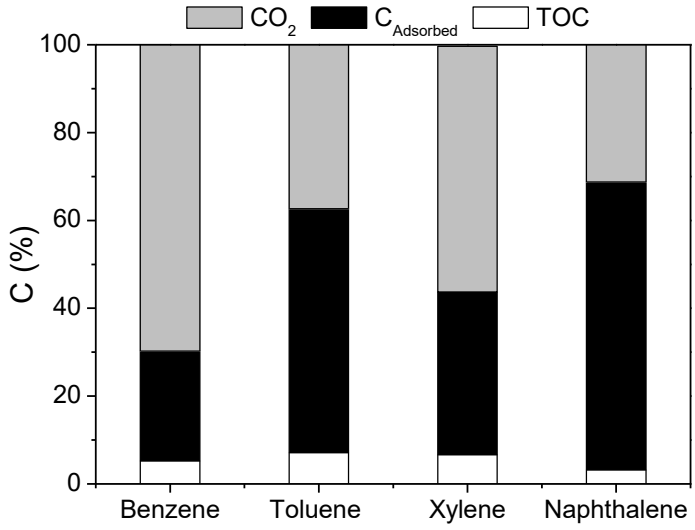

Figure S4. Carbon balance at t:15 min.

5.3. Intensification of Catalytic Wet Peroxide Oxidation with Microwave radiation: activity and stability of carbon materials

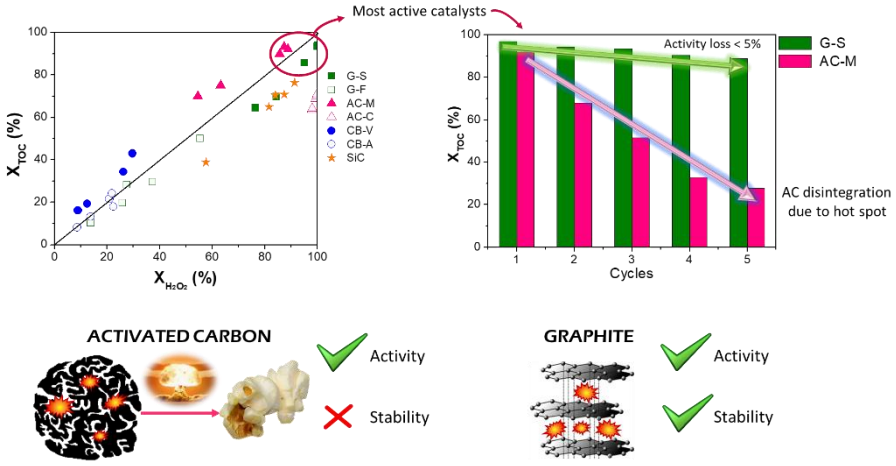

Separation and Purification Technology 209 (2019) 301–306

Contents lists available at ScienceDirect

Separation and Purification Technology

journal homepage: www.elsevier.com/locate/seppur

Intensification of catalytic wet peroxide oxidation with microwave radiation: Activity and stability of carbon materials

Alicia L. Garcia-Costa*, Juan A. Zazo, Juan J. Rodriguez, Jose A. Casas

Chemical Engineering Departamental Section, School of Science, Universidad Autonoma de Madrid, Ctra. Colmenar Viejo km. 15, Madrid 28049, Spain

ARTICLE INFO

Keywords:
CWPO
Microwave
Activated carbon
Graphite
Hot spot

ABSTRACT

Several commercial carbon materials have been tested as catalysts in the Microwave-assisted Catalytic Wet Peroxide Oxidation process (MW-CWPO). Two graphites (G-F and G-S), two activated carbons (AC-M and AC-C), two carbon blacks (CB-V and CB-A) and silicon carbide (SiC) were selected due to their MW-absorbing properties. Phenol (100 mg L^{-1}) was used as target pollutant, operating in batch at pH_0 3, 120 °C, 500 mg L^{-1} catalyst load and the theoretical stoichiometric amount of H_2O_2 (500 mg L^{-1}). All carbon materials showed to be active in terms of H_2O_2 decomposition and phenol oxidation. Nonetheless, G-S and AC-M stood out as the most active materials in terms of TOC removal, with values of 94 and 93% TOC elimination, respectively. On the other hand, both carbon blacks and G-F yielded a significantly lower TOC degradation. Surface chemistry seems to rule the activity of graphites, in particular the pH slurry (4.5 for G-S and 8.4 for G-F). The most active catalysts, G-S and AC-M were used in 5 consecutive cycles in order to study their stability. While G-S remained active, AC-M.

1. Introduction

Public and governmental concern on water quality challenges engineers to find new or enhanced technologies for wastewater treatment, particularly when facing bio-refractory pollutants. Catalytic Wet Peroxidation (CWPO) appears to be a potential solution. This Advanced Oxidation Process (AOP) consists a heterogeneous version of the Fenton process, based on the redox decomposition of H_2O_2 into hydroxyl ($HO^{\cdot}$) and hydroperoxyl radicals ($HOO^{\cdot}$). These species present high oxidation potentials, high reactivity and low selectivity, allowing the breakdown of organic recalcitrant pollutants. Furthermore, this is an environmentally friendly technology, since H_2O_2 decomposition yields non-toxic byproducts. CWPO catalysts frequently consist on a metallic phase (Fe, Cu) supported on activated carbon, alumina or other porous materials [1–5]. Nonetheless, catalyst deactivation due to metal leaching is usual, generating a new environmental problem. To overcome this issue, several authors have successfully employed bare carbon materials such as activated carbon, graphite or carbon black as CWPO catalysts [6–10].

CWPO intensification has been studied in the past decades, addressed to improve both the overall efficiency of the process and the catalyst stability [11]. In this sense, several strategies have been checked, like working at higher temperature [10,12], or applying different radiations, such as UV–vis [13,14], ultrasounds [15] and microwaves (MW) [16–22]. Within these new processes, microwave-assisted CWPO (MW-CWPO) offers a promising way allowing to work at higher temperature with a more efficient heating. Besides, when using MW absorbers, such as carbon materials, hot spot formation on their surface can occur. Delocalized π-electrons in the surface of carbon materials are free to move. The kinetic energy of these electrons increases upon MW irradiation, generating micro-plasmas, or hot spots, and ionizing the surrounding atmosphere These hot spots may reach up to 1200 °C and have a synergistic effect on CWPO, boosting $HO_X^{\cdot}$ generation [22–25].

Table 1 summarizes the most recent applications of MW-CWPO for wastewater treatment. Research efforts are being addressed on the development of complex nanocomposites and their applications in MW-CWPO, with some outstanding results [26–29]. Nonetheless, a better knowledge is needed on key issues such as H_2O_2 decomposition, pollutants mineralization, degradation pathways and catalysts stability. Furthermore, even the reported operating conditions need to be clarified in some cases. Thus, additional systematic research is required to better understand the MW-CWPO process.

Previous work has shown that bare activated carbon (AC) yielded practically the same activity than Fe/AC catalysts (Fe: 4 wt% as Fe_2O_3) in MW-CWPO process, due to its MW absorbing properties, [30]. Hence, the use of carbon materials can offer a low-cost and feasible alternative to tailor-made traditional CWPO catalysts.

* Corresponding author.
E-mail address: alicial.garcia@uam.es (A.L. Garcia-Costa).

https://doi.org/10.1016/j.seppur.2018.07.054
Received 23 April 2018; Received in revised form 19 July 2018; Accepted 20 July 2018
Available online 20 July 2018
1383-5866/

Table 1
Recent works on MW-CWPO.

Pollutant	Catalyst	Operating conditions	Results	Ref.
Methyl orange (MO)	$NiFeMnO_4$	C_{MO}: 30 mg L^{-1} C_{cat}: 1 g L^{-1} C_{H2O2}: 30 mg L^{-1} t: 60 min pH_0: 2–3 T: 50 °C P: 750 W	X_{MO}: 97%	[26]
Orange G (OG)	rGO-TiO_2	C_{MO}: 4.5 mg L^{-1} C_{cat}, C_{H2O2}, t and pH_0: unknown T: 30–120 °C P: 300 W	X_{OG}: 90%	[27]
Perfluorooctanoic acid (PFOA)	Pb-$BiFeO_3$/rGO	C_{PFOA}: 50 mg L^{-1} C_{cat}: 1 g L^{-1} C_{H2O2}: 44 mg L^{-1} t: 5 min pH_0: 5 T: unknown P: 500 W	X_{PFOA}: 87% X_{TOC}: 52%	[28]
Phenol	CuO_X/GAC	C_{Phenol}: 100 mg L^{-1} C_{cat}: 3 g L^{-1} C_{H2O2}: 600 mg L^{-1} t: 5 min pH_0: 4 T: unknown P: 400 W	X_{Phenol}: 100% X_{COD}: 90%	[29]
Phenol	Fe/AC	C_{Phenol}: 100 mg L^{-1} C_{cat}: 0.1 g L^{-1} C_{H2O2}: 500 mg L^{-1} t: 60 min pH_0: 3 T: 120 °C P: variable P_{MAX}: 1800 W	X_{Phenol}: 100% X_{H2O2}: 100% X_{TOC}: 87%	[30]
Phenol	AC	C_{Phenol}: 100 mg L^{-1} C_{cat}: 0.1 g L^{-1} C_{H2O2}: 500 mg L^{-1} t: 60 min pH_0: 3 T: 120 °C P: variable P_{MAX}: 1800 W	X_{Phenol}: 100% X_{H2O2}:100% X_{TOC}: 80%	[30]

Table 2
Porous texture and pH slurry of the carbon materials.

Material	S_{BET} ($m^2 g^{-1}$)	A_{ext} ($m^2 g^{-1}$)	pH slurry
G-F	7	7	8.4
G-S	12	12	4.5
CB-A	74	74	6.7
CB-V	238	152	6.6
AC-C	872	73	6.8
AC-M	991	169	6.5
SiC	< 2	< 2	7

Phenol is one of the most characteristic pollutants in industrial wastewater and its degradation has been widely studied [29–32]. Therefore, it represents an interesting pollutant when comparing the performance of different catalysts in new processes, such as MW-CWPO. In this work, the activity of activated carbon, graphite, carbon black and silicon carbide as MW-CWPO catalysts for phenol oxidation has been tested. The stability of the most active materials upon consecutive runs has also been checked.

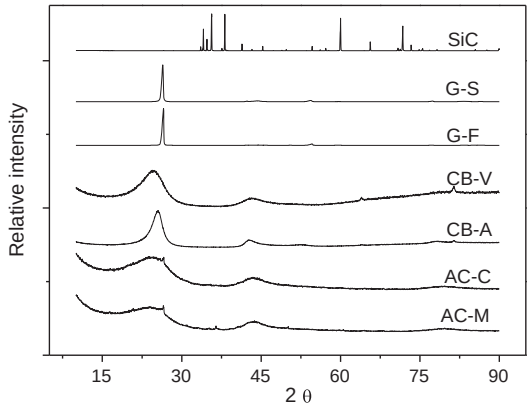

Fig. 1. XRD patterns of the carbon materials.

2. Materials and methods

2.1. Reactants

Phenol was supplied by Sigma-Aldrich and H_2O_2 (30% w/v) by Panreac. The respective aqueous solutions were prepared at pH_0 3 using HCl (37% w/v; Panreac).

Activated carbons were supplied by Merck (AC-M, ref.: 102514) and Chemviron (AC-C), carbon blacks by Alfa-Aesar (CB-A, ref.: 1333-86-4) and Vulcan (CB-V, ref.: CC72R), Graphite from Fluka (G-F, ref.: 1249167) and Sigma-Aldrich (G-S, ref.: 282863) and silicon carbide by Goodfellow (SiC). All these materials were used as received. All samples were supplied in powder, except for ACs, which were grounded and sieved to achieve a particle size < 150 μm.

H_2SO_4 (96 wt%), H_3PO_4 (85 wt%) acetonitrile, $TiOSO_4$, Na_2CO_3 and $NaHCO_3$, supplied by Sigma-Aldrich, were used in the analytic procedure. All reagents are analytical grade and they were used as received without further purification. Working standard solutions of phenol, catechol, resorcinol, hydroquinone, p-benzoquinone, and organic acids (fumaric, malonic, maleic, acetic and formic from Sigma-Aldrich and oxalic from Panreac) were prepared for calibration. Ultrapure water was used throughout the work.

2.2. MW-CWPO experiments

MW-CWPO runs were performed in high pressure PTFE reaction vessels located in a microwave furnace (flexiWAVE, Milestone). The experiments were conducted in batch using 100 mL stoppered PTFE reactors which were initially loaded with aqueous phenol solution (100 mg L^{-1}) at pH_0 = 3 and 500 mg L^{-1} of catalyst H_2O_2 was added at 500 mg L^{-1}, corresponding to the theoretical stoichiometric amount for complete mineralization of phenol. Stirring was fixed at 400 rpm, which allowed maintaining the catalyst in suspension and avoiding external mass-transfer limitation. Heating rate was set at 80 °C/min to reach the reaction temperature 120 °C, which was maintained for 15 min. During reaction, the pressure rose up above 2 bar. All the experiments were done by triplicate, being the standard deviation always < 5%.

2.3. Catalyst characterization

The porous texture of the supports and catalysts was characterized by 77 K N_2 adsorption/desorption using a Micromeritics Tristar apparatus. The specific surface area (S_{BET}) and the external or non-microporous area (A_{ext}) were calculated by the BET and t-method, respectively. X-Ray Diffraction (XRD) patterns were obtained in a D5000 X-

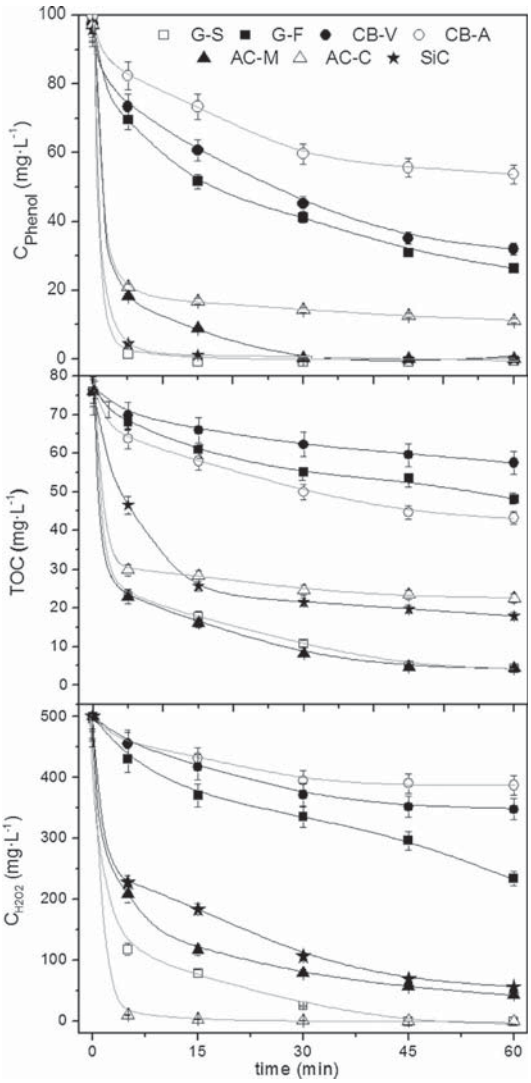

Fig. 2. Phenol, TOC and H_2O_2 evolution upon MW-CWPO. $C_{Phenol,0}$: 100 mg L^{-1}, C_{cat}: 500 mg L^{-1}, $C_{H2O2,0}$: 500 mg L^{-1}, T: 120 °C, pH_0: 3.

ray diffractometer (Siemens), using Cu Kα (8.04 keV) radiation and a step of 0.02°/s for 2Θ = 5–100°. The pH slurry of the carbon materials was determined following the ASTM D3838 – 05 method. Thermogravimetric analysis (TGA) of the fresh and used catalysts were performed in a thermoscale TGA Q500 (TA Instruments). Runs were conducted under N_2 flow up to 1000 °C, reached at 10 °C/min heating rate.

2.4. Analytical methods

Samples were periodically withdrawn from the reactors and immediately analyzed after filtration through fiber glass filters (Albet FV-C). Phenol and aromatic intermediates were identified and quantified by means of an Ultra HPLC (Thermo Scientific Ultimate 3000) with a Diode Array detector (Dionex Ultimate 3000). An ion-exclusion column (ZORBAX Eclipse Plus C18, 100 mm, 1.8 μm) was used as stationary

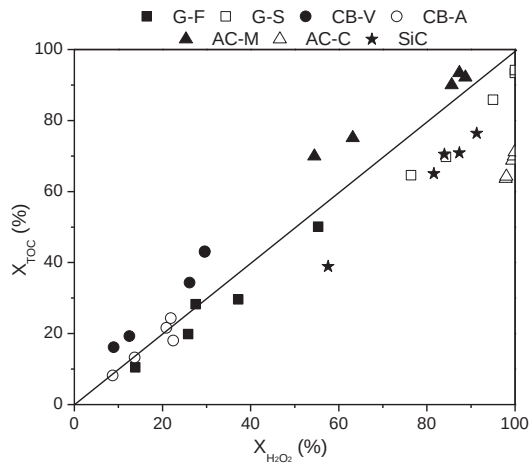

Fig. 3. H_2O_2 efficiency in MW-CWPO. $C_{Phenol,0}$: 100 mg L^{-1}, C_{cat}: 500 mg L^{-1}, $C_{H2O2,0}$: 500 mg L^{-1}, T: 120 °C, pH_0: 3.

phase and 4 mM H_2SO_4 aqueous solution at 1 mL/min as mobile phase. UV detector at 210 nm wavelength was used for phenol, resorcinol, catechol and hydroquinone and at 246 nm for p-benzoquinone. Short-chain organic acids were analyzed in an ion chromatograph with chemical suppression (Metrohm 790 IC) using a conductivity detector. A Metrosep A supp 5-250 column (25 cm long, 4 mm diameter) was used as stationary phase and 0.7 mL/min of a 3.2 mM/1 mM aqueous solution of Na_2CO_3 and $NaHCO_3$, respectively, as mobile phase. Total Organic Carbon was measured using a TOC analyzer (Shimadzu TOC-VSCH). Residual H_2O_2 in the liquid phase was determined by colorimetric titration with an Agilent spectrophotometer using the $TiOSO_4$ method [33].

3. Results and discussion

3.1. Materials characterization

Porous texture and pH slurry of the selected carbon materials are shown in Table 2. Textural properties vary significantly depending on the type of material. Activated carbons present a high surface area, corresponding mostly to microporosity, opposite to the graphites and SiC, which are essentially non-porous materials. The two carbon blacks differ significantly in their porous texture, showing CB-V a more developed porosity with both micro and mesopores. All families presented similar pH slurry values, close to 7, except for the graphites, being G-F a basic material in contrast to G-S, with acidic pH slurry value.

XRD patterns are collected in Fig. 1. SiC is a crystalline material, different to the rest of carbon materials selected. Graphites show the characteristic 0 0 2 diffraction peak at 2Θ = 26°, while carbon blacks and activated carbons are amorphous materials, with larger turbostratic domains in the case of the former.

3.2. Activity in MW-CWPO process

As indicated before, all these materials were tested as catalysts in the MW-CWPO degradation of phenol. Phenol concentration, Total Organic Carbon (TOC) and H_2O_2 evolution are shown in Fig. 2. Only G-S, AC-M and SiC, allowed complete conversion of phenol, being the two former highly efficient in terms of mineralization in a relatively short time. Regarding H_2O_2 decomposition, AC-C showed the highest activity, although with much lower efficiency towards phenol breakdown and mineralization. $HO_X^{\cdot}$ radicals auto scavenging reactions can occur

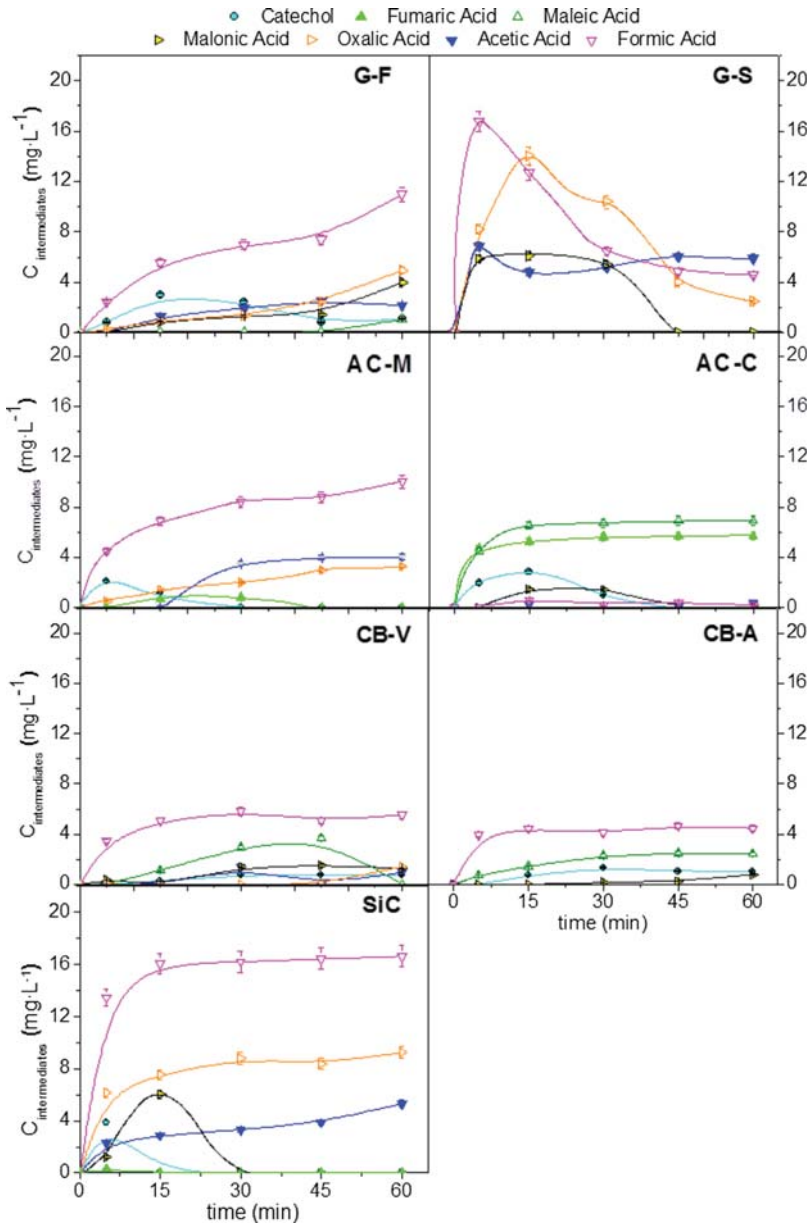

Fig. 4. Time-course of reaction byproducts upon MW-CWPO of phenol. $C_{Phenol,0}$: 100 mg L^{-1}, C_{cat}: 500 mg L^{-1}, $C_{H2O2,0}$: 500 mg L^{-1}, T: 120 °C, pH_0: 3.

on the surface of AC-C, giving rise to H_2O and O_2 in a higher extent. Both carbon blacks (CB-A and CB-V) and the graphite G-F showed a very low activity in MW-CWPO.

In the case of graphites, the surface chemistry seems to play a key role in the process. G-S is the most acidic and active material of this family, whereas G-F has a basic character with pH_{slurry}: 8.4, leading to a much lower activity for H_2O_2 decomposition.

One of the critical issues in CWPO is to find catalysts that maximize the H_2O_2 consumption efficiency. Fig. 3 shows the relation between H_2O_2 consumption and TOC removal. All the runs employed the stoichiometric amount needed for complete phenol mineralization. Hence, data on the diagonal would indicate a 100% effectiveness in H_2O_2 consumption. Data above the diagonal indicates phenol or intermediates adsorption on the catalyst, whereas data below that line would imply an inefficient H_2O_2 use. As pointed out from Fig. 2, AC-C is very active for H_2O_2 decomposition but radicals can recombine leading to a low TOC removal. AC-M and CB-V, with the highest specific within their respective families provide a higher contribution of adsorption. Despite G-S shows a lower H_2O_2 efficiency than G-F or CB-A, its higher activity results promising for MW-CWPO.

Fig. 4 shows the evolution of detected byproducts, aromatic and short-chain acids. In all runs, catechol was the only aromatic

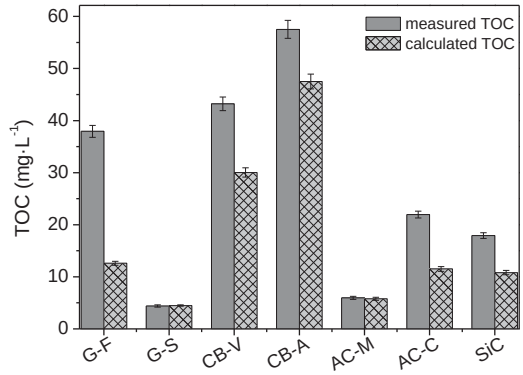

Fig. 5. Unidentified TOC after 60 min reaction time.

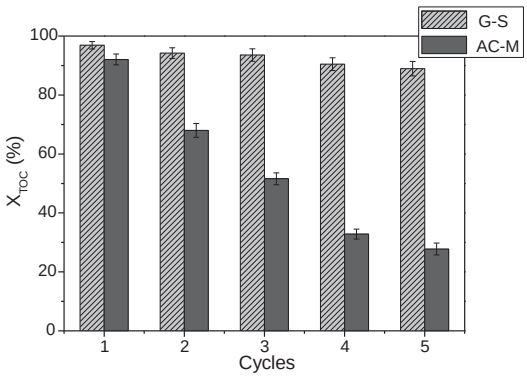

Fig. 6. G-S and AC-M stability in MW-CWPO through 5 reaction cycles.

intermediate detected, always in very low concentrations ($< 4\ mg\ L^{-1}$). With G-S aromatic intermediates were not detected throughout the reaction. Thus, phenol breakdown in MW-CWPO goes through a very rapid ring opening, as was described in a previous work [30]. Regarding the short chain acids, oxalic and formic are known to be highly resistant to CWPO. Hence, it should be remarked that G-S is able to oxidize these two acids after their formation, opposite to the rest of materials tested.

Besides aromatic and short-chain acids, condensation byproducts may arise in the oxidation of phenol [7,32,34]. These compounds have not been yet identified. Nonetheless, they can be assessed in the liquid phase as the difference between the measured TOC and that calculated identified species, as depicted in Fig. 5. Under the working conditions, the C balance closed for G-S and AC-M. Thus, no oligomeric byproducts were remaining in the effluent. These byproducts can lead to catalyst deactivation due to fouling, as it seems to happen with G-F. Therefore, based in their high activity and complete removal of aromatic intermediates and condensation byproducts, G-S and AC-M were selected for further stability tests.

3.3. G-S and AC-M stability in MW-CWPO process

The stability of G-S and AC-M was tested in 5 consecutive cycles. The results are shown in Fig. 6. G-S remained active under the selected operating conditions, since mineralization degree was always above 85%. In contrast AC-M suffered a progressive loss of activity in each cycle. This can be ascribed to the catalyst structure and porous texture. AC-M is mostly a microporous solid, with only 17% of its high BET surface area corresponding to external or non-microporous area, whereas G-S can be considered a non-porous carbon of fairly small surface area. When hot spot are formed inside these microspores, confined vapor is generated. The pressure increases until the AC crumbles in the so called popcorn effect. These changes in the material seem to affect its stability favoring deactivation by fouling. On the other hand, graphite is a highly ordered and layered material. Hot spot formation on the surface of those layers is followed by a rapid energy dissipation. Thus, the structure of the material remains intact, as does the activity.

To learn on the catalyst fouling, termogravimetric analyses (TGA) under N_2 were performed for the fresh and used materials after 1 and 5 cycles Fig. 7. Results are shown in Fig. 6. G-S showed a weight loss below 2%, while this was much higher for AC-M, increasing upon the successive cycles. This proves that the active sites on AC-M are progressively covered, hindering its activity by fouling.

4. Conclusions

Carbon materials of different nature have been tested in MW-CWPO using phenol as target pollutant. Carbon blacks showed a very low activity in this process. SiC exhibited a high initial activity but a rapid deactivation. Activated carbons yielded a good activity but an inefficient H_2O_2 consumption. AC-C allowed complete H_2O_2 decomposition in 15 min, hindering the reaction due to a lack of oxidant and rapid radical recombination. On the other hand, when using AC-M, 93% mineralization was achieved. The activity of graphite relies on its surface chemistry. G-F, with basic pH_{slurry}, showed low activity for both H_2O_2 conversion and TOC removal, yielding a relatively high amount of

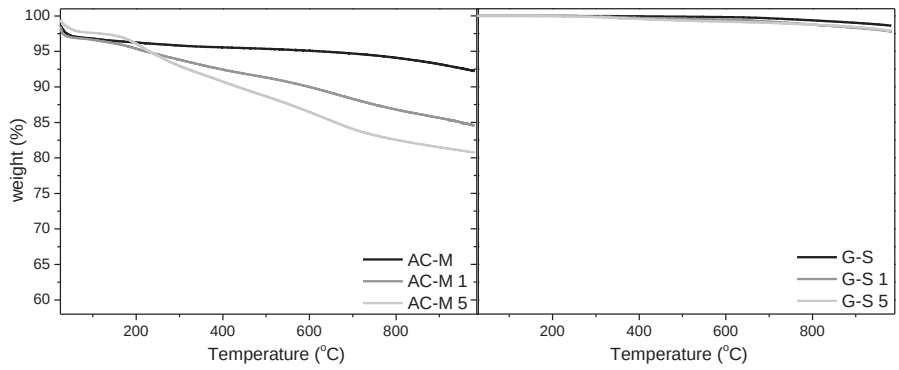

Fig. 7. Termogravimetric assays for fresh and used materials after one and five MW-CWPO cycles.

condensation byproducts, favoring its deactivation by fouling. In contrast, G-S, with acid pH_{slurry}, allowed complete phenol conversion and 94% mineralization. Intermediates analyses reveal a very quick ring opening with no aromatic intermediates or condensation byproducts in aqueous phase after 60 min reaction with G-S and AC-M. These two materials were subjected to stability tests, finding that AC-M crumbled and lost its activity in consecutive runs due to the popcorn effect. Contrarily, the ordered laminar structure of graphite allows energy dissipation when hot spots are formed, being G-S stable upon 5 consecutive runs.

Acknowledgements

Authors would like to thank the Spanish Ministerio de Economia y Competitividad (MINECO) for financial support through project CTM2016-76454-R. A.L. Garcia-Costa acknowledges the European Social Fund and MINECO for PhD. grant BES-2014-067598.

References

[1] J.A. Zazo, A.F. Fraile, A. Rey, A. Bahamonde, J.A. Casas, J.J. Rodriguez, Optimizing calcination temperature of Fe/activated carbon catalysts for CWPO, Catal. Today 143 (2009) 341–346.
[2] A. Santos, P. Yustos, A. Quintanilla, G. Ruiz, F. Garcia-Ochoa, Study of the copper leaching in the wet oxidation of phenol with CuO-based catalysts: causes and effects, Appl. Catal. B-Environ. 61 (2005) 323–333.
[3] H.S. Park, J.R. Koduru, K.H. Choo, B. Lee, Activated carbons impregnated with iron oxide nanoparticles for enhanced removal of bisphenol a and natural organic matter, J. Hazard. Mater. 286 (2015) 315–324.
[4] S.A. Messele, O. Soares, J.J.M. Orfao, F. Stuber, C. Bengoa, A. Fortuny, A. Fabregat, J. Font, Zero-valent iron supported on nitrogen-containing activated carbon for catalytic wet peroxide oxidation of phenol, Appl. Catal. B-Environ. 154 (2014) 329–338.
[5] M. Munoz, Z.M. de Pedro, N. Menendez, J.A. Casas, J.J. Rodriguez, A ferromagnetic gamma-alumina-supported iron catalyst for CWPO application to chlorophenols, Appl. Catal. B-Environ. 136 (2013) 218–224.
[6] C.M. Dominguez, P. Ocon, A. Quintanilla, J.A. Casas, J.J. Rodriguez, Highly efficient application of activated carbon as catalyst for wet peroxide oxidation, Appl. Catal. B-Environ. 140 (2013) 663–670.
[7] C.M. Dominguez, P. Ocon, A. Quintanilla, J.A. Casas, J.J. Rodriguez, Graphite and carbon black materials as catalysts for wet peroxide oxidation, Appl. Catal. B-Environ. 144 (2014) 599–606.
[8] R.S. Ribeiro, A.M.T. Silva, J.L. Figueiredo, J.L. Faria, H.T. Gomes, Removal of 2-nitrophenol by catalytic wet peroxide oxidation using carbon materials with different morphological and chemical properties, Appl. Catal. B-Environ. 140 (2013) 356–362.
[9] R.S. Ribeiro, A.M.T. Silva, L.M. Pastrana-Martinez, J.L. Figueiredo, J.L. Faria, H.T. Gomes, Graphene-based materials for the catalytic wet peroxide oxidation of highly concentrated 4-nitrophenol solutions, Catal. Today 249 (2015) 204–212.
[10] M.T. Pinho, H.T. Gomes, R.S. Ribeiro, J.L. Faria, A.M.T. Silva, Carbon nanotubes as catalysts for catalytic wet peroxide oxidation of highly concentrated phenol solutions: towards process intensification, Appl. Catal. B-Environ. 165 (2015) 706–714.
[11] G. Pliego, J.A. Zazo, P. Garcia-Munoz, M. Munoz, J.A. Casas, J.J. Rodriguez, Trends in the intensification of the fenton process for wastewater treatment: an overview, Crit. Rev. Environ. Sci. Technol. 45 (2015) 2611–2692.
[12] M. Munoz, P. Dominguez, Z.M. de Pedro, J.A. Casas, J.J. Rodriguez, Naturally-occurring iron minerals as inexpensive catalysts for CWPO, Appl. Catal. B-Environ. 203 (2017) 166–173.
[13] P. Liu, C.L. Li, Q. Han, G. Lu, X.Q. Dong, F. Ji, J.H. Xu, Phenol degradation by UV-enhanced catalytic wet peroxide oxidation process, J. Adv. Oxid. Technol. 17 (2014) 127–132.
[14] J.A. Zazo, G. Pliego, P. García-Muñoz, J.A. Casas, J.J. Rodriguez, UV-LED assisted catalytic wet peroxide oxidation with a Fe(II)-Fe(III)/activated carbon catalyst, Appl. Catal. B: Environ. 192 (2016) 350–356.
[15] R. Molina, F. Martinez, J.A. Melero, D.H. Bremner, A.G. Chakinala, Mineralization of phenol by a heterogeneous ultrasound/Fe-SBA-15/H2O2 process: multivariate study by factorial design of experiments, Appl. Catal. B-Environ. 66 (2006) 198–207.
[16] X.D. Qi, Z.H. Li, Efficiency optimization of pharmaceutical wastewater treatment by a microwave-assisted fenton-like process using special supported catalysts, Pol. J. Environ. Stud. 25 (2016) 1205–1214.
[17] W. Pan, G. Zhang, T. Zheng, P. Wang, Degradation of p-nitrophenol using CuO/Al_2O_3 as a Fenton-like catalyst under microwave irradiation, RSC Adv. 5 (2015) 27043–27051.
[18] A.B. Ahmed, B. Jibril, S. Danwittayakul, J. Dutta, Microwave-enhanced degradation of phenol over Ni-loaded ZnO nanorods catalyst, Appl. Catal. B-Environ. 156 (2014) 456–465.
[19] A.Y. Atta, B.Y. Jibril, T.K. Al-Waheibi, Y.M. Al-Waheibi, Microwave-enhanced catalytic degradation of 2-nitrophenol on alumina-supported copper oxides, Catal. Commun. 26 (2012) 112–116.
[20] N.N. Wang, T. Zheng, J.P. Jiang, P. Wang, Cu(II)-Fe(II)-H_2O_2 oxidative removal of 3-nitroaniline in water under microwave irradiation, Chem. Eng. J. 260 (2015) 386–392.
[21] G.H. Zhao, B.Y. Lv, Y. Jin, D.M. Li, P-Chlorophenol wastewater treatment by microwave-enhanced catalytic wet peroxide oxidation, Water Environ. Res. 82 (2010) 120–127.
[22] Z. Liu, H. Meng, H. Zhang, J. Cao, K. Zhou, J. Lian, Highly efficient degradation of phenol wastewater by microwave induced H_2O_2-CuO_x/GAC catalytic oxidation process, Sep. Purif. Technol. 193 (2018) 49–57.
[23] N. Remya, J.-G. Lin, Current status of microwave application in wastewater treatment—a review, Chem. Eng. J. 166 (2011) 797–813.
[24] N. Wang, P. Wang, Study and application status of microwave in organic wastewater treatment – a review, Chem. Eng. J. 283 (2016) 193–214.
[25] J.A. Menéndez, A. Arenillas, B. Fidalgo, Y. Fernández, L. Zubizarreta, E.G. Calvo, J.M. Bermúdez, Microwave heating processes involving carbon materials, Fuel Process. Technol. 91 (2010) 1–8.
[26] Y. Lei, X. Lin, H. Liao, New insights on microwave induced rapid degradation of methyl orange based on the joint reaction with acceleration effect between electron hopping and Fe^{2+}-H_2O_2 reaction of $NiFeMnO_4$ nanocomposites, Sep. Purif. Technol. 192 (2018) 220–229.
[27] A. Anshuman, S. Saremi-Yarahmadi, B. Vaidhyanathan, Enhanced catalytic performance of reduced graphene oxide–TiO_2 hybrids for efficient water treatment using microwave irradiation, RSC Adv. 8 (2018) 7709–7715.
[28] S. Li, G.S. Zhang, W. Zhang, H.S. Zheng, W.Y. Zhu, N. Sun, Y.J. Zheng, P. Wang, Microwave enhanced fenton-like process for degradation of perfluorooctanoic acid (PFOA) using Pb-$BiFeO_3$/rGO as heterogeneous catalyst, Chem. Eng. J. 326 (2017) 756–764.
[29] Z. Liu, H. Meng, H. Zhang, J. Cao, K. Zhou, J. Lian, Highly efficient degradation of phenol wastewater by microwave induced H2O2-CuOx/GAC catalytic oxidation process, Sep. Purif. Technol. 193 (2018) 49–57.
[30] A.L. Garcia-Costa, J.A. Zazo, J.J. Rodriguez, J.A. Casas, Microwave-assisted catalytic wet peroxide oxidation comparison of Fe catalysts supported on activated carbon and gamma-alumina, Appl. Catal. B-Environ. 218 (2017) 637–642.
[31] A. Srikhaow, S.M. Smith, K. Uraisin, K. Suttiponparnit, C. Kongmark, C. Chuaicham, Catalytic remediation of phenol contaminated wastewater using Cu-Zn hydroxide nitrate, Rsc Adv. 6 (2016) 36766–36774.
[32] J.A. Zazo, J.A. Casas, A.F. Mohedano, M.A. Gilarranz, J.J. Rodriguez, Chemical pathway and kinetics of phenol oxidation by Fenton's reagent, Environ. Sci. Technol. 39 (2005) 9295–9302.
[33] G.M. Eisenberg, Colorimetric determination of hydrogen peroxide, Ind. Eng. Chem.-Anal. Ed. 15 (1943) 327–328.
[34] M.E. Suarez-Ojeda, F. Stuber, A. Fortuny, A. Fabregat, J. Carrera, J. Font, Catalytic wet air oxidation of substituted phenols using activated carbon as catalyst, Appl. Catal. B-Environ. 58 (2005) 105–114.

5.4.Microwave-assisted Catalytic Wet Peroxide Oxidation: energy optimization

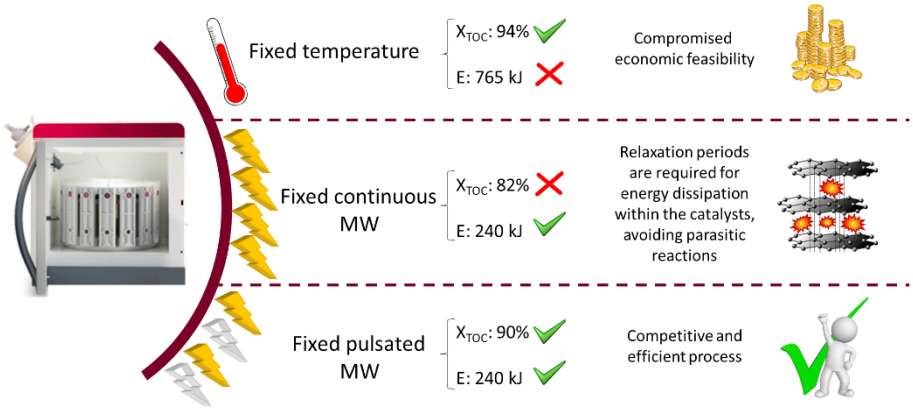

Separation and Purification Technology 215 (2019) 62–69

Contents lists available at ScienceDirect

Separation and Purification Technology

journal homepage: www.elsevier.com/locate/seppur

Microwave-assisted catalytic wet peroxide oxidation: Energy optimization

Alicia L. Garcia-Costa*, Juan A. Zazo, Jose A. Casas

Chemical Engineering Department, School of Science, Universidad Autonoma de Madrid, Ctra. Colmenar Viejo Km. 15, 28049 Madrid, Spain

ARTICLE INFO

Keywords:
Wastewater treatment
Graphite
Microwave
AOP intensification
Hot spot
Metal-free catalyst

ABSTRACT

Over the past few years, microwave technology (MW) has been successfully coupled to different advanced oxidation processes for wastewater treatment. This intensification method provides a rapid and homogeneous heating and, in presence of microwave absorbing materials, hot spots can be generated. These have shown a significant contribution on the overall efficiency of the process. Up to the date, there is no information on the influence of the radiation mode on the system. To gain knowledge on this issue, three different operation modes were studied in the MW-assisted catalytic wet peroxide oxidation of phenol: (i) controlled temperature (120 °C), (ii) controlled continuous MW and (iii) controlled pulsated MW. Other experimental conditions were $[Phenol]_0$: 100 mg·L^{-1}, $[H_2O_2]_0$: 500 mg·L^{-1}, [graphite]: 500 mg·L^{-1}, pH_0:3. The pulsated method reached 90% mineralization degree and complete H_2O_2 decomposition using 240 kJ, three times less energy than the controlled temperature run. Continuous MW showed a slightly inferior performance (X_{TOC}: 82%), ascribed to a worse energy dissipation from the hot spots on the material. After reaction, only biodegradable short chain carboxylic acids remain in the effluent and there are no significant modifications on the catalyst crystallinity, despite the extreme conditions produced by hot spot formation. Under these conditions TOC abatement follows a pseudo-second kinetic order ($E_{A,TOC} \approx 30–40$ kJ·mol^{-1}), whereas H_2O_2 decomposition fits by a pseudo-first order ($E_{A,H2O2} \approx 33–52$ kJ·mol^{-1}). Additionally, the specific energy consumption (EC_{TOC}) for the controlled power runs was lower than that of other intensified AOP, making MW-CWPO a competitive technology for wastewater treatment.

1. Introduction

Advanced Oxidation Processes (AOP) have arisen as promising techniques for wastewater detoxification, especially when facing acutely toxic and/or recalcitrant contaminants. These methods are based on the generation of strongly oxidizing agents such as hydroxyl and hydroperoxyl radicals ($HO_X^{\cdot}$). Among the existing AOP, Fenton is the most commonly used. This process uses iron salts in the catalytic decomposition of H_2O_2, giving rise to $HO_X^{\cdot}$. Despite its ease of operation and high efficiency, this treatment generates additional waste, as dissolved iron needs to be recovered as $Fe(OH)_3$ sludge prior to the effluent discharge [1,2].

In order to overcome this drawback, Catalytic Wet Peroxide Oxidation (CWPO) emerges as a feasible alternative, supporting the metal (typically iron or copper) onto a porous solid such as alumina, activated carbon, etc. [3–5]. Nonetheless, at the usual operating pH, active phase leaching may occur, causing additional water pollution and catalyst deactivation. In this scenario, free-metal catalysis arises, typically using carbonaceous materials such as activated carbon, graphite, carbon black, etc. These have been successfully applied in CWPO, with a sensibly lower activity but greater stability than the metal doped catalysts [6–8].

The current trend in AOP goes through process intensification to boost either the activity or the stability of the catalysts. This enhancement can be achieved by increasing the temperature [9], with electrochemical methods [10] or applying different kinds of radiation such as ultrasounds [11,12], UV–vis light [13,14] or microwaves (MW) [15–17]. MW-assisted AOPs present a promising technology, as they combine homogeneous heating of the bulk reaction by dipole polarization, as well as other MW non-thermal effects, related to the MW absorbing properties of the materials. Materials with high loss factor (tan δ), can absorb a great amount of radiation, releasing the energy as hot spots on their surface. These hot spots are micro-plasma regions in which temperature rises up to 1200 °C [18]. A previous work revealed a higher activity when using carbon based catalysts, which are MW absorbers, in comparison to alumina, transparent to this kind of radiation [19]. Furthermore, in that work we observed that the non-thermal effects had a significant contribution on phenol degradation, presenting activated carbon (AC) practically the same activity as a Fe/AC catalyst. Further research revealed the importance of the catalyst structure [20],

* Corresponding author.
E-mail address: alicial.garcia@uam.es (A.L. Garcia-Costa).

https://doi.org/10.1016/j.seppur.2019.01.006
Received 12 November 2018; Received in revised form 26 December 2018; Accepted 3 January 2019
Available online 04 January 2019
1383-5866/

Table 1
Recent MW-CWPO applications.

Operation mode	Pollutant	Catalyst	Operating conditions	Results	Ref.
Controlled temperature	Phenol	AC, Graphite	C_{Phenol}: 100 mg·L^{-1}, C_{cat}: 0.1 g·L^{-1}, C_{H2O2}: 500 mg·L^{-1} t: 60 min, pH_0: 3 T: 120 °C, P: variable, P_{MAX}: 1800 W	X_{Phenol}: 100% X_{H2O2}:100% X_{TOC}: 93–94%	[19,20]
	Benzene, Toluene, Xylene, Naphthalene (BTXN)	AC	C_{BTX}: 100 mg·L^{-1}, C_N: 30 mg·L^{-1}, C_{cat}: 1 g·L^{-1}, C_{H2O2}: stoichiometric t: 60 min, pH_0: 3 T: 120 °C, P: variable, P_{MAX}: 1800 W	X_{BTXN}: 100% X_{H2O2}:100% X_{TOC}: 90%	[26]
	Humic acid	CuO-Co_3O_4/AC	$C_{HumicAcid}$: 100 mg·L^{-1}, C_{cat}: 0.5 g·L^{-1}, C_{H2O2}: 315 mg·L^{-1} t: 60 min, pH_0: 7 T: 80 °C, P_{MAX}: 800 W	$X_{HumicAcid}$: 90% $Cu_{Leached}$: 0.3 mg·L^{-1} $Co_{Leached}$: 0.1 mg·L^{-1}	[27]
	Orange G (OG)	rGO-TiO_2	C_{MO}: 4.5 mg·L^{-1}, C_{cat}, C_{H2O2}, t and pH_0: not reported T: 30–120 °C, P_{MAX}: 300 W	X_{OG}: 90%	[28]
Fixed MW power	Phenol	CuO_X/GAC	C_{Phenol}: 100 mg·L^{-1}, C_{cat}: 3 g·L^{-1}, C_{H2O2}: 600 mg·L^{-1} t: 5 min, pH_0: 4 T: not reported, P: 400 W	X_{Phenol}: 100% X_{COD}: 90% $Cu_{Leached}$: 21 mg·L^{-1}	[29]
	Rhodamine B (RhB)	$BiFeO_3$	C_{RhB}: 30 mg·L^{-1}, C_{cat}: 1 g·L^{-1}, C_{H2O2}: 44 mg·L^{-1} t: 6 min, pH_0: 4 T_{MAX}: 170–190 °C, P: 300 W	X_{RhB}: 94.8% $Fe_{Leached}$: 60 mg·L^{-1} $Bi_{Leached}$: 40 mg·L^{-1}	[30]
	Perfluorooctanoic acid (PFOA)	Pb-$BiFeO_3$/rGO	C_{PFOA}: 50 mg·L^{-1}, C_{cat}: 1 g·L^{-1}, C_{H2O2}: 44 mg·L^{-1} t: 5 min, pH_0: 5 T: not reported, P: 500 W	X_{PFOA}: 87% X_{TOC}: 52% $Fe_{Leached}$: 0.05 mg·L^{-1} $Bi_{Leached}$: 0.03 mg·L^{-1} $Pb_{Leached}$: 0.08 mg·L^{-1}	[31]
	Methyl orange (MO)	$NiFeMnO_4$	C_{MO}: 30 mg·L^{-1}, C_{cat}: 1 g·L^{-1}, C_{H2O2}: 30 mg·L^{-1} t: 6 min, pH_0: 2–3 T: 50 °C, P: 750 W	X_{MO}: 97%	[32]

where highly ordered materials such as graphite present a higher stability than AC. Hot spot formation inside the AC micropores leads to material crumbling and catalyst deactivation by fouling. Both works were performed heating the solution at P_{MAX}: 1800 W until the working temperature was reached (120 °C). Afterwards the MW-furnace modulated the radiation to keep that temperature, working in average at around P: 215 W throughout the process. This strategy allows to compare our results to those obtained in absence of MW. Nonetheless, hot spot formation is intrinsically related to the radiation. Thus, the current operating mode may imply an inefficient energy consumption.

So far, MW-CWPO has been widely studied in the degradation of a large variety of contaminants with great results, as may be seen in Table 1. Nonetheless, the metal leaching presented in some works [29,30] cannot be neglected, as they exceed the environmental regulations for effluent disposal. Furthermore, some authors are obscure about the operating conditions, reporting mysterious situations in which, operating at a fixed power, temperature is allegedly kept constant inside the microwave. In this sense, no studies have yet been conducted to determine the optimal operating conditions in terms of energy consumption. This paper aims to gain depth in this issue, working in three different scenarios at: (i) fixed temperature, (ii) fixed energy with continuous MW irradiation and (iii) fixed energy with MW pulsation. In order to do so, graphite was selected as metal-free catalyst and phenol as target compound. This aromatic pollutant has been widely studied because of its presence in industrial effluents but still nowadays, it remains an interesting contaminant when testing new catalysts or processes [21–25].

2. Materials and methods

2.1. Reactants

Phenol was supplied by Sigma-Aldrich and H_2O_2 (30% w/v) by Panreac. The respective aqueous solutions were prepared at pH_0 3 using HCl (37% w/v; Panreac). H_2SO_4 (96 wt%), H_3PO_4 (85 wt%) acetonitrile, $TiOSO_4$, Na_2CO_3 and $NaHCO_3$, supplied by Sigma-Aldrich, were used in the analytic procedure. All reagents are analytical grade and they were used as received without further purification. Working standard solutions of phenol, catechol, resorcinol, hydroquinone, p-benzoquinone, and organic acids (fumaric, malonic, maleic, acetic and formic from Sigma-Aldrich and oxalic from Panreac) were prepared for calibration. Ultrapure water was used throughout the work.

Commercial graphite provided by Sigma-Aldrich (ref.: 282863) was used as catalyst as received. This material was characterized elsewhere [6,20]. In brief, it presents S_{BET}: 12 m^2/g, C: 97.3%, Ashes: 0.5%, pH_{SLURRY}: 4.5.

2.2. MW-CWPO experiments

MW-CWPO runs were performed in high pressure PTFE reaction vessels located in a microwave furnace (flexiWAVE, Milestone). The experiments were conducted in batch using 100 mL stoppered PTFE reactors which were initially loaded with aqueous phenol solution (100 mg·L^{-1}) at pH_0 = 3 and 500 mg·L^{-1} of catalyst. H_2O_2 was added at 500 mg·L^{-1}, corresponding to the theoretical stoichiometric amount for complete mineralization of phenol. Stirring was fixed at 400 rpm, which allowed maintaining the catalyst in suspension and avoiding external mass-transfer limitation.

For the controlled temperature experiment, the heating rate was set at 80 °C/min to reach the reaction temperature 120 °C, which was maintained for 15 min. In the fixed power experiments, two different operation modes were selected, continuous and pulsed radiation. The continuous runs were conducted fixing a given power (200 W, 400 W, 1800 W) thus, temperature rose during the experiments. For the pulse operation, the microwave radiation was applied at 800 W and 1800 W in regular time periods. All the experiments were done by triplicate, being the standard deviation always less than 5%.

2.3. Analytical methods

Samples were periodically withdrawn from the reactors and immediately analyzed after filtration through fiber glass filters (Albet FV-C). Phenol and aromatic intermediates were identified and quantified by means of an Ultra HPLC (Thermo Scientific Ultimate 3000) with a Diode Array detector (Dionex Ultimate 3000). An ion-exclusion column (ZORBAX Eclipse Plus C18, 100 mm, 1.8 μm) was used as stationary phase. As mobile phase 4 mM H_2SO_4 aqueous solution at 1 mL·min^{-1}. UV detector at 210 nm wavelength was used for phenol, resorcinol, catechol and hydroquinone and at 246 nm for p-benzoquinone. Short-chain organic acids were analyzed in an ion chromatograph with

Table 2
Operating conditions. Applied energy.

Operation mode	Run	Label	P (W)	t (s)	Energy (kJ)
Controlled temperature	120 °C	T.120	≈212	3600	≈765
Controlled applied power	Continuous – 200 W	C.200	200	600	120
	Continuous – 400 W	C.400	400	600	240
	Continuous – 1800 W	C.1800	1800	133	240
	Pulses – 800 W	P.800	800	25 × 12 s	240
	Pulses – 1800 W	P.1800	1800	10 × 6 s 15 × 5 s	240

chemical suppression (Metrohm 790 IC) using a conductivity detector. A Metrosep A supp 5-250 column (25 cm long, 4 mm diameter) was used as stationary phase and 0.7 mL·min^{-1} of a 3.2 mM/1 mM aqueous solution of Na_2CO_3 and $NaHCO_3$, respectively, as mobile phase. Total Organic Carbon was measured using a TOC analyzer (Shimadzu TOC-VSCH). Residual H_2O_2 in the liquid phase was determined by colorimetric titration with an Agilent spectrophotometer using the $TiOSO_4$ method [33].

X-Ray Diffraction (XRD) patterns for the fresh and used catalyst were collected in a Siemens Model D5000X-ray diffractometer, using Cu Kα (8.04 keV) radiation and a step of 0.02°·s^{-1} for 2Θ = 20–90°. Thermogravimetric analyses (TGA) were performed in a TGA Q500 thermoscale (TA Instruments) in air atmosphere from 25 to 950 °C, reached at 10 °C/min heating rate.

3. Results and discussion

3.1. MW-CWPO Optimization

Various runs were carried out to determine the best operating conditions in terms of MW-radiation mode. Table 2 summarizes the experimental plan. For the controlled temperature run, the average applied power was obtained by integration using the own Flexiwave furnace software. Usually, the energy consumption in this MW-assisted processes is very high and can compromise the economic feasibility of these at larger scale. Therefore, to reduce the operating cost, the applied energy was reduced to one third, working at maximum 240 kJ. Results for TOC removal, H_2O_2 consumption and temperature evolution are collected in Fig. 1. An energy of 120 kJ was not enough to reach total H_2O_2 consumption at 10 min, mainly having a partial oxidation reaction. Nonetheless, working at 240 kJ complete H_2O_2 decomposition was achieved, with significant differences in the mineralization degree depending on the irradiation mode. The continuous runs could only achieve an 82% TOC removal, whereas the pulsated runs reached 90% mineralization. The non-radiated periods in the MW-pulses-CWPO allow the relaxation of graphite, with the consequent dissipation of the heat generated at the hot spots and an enhanced overall efficiency.

It should be noticed that working at very short reaction time and high power (C.1800) there was a great overheating, reaching 230 °C. This supposes an increase of 60 °C above the maximum temperature reached in the other runs with 240 kJ. This fact was ascribed to a limited heat dissipation throughout the reactor vessel in relation to the C.400 run, in which the same amount of energy was radiated in a more prolonged time.

Working at the stoichiometric dose of H_2O_2 for complete phenol mineralization, the oxidant consumption efficiency (ε) can be defined as the ratio between TOC and H_2O_2 conversions (Eq. (1)). This is one of the key parameters in AOPs, as this reagent usually is amongst the most expensive operating costs. Also, to compare the MW-CWPO process with other intensified AOP, the specific energy consumption per TOC mass at the final point of reaction (EC_{TOC}) was determined. This parameter has been estimated according to Eq. (2), where E is the applied energy (kWh), ΔTOC is the experimental abated TOC and V_s is the treated volume (0.30 L). The values for ε and EC_{TOC} are collected in Table 3.

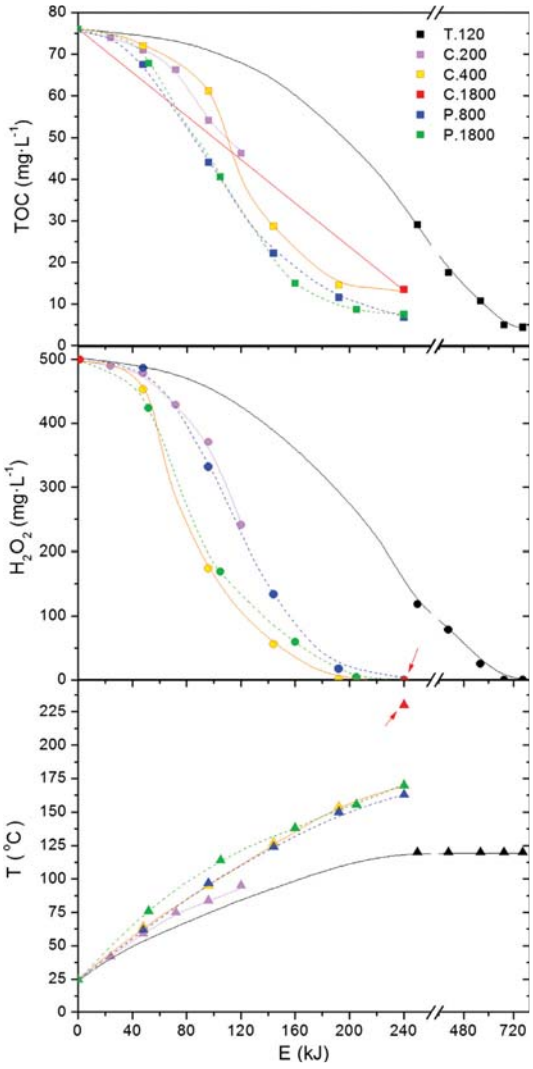

Fig. 1. TOC, H_2O_2 and temperature evolution for the runs in Table 2. $C_{Phenol,0}$: 100 mg·L^{-1}, C_{cat}: 500 mg·L^{-1}, $C_{H2O2,0}$: 500 mg·L^{-1}, pH_0: 3.

$$\varepsilon = \frac{X_{TOC}}{X_{H2O2}} \quad (1)$$

Table 3
H_2O_2 consumption efficiency (ε) and specific energy consumption (EC_{TOC}).

Run	ε	EC_{TOC} (kWh·g_{TOC}^{-1})	X_{PHENOL} (%)	X_{TOC} (%)
T.120	0.94	19.8	100	94
C.200	0.76	7.5	100	76
C.400	0.82	7.1	100	82
C.1800	0.82	7.1	100	82
P.800	0.91	6.4	100	91
P.1800	0.90	6.5	100	90

$$EC_{TOC}\,(\mathrm{kWh\cdot g_{TOC}^{-1}}) = \frac{E}{\Delta TOC\hat{A}\cdot V_s} \quad (2)$$

Working at high power in continuous mode does not imply a great improvement in terms of H_2O_2 efficiency. However, the pulse mode achieves a 90% efficiency degree, regardless of the applied power. In terms of energy consumption, EC_{TOC} decreases drastically when working at fixed power in relation to the temperature controlled run, with a slight enhancement by MW pulsation. In relation to other intensified AOP, as shown in Table 4, MW-CWPO presents a lower EC_{TOC} than UV-assisted CWPO or persulfate electro activation. This is an immature technology, which needs to be further investigated, especially in terms of reactor design in order to be competitive against other AOPs such as the electro-oxidation processes. Nonetheless, these kind of water treatments use either expensive (BDD) or potentially polluting (PbO_2) electrodes and require a rather high amount of salts in the medium to ensure a good conductivity, limiting their real application.

Besides TOC and H_2O_2, the final products were also analyzed. In all cases, phenol was completely eliminated. Fig. 2 shows the evolution of the intermediates. The detected intermediates coincide with those reported in literature for phenol AOPs by other authors [39–42]. Phenol is rapidly converted into hydroxylated compounds (hydroquinone, benzoquinone and catechol), which are further oxidized opening the aromatic ring and giving rise to short-chain acids, mainly oxalic, acetic and formic acids. Comparing the different processes, aromatic intermediates depletion rate is greatly enhanced when working in pulsated mode, as depicted by the significantly lower concentration of hydroquinone seen in P.800 in comparison with that of C.400. In relation to short-chain acid formation it should be noted that, oxalic and formic, which are usually refractory for the Fenton process [39], start degrading after 160 kJ and are almost completely eliminated in the 240 kJ runs.

Nevertheless, the carbon associated to the reaction by-products does not add up in relation to the measured TOC. Several authors have described the formation of condensed by-products (CBP), oligomers formed by aromatic intermediates condensation in the very first stages of the oxidation of phenol or other aromatic pollutants [39,43]. These oligomers have not been yet identified, but they can be quantified as the difference between the measured TOC by a TOC analyzer and the calculated TOC, as the sum of carbon from the oxidation products, which is typical in these kind of oxidation processes [42]. These data are collected in Fig. 3. There is a great formation of CBP in all cases at the beginning of the process. Above 80 kJ, these species start to breakdown, due to the temperature increase. Still, for the continuous mode treatments, some oligomers contribute to the residual TOC after reaction. Thus, CBP are highly stable and cannot be fully eliminated even at 230 °C when using H_2O_2 at the stoichiometric amount. A rational use of MW radiation is essential for their elimination, achieving complete CBP destruction in the pulsated runs.

3.2. Catalyst characterization after reaction

Catalysts have been exposed to a highly aggressive environment in MW-CWPO due to hot spot formation on their surface. To analyze their impact on the catalyst, XRD patterns were recorded before and after reaction, as shown in Fig. 4. Previous work reports a great stability of graphite in MW-CWPO, ascribing it to its capability of dissipating the heat generated by the hot spots thanks to its laminar structure [20]. This structure, which confers graphite a characteristic crystallinity at 2Θ: 26–27, is maintained in all trials.

Also, thermogravimetric analyses (TGA) in air atmosphere of the fresh and used catalysts were carried out to study whether the CBP are completely removed or adsorbed onto the graphite surface. Results are shown in Fig. 5. There is a similar weight loss profile in all cases, consistent to that of the fresh graphite. Thus, despite CBP remain in the aqueous media for C.200 according to Fig. 3, these are not adsorbed onto the catalyst due to hot spot formation.

3.3. Kinetic model

In order to study the kinetics of the MW-CWPO process, temperature must be taken into account as a variable using the Arrhenius equation, due to the different temperature profiles obtained as seen in Fig. 1. This was integrated into the kinetic model, which follows a pseudo-second order for TOC (Eq. (3)) and pseudo-first order for H_2O_2 (Eq. (4)) [39].

Table 4
Intensified AOP EC_{TOC}.

Process/Pollutant	Operating conditions	Results	EC_{TOC} (kWh·g_{TOC}^{-1})	[Ref]
UV-TiO_2/Valproic acid (VA)	$[VA]_0$ = 50 mg·L^{-1} $[TiO_2]$ = 0.1 g·L^{-1} Energy source: Xe lamp	X_{VA} = 73% X_{TOC} = 1.6%	8.6	[34]
UV-CWPO/Phenol	$[Phenol]_0$ = 100 mg·L^{-1} $[H_2O_2]_0$ = 500 mg·L^{-1} $[FeTiO_3]$ = 450 mg·L^{-1} Energy source: solar lamp	X_{Phenol} = 100% X_{TOC} = 95%	22.2	[35]
Thermal + Electro persulfate/Phenol	$[Phenol]_0$ = 100 mg·L^{-1} $[S_2O_8^{2-}]_0$ = 2.85 g·L^{-1} Electrodes: sacrificial Fe i = 1 mA·cm^{-2} T: 90 °C	X_{Phenol} = 98% X_{TOC} = 80%	9.3	[36]
Electro-oxidation/Phenol	$[Phenol]_0$ = 50 mg·L^{-1} Anode: PbO_2 i = 50 mA·cm^{-2} $[Na_2SO_4]$ = 7.1 g·L^{-1} (electrolyte)	X_{Phenol} = 100% X_{TOC} = 85%	3.8	[37]
Electro-oxidation/Phenol	$[Phenol]_0$ = 1.82 g·L^{-1} Anode: BDD i = 147 mA·cm^{-2} $[H_2SO_4]$ = 9.8 g·L^{-1} (electrolyte)	X_{Phenol} = 100% X_{TOC} = 80%	0.2	[38]

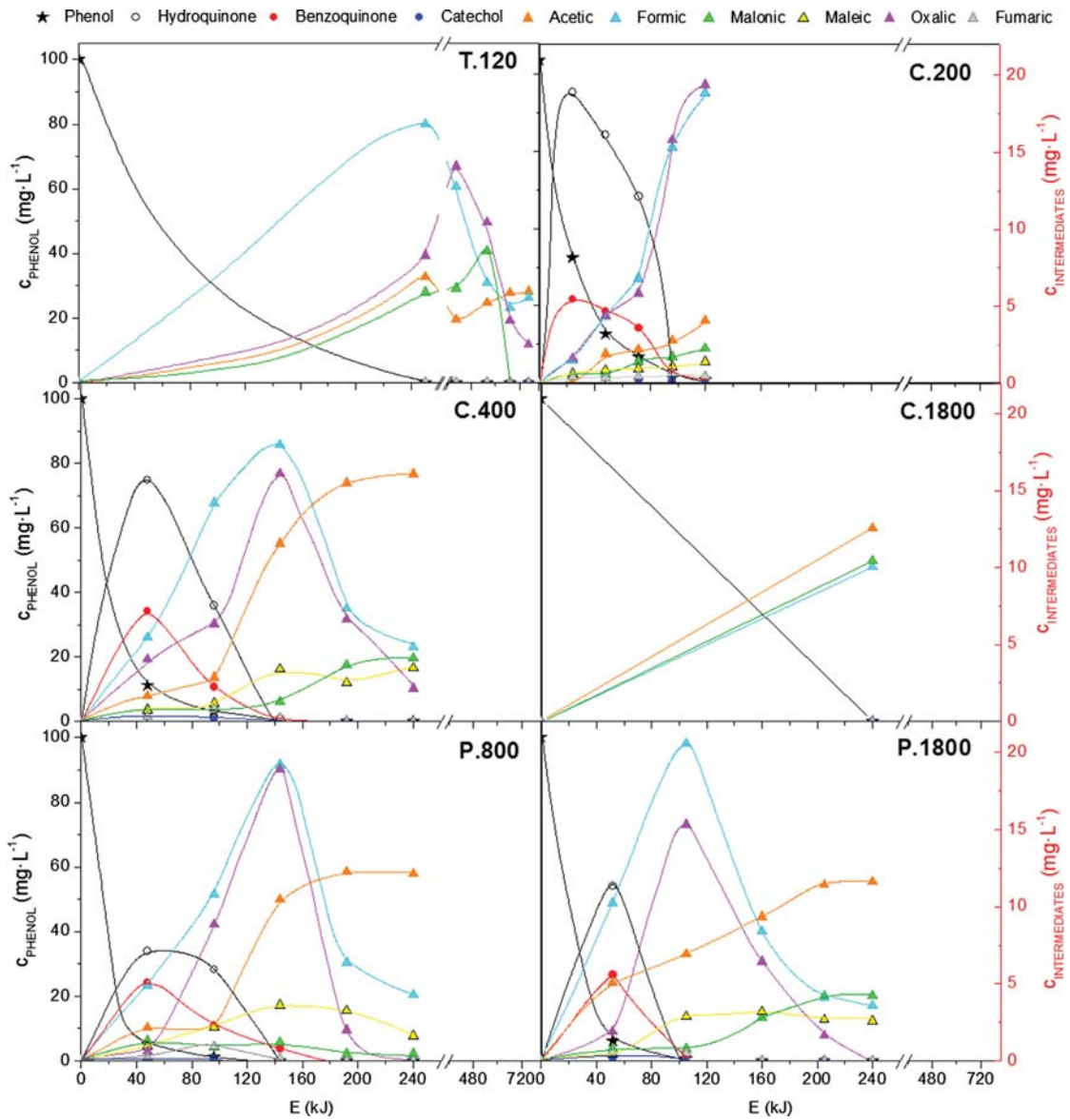

Fig. 2. Phenol and intermediates evolution upon MW-CWPO. $C_{Phenol,0}$: 100 mg·L^{-1}, C_{cat}: 500 mg·L^{-1}, $C_{H2O2,0}$: 500 mg·L^{-1}, pH_0: 3.

Experimental data were fitted by the proposed equations, as can be seen in Fig. 6. There is a good reproduction with a slight deviation in P.1800 for both TOC and H_2O_2.

$$-r_{(TOC)} = k_{TOC}\cdot TOC^2 = k_{0,TOC}\cdot e^{\left(\frac{-E_{A,TOC}}{R\cdot T}\right)}\cdot TOC^2 \quad (3)$$

$$-r_{(H_2O_2)} = k_{H2O2}\cdot H_2O_2 = k_{0,H2O2}\cdot e^{\left(\frac{-E_{A,H2O2}}{R\cdot T}\right)}\cdot H_2O_2 \quad (4)$$

Activation energies and pre-exponential factors obtained by fitting are collected in Table 5. $E_{A,\ TOC}$ is lower than the one reported for non-assisted CWPO of phenol ($E_{A,\ TOC}$: 55–57 kJ·mol^{-1}) [40,44]. However, $E_{A,\ H2O2}$ is similar to that reported by Diaz de Tuesta et al. [42] for phenol CWPO using carbon black as catalyst ($E_{A,\ H2O2}$: 43 kJ·mol^{-1}). Thus, MW non-thermal effects seem to have a greater influence on the organic pollutants abatement, rather than on the H_2O_2 decomposition.

In order to compare the behavior of the system with the results obtained at fixed temperature (T.120), the apparent kinetic constants at 120 °C have been calculated for C.400 and P.800 using Eqs. (3) and (4) as well as the parameters collected in Table 5. These runs were chosen because they both present a very similar temperature profile (Fig. 1). The apparent kinetic constants (k_{app}) are collected in Table 6. For the sake of comparison, the experimental data for these runs is collected in Fig. 7, which shows the reaction efficiency in terms of H_2O_2 consumption and TOC removal. Working at the stoichiometric amount of H_2O_2 needed for complete phenol mineralization, the ideal situation would be to work as close as possible to the diagonal, where each

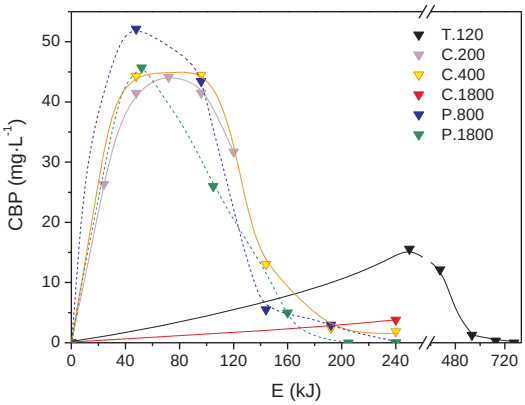

Fig. 3. Unidentified TOC after reaction.

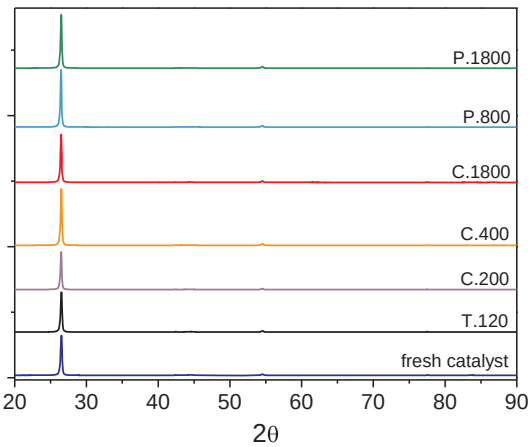

Fig. 4. XRD patterns of the fresh and used catalysts.

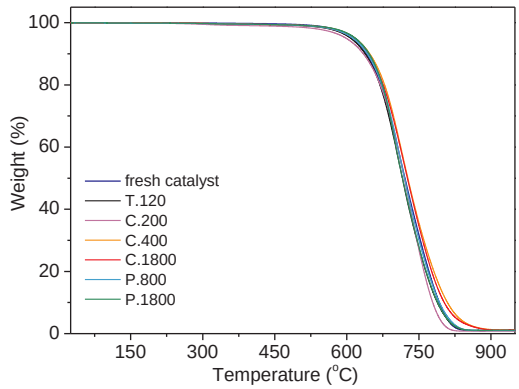

Fig. 5. TGA curves of the fresh and used catalysts.

fraction of decomposed H_2O_2 is efficiently employed for pollutant mineralization. Towards the end of the reaction there is always a higher deviation due to the presence of refractory byproducts (acetic acid).

As reflected in Table 6, in the same temperature conditions, for continuous MW radiation there is a faster H_2O_2 decomposition, which is not translated in a higher mineralization degree. This process is inefficient in terms of H_2O_2 efficiency, as revealed by the deviation from the diagonal in Fig. 7. For the fixed temperature run (T.120), the H_2O_2 decomposition rate is relatively slow, although the effectiveness of the process is higher, as revealed by the $k_{app,TOC}$ and the greater approach to the diagonal. Nonetheless, with MW pulses, an equilibrium between H_2O_2 decomposition and $HO_X^{\cdot}$ exploitation towards the pollutant mineralization is reached. For this run, the experimental data are very close to the ideal performance, with a high $k_{app,TOC}$ and a medium $k_{app,H2O2}$. Hence, the pulsated-MW process, which combines hot spot formation and catalyst relaxation, gives rise to a moderate H_2O_2 decomposition rate with a high efficiency towards TOC removal, as it has

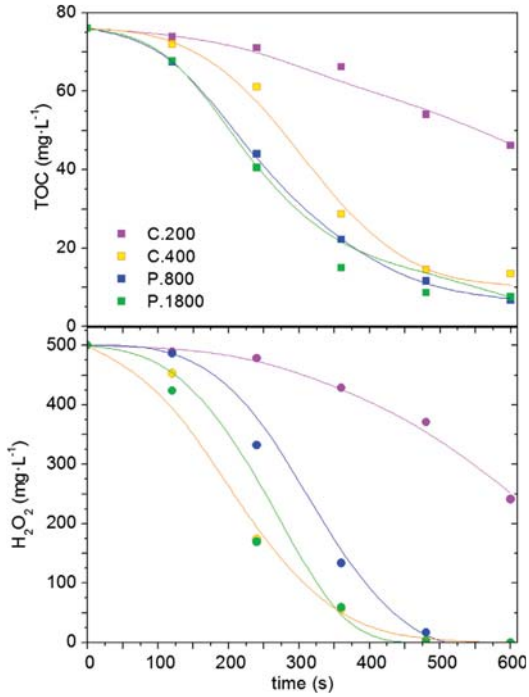

Fig. 6. Experimental (symbols) and estimated (curves) time-course of TOC and H_2O_2.

Table 5
Activation energy and pre-exponential factors for TOC and H_2O_2.

Run	TOC			H_2O_2		
	$E_{A,TOC}$ (kJ·mol^{-1})	$k_{0,TOC}$ (L·mg^{-1}·s^{-1})	r^2	$E_{A,H2O2}$ (kJ·mol^{-1})	$k_{0,H2O2}$ (s^{-1})	r^2
C.200	29.7	0.23	0.984	52.1	$2.81 \cdot 10^5$	0.997
C.400	40.9	11.68	0.991	37.4	$4.96 \cdot 10^2$	0.998
P.800	32.9	1.91	0.999	46.5	$4.22 \cdot 10^3$	0.996
P.1800	37.1	4.74	0.977	33.0	$1.22 \cdot 10^2$	0.981

Table 6
Apparent kinetic constant for T = 120 °C.

Run	TOC $k_{app,TOC} \cdot 10^5$ (L·mg^{-1}·s^{-1})	H_2O_2 $k_{app,H2O2} \cdot 10^3$ (s^{-1})
T.120	6.26	1.10
C.400	4.27	5.39
P.800	8.09	2.81

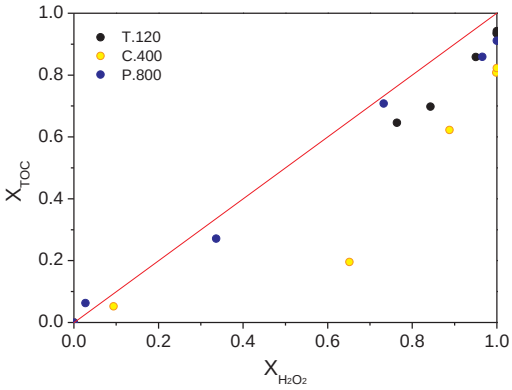

Fig. 7. H_2O_2 efficiency in MW-CWPO for T.120, C.400 and P.800. $C_{Phenol,0}$: 100 mg·L^{-1}, C_{cat}: 500 mg·L^{-1}, $C_{H2O2,0}$: 500 mg·L^{-1}, pH_0: 3.

been demonstrated both experimentally and with the simulation at constant temperature.

4. Conclusions

The MW application mode plays a key role in the MW-CWPO process. MW pulsation allows a faster and higher mineralization degree in relation to the continuous MW radiation, with a better H_2O_2 consumption efficiency (ε: 90%) at 240 kJ. This implies a high energy saving with respect to the controlled temperature experience (120 °C), which requires three times more energy to reach similar results. In this sense, we have successfully developed a fast and efficient procedure for phenolic wastewater treatment (t: 10 min, X_{TOC}: 90%) without compromising the effluent quality, as the only remaining products are readily biodegradable short chain acids. The proposed MW-pulse-CWPO is also competitive in terms of energy consumption against other technologies such as UV-assisted CWPO and persulfate combined thermal and electric activation. In regard with the catalyst, despite the extreme conditions to which they are subjected, graphite maintains its crystallinity and no organic deposits remain adsorbed after reaction. The MW-CWPO follows a pseudo-second order kinetics for TOC abatement and pseudo-first order for H_2O_2 decomposition with lower $E_{A,TOC}$ than the non-assisted process due to the microwave non-thermal effects.

Acknowledgements

Authors would like to thank the Spanish Ministerio de Economia y Competitividad (MINECO) for financial support through project CTM2016-76454-R. A.L. Garcia-Costa acknowledges the European Social Fund and MINECO for PhD. grant BES-2014-067598.

References

[1] V. Kavitha, K. Palanivelu, Destruction of cresols by Fenton oxidation process, Water Res. 39 (2005) 3062–3072.
[2] W.Z. Tang, C.P. Huang, 2,4-Dichlorophenol oxidation kinetics by Fenton's reagent, Environ. Technol. 17 (1996) 1371–1378.
[3] M. Munoz, Z.M. de Pedro, N. Menendez, J.A. Casas, J.J. Rodriguez, A ferromagnetic gamma-alumina-supported iron catalyst for CWPO Application to chlorophenols, Appl. Catal. B-Environ. 136 (2013) 218–224.
[4] J.A. Zazo, J. Bedia, C.M. Fierro, G. Pliego, J.A. Casas, J.J. Rodriguez, Highly stable Fe on activated carbon catalysts for CWPO upon FeCl3 activation of lignin from black liquors, Catal. Today 187 (2012) 115–121.
[5] R. Molina, F. Martinez, J.A. Melero, D.H. Bremner, A.G. Chakinala, Mineralization of phenol by a heterogeneous ultrasound/Fe-SBA-15/H_2O_2 process: multivariate study by factorial design of experiments, Appl. Catal. B-Environ. 66 (2006) 198–207.
[6] C.M. Dominguez, P. Ocon, A. Quintanilla, J.A. Casas, J.J. Rodriguez, Graphite and carbon black materials as catalysts for wet peroxide oxidation, Appl. Catal. B-Environ. 144 (2014) 599–606.
[7] C.M. Dominguez, P. Ocon, A. Quintanilla, J.A. Casas, J.J. Rodriguez, Highly efficient application of activated carbon as catalyst for wet peroxide oxidation, Appl. Catal. B-Environ. 140 (2013) 663–670.
[8] A. Dhaouadi, N. Adhoum, Heterogeneous catalytic wet peroxide oxidation of paraquat in the presence of modified activated carbon, Appl. Catal. B 97 (2010) 227–235.
[9] J.A. Zazo, G. Pliego, S. Blasco, J.A. Casas, J.J. Rodriguez, Intensification of the Fenton process by increasing the temperature, Ind. Eng. Chem. Res. 50 (2011) 866–870.
[10] G. Coria, I. Sires, E. Brillas, J.L. Nava, Influence of the anode material on the degradation of naproxen by Fenton-based electrochemical processes, Chem. Eng. J. 304 (2016) 817–825.
[11] L.P. Ramteke, P.R. Gogate, Treatment of toluene, benzene, naphthalene and xylene (BTNXs) containing wastewater using improved biological oxidation with pretreatment using Fenton/ultrasound based processes, J. Ind. Eng. Chem. 28 (2015) 247–260.
[12] E. Psillakis, G. Goula, N. Kalogerakis, D. Mantzavinos, Degradation of polycyclic aromatic hydrocarbons in aqueous solutions by ultrasonic irradiation, J. Hazard. Mater. 108 (2004) 95–102.
[13] I.A. Ricardo, C.E.S. Paniagua, V.A.B. Paiva, B.R. Goncalves, R.M.F. Sousa, A.E.H. Machado, A.G. Trovo, Degradation and initial mechanism pathway of chloramphenicol by photo-Fenton process at circumneutral pH, Chem. Eng. J. 339 (2018) 531–538.
[14] P. Liu, C.L. Li, Q. Han, G. Lu, X.Q. Dong, F. Ji, J.H. Xu, Phenol degradation by UV-enhanced catalytic wet peroxide oxidation process, J. Adv. Oxid. Technol. 17 (2014) 127–132.
[15] Z.H. Liu, R.L. Liu, T.M. Mu, Z.H. Zuo, C.Y. Tao, Degradation of methyl orange solution by microwave-assisted catalysis of H_2O_2 with chromium residue, Spectrosc. Spectr. Anal. 28 (2008) 1900–1904.
[16] G.Y. Zhang, P. Wang, Y. Shi, H.J. Ma, G. Hong, Microwave Irradiation Treatment of Phenol in Water based on Fenton Process, Harbin Institute Technology Publishers, Harbin, 2004.
[17] J. Sanz, J.I. Lombrada, A.M. De Luis, M. Ortueta, F. Varona, Microwave and Fenton's reagent oxidation of wastewater, Environ. Chem. Lett. 1 (2003) 45–50.
[18] N. Wang, P. Wang, Study and application status of microwave in organic wastewater treatment – a review, Chem. Eng. J. 283 (2016) 193–214.
[19] A.L. Garcia-Costa, J.A. Zazo, J.A. Casas, J.J. Rodriguez, Microwave-assisted catalytic wet peroxide oxidation. Comparison of Fe catalysts supported on activated carbon and g-alumina, Appl. Catal. B 218 (2017) 5.
[20] A.L. Garcia-Costa, J.A. Zazo, J.J. Rodriguez, J.A. Casas, Intensification of catalytic wet peroxide oxidation with microwave radiation: activity and stability of carbon materials, Sep. Purif. Technol. 209 (2019) 301–306.
[21] N. Tian, X.K. Tian, Y.L. Nie, C. Yang, Z.X. Zhou, Y. Li, Biogenic manganese oxide: an efficient peroxymonosulfate activation catalyst for tetracycline and phenol degradation in water, Chem. Eng. J. 352 (2018) 469–476.
[22] P. Liang, Q.C. Wang, J. Kang, W.J. Tian, H.Q. Sun, S.B. Wang, Dual-metal zeolitic imidazolate frameworks and their derived nanoporous carbons for multiple environmental and electrochemical applications, Chem. Eng. J. 351 (2018) 641–649.
[23] Y.J. Choe, J.Y. Byun, S.H. Kim, J. Kim, Fe3S4/Fe7S8-promoted degradation of phenol via heterogeneous, catalytic H_2O_2 scission mediated by S-modified surface Fe^{2+} species, Appl. Catal. B-Environ. 233 (2018) 272–280.
[24] W.L. Yang, M.H. Zhou, L. Liang, Highly efficient in-situ metal-free electrochemical advanced oxidation process using graphite felt modified with N-doped graphene, Chem. Eng. J. 338 (2018) 700–708.
[25] A. Jawad, J. Lang, Z.W. Liao, A. Khan, J. Ifthikar, Z.N. Lv, S.J. Long, Z.L. Chen, Z.Q. Chen, Activation of persulfate by CuOx@Co-LDH: a novel heterogeneous system for contaminant degradation with broad pH window and controlled leaching, Chem. Eng. J. 335 (2018) 548–559.
[26] A.L. Garcia-Costa, L. Lopez-Perela, X. Xu, J.A. Zazo, J.J. Rodriguez, J.A. Casas, Activated carbon as catalyst for microwave-assisted wet peroxide oxidation of aromatic hydrocarbons, Environ. Sci. Pollut. Res. (2018).
[27] X.S. Yao, Q.T. Lin, L.Z. Zeng, J.X. Xiang, G.C. Yin, Q.J. Liu, Degradation of humic acid using hydrogen peroxide activated by CuO-Co_3O_4@AC under microwave irradiation, Chem. Eng. J. 330 (2017) 783–791.
[28] A. Anshuman, S. Saremi-Yarahmadi, B. Vaidhyanathan, Enhanced catalytic performance of reduced graphene oxide–TiO_2 hybrids for efficient water treatment using microwave irradiation, RSC Adv. 8 (2018) 7709–7715.
[29] Z. Liu, H. Meng, H. Zhang, J. Cao, K. Zhou, J. Lian, Highly efficient degradation of phenol wastewater by microwave induced H_2O_2-CuOx/GAC catalytic oxidation process, Sep. Purif. Technol. 193 (2018) 49–57.
[30] S. Li, G.S. Zhang, H.S. Zheng, N.N. Wang, Y.J. Zheng, P. Wang, Microwave-assisted synthesis of $BiFeO_3$ nanoparticles with high catalytic performance in microwave-enhanced Fenton-like process, RSC Adv. 6 (2016) 82439–82446.
[31] S. Li, G.S. Zhang, W. Zhang, H.S. Zheng, W.Y. Zhu, N. Sun, Y.J. Zheng, P. Wang, Microwave enhanced Fenton-like process for degradation of perfluorooctanoic acid (PFOA) using Pb-$BiFeO_3$/rGO as heterogeneous catalyst, Chem. Eng. J. 326 (2017) 756–764.
[32] Y. Lei, X. Lin, H. Liao, New insights on microwave induced rapid degradation of methyl orange based on the joint reaction with acceleration effect between electron hopping and Fe^{2+}-H_2O_2 reaction of $NiFeMnO_4$ nanocomposites, Sep. Purif. Technol. 192 (2018) 220–229.
[33] G.M. Eisenberg, Colorimetric determination of hydrogen peroxide, Ind. Eng. Chem.-Anal. Ed. 15 (1943) 327–328.
[34] D. Haranaka-Funai, F. Didier, J. Gimenez, P. Marco, S. Esplugas, A. Machulek,

Photocatalytic treatment of valproic acid sodium salt with TiO_2 in different experimental devices: an economic and energetic comparison, Chem. Eng. J. 327 (2017) 656–665.
[35] P. Garcia-Munoz, G. Pliego, J.A. Zazo, A. Bahamonde, J.A. Casas, Ilmenite ($FeTiO_3$) as low cost catalyst for advanced oxidation processes, J. Environ. Chem. Eng. 4 (2016) 542–548.
[36] J.E. Silveira, T.O. Cardoso, M. Barreto-Rodrigues, J.A. Zazo, J.A. Casas, Electro activation of persulfate using iron sheet as low-cost electrode: the role of the operating conditions, Environ. Technol. 39 (2018) 1208–1216.
[37] X.Y. Duan, F. Ma, Z.X. Yuan, L.M. Chang, X.T. Jin, Electrochemical degradation of phenol in aqueous solution using PbO_2 anode, J. Taiwan Inst. Chem. Eng. 44 (2013) 95–102.
[38] E. Weiss, K. Groenen-Serrano, A. Savall, A comparison of electrochemical degradation of phenol on boron doped diamond and lead dioxide anodes, J. Appl. Electrochem. 38 (2008) 329–337.
[39] J.A. Zazo, J.A. Casas, A.F. Mohedano, M.A. Gilarranz, J.J. Rodriguez, Chemical pathway and kinetics of phenol oxidation by Fenton's reagent, Environ. Sci. Technol. 39 (2005) 9295–9302.
[40] N.S. Inchaurrondo, P. Massa, R. Fenoglio, J. Font, P. Haure, Efficient catalytic wet peroxide oxidation of phenol at moderate temperature using a high-load supported copper catalyst, Chem. Eng. J. 198 (2012) 426–434.
[41] J. Iniesta, P.A. Michaud, M. Panizza, G. Cerisola, A. Aldaz, C. Comninellis, Electrochemical oxidation of phenol at boron-doped diamond electrode, Electrochim. Acta 46 (2001) 3573–3578.
[42] J.L.D. de Tuesta, A. Quintanilla, J.A. Casas, J.J. Rodriguez, Kinetic modeling of wet peroxide oxidation with a carbon black catalyst, Appl. Catal. B-Environ. 209 (2017) 701–710.
[43] M.E. Suarez-Ojeda, F. Stuber, A. Fortuny, A. Fabregat, J. Carrera, J. Font, Catalytic wet air oxidation of substituted phenols using activated carbon as catalyst, Appl. Catal. B-Environ. 58 (2005) 105–114.
[44] E.V. Rokhina, E. Repo, J. Virkutyte, Comparative kinetic analysis of silent and ultrasound-assisted catalytic wet peroxide oxidation of phenol, Ultrason. Sonochem. 17 (2010) 541–546.


UAM
Universidad Autónoma
de Madrid